Tailor-made thin radionuclide layers for targets and recoil ion sources in nuclear applications

Dissertation

zur Erlangung des Grades
„Doktor der Naturwissenschaften“
im Promotionsfach Chemie
am Fachbereich Chemie, Pharmazie und Geowissenschaften
der Johannes Gutenberg-Universität
in Mainz

Raphael Haas
geb. in Wiesbaden

JOHANNES GUTENBERG UNIVERSITÄT MAINZ

JG|U

Mainz, den 25. September 2020

1. Gutachter: [redacted]
2. Gutachter: [redacted]

Raphael Haas
Department Chemie - Standort TRIGA
Fritz-Strassmann-Weg 2
55128 Mainz
raphhaas@uni-mainz.de

Declaration of academic integrity

With this statement I declare that I have completed the PhD thesis entitled with "Tailor-made thin radionuclide layers for targets and recoil ion sources in nuclear applications" self-directed. The thoughts taken directly or indirectly from external sources as well as other resources are properly marked as such. I have not or had not submitted the work now submitted as a dissertation as an examination paper for a state or other scientific examination. I did not submit the present work or parts of it as a dissertation to another faculty or department.

Hiermit versichere ich, dass ich die vorliegende Dissertation mit dem Titel "Tailor-made thin radionuclide layers for targets and recoil ion sources in nuclear applications" selbständig angefertigt habe. Die direkt oder indirekt aus externen Quellen entnommenen Gedanken sowie andere Hilfsmittel und Materialien sind ordnungsgemäß als solche gekennzeichnet. Ich habe oder hatte die jetzt als Dissertation vorgelegte Arbeit nicht als Prüfungsarbeit für eine staatliche oder andere wissenschaftliche Prüfung eingereicht. Ich hatte weder die jetzt als Dissertation vorgelegte Arbeit noch Teile davon bei einer anderen Fakultät beziehungsweise einem anderen Fachbereich als Dissertation eingereicht.

Mainz, den 25.09.2020

Abstract

The present work deals with the production and characterization of thin inorganic layers consisting of natural isotopes and exotic radionuclides by different methods. These layers are usually deposited on thin substrates and are used, e.g., as targets in accelerator experiments and other nuclear applications for nuclear reaction studies and the synthesis of superheavy elements. With steadily increasing beam intensities of new accelerator facilities, the targets have to withstand increasing power inputs. They also have to contain more material, since the cross sections for the synthesis of the heaviest known elements are extremely small. For off-line studies of the chemical reactions of targets with low energetic electron and ion beams, a pilot experiment for "Off-line Deposit Irradiations" (ODIn) of thin layers was constructed, characterized and commissioned with lead targets. This experiment will help to develop a method to condition targets suitable for future accelerator experiments. Furthermore, the fabrication methods in this work were used for the production of thin radioactive samples, so-called recoil ion sources, which are used for the generation of particle beams of their emitted recoil ions and thus have different requirements in contrast to targets. The goal was the production of ideal recoil ions sources consisting of single atomic layers (monolayers) of alpha-decaying radionuclides. They will be used for quantum logic spectroscopy in the "Trapping And Cooling of Thorium Ions with Calcium" (TACTICa) collaboration. The aim of the TACTICa experiment is to study the isomer ^{229m}Th trapped inside a coulomb crystal of $^{40}Ca^{+}$ ions in a Paul trap. The ^{229}Th is a nuclide of high interest due to its low lying isomeric state at (8.28 ± 0.17) eV. The precisely known energy and half-life of the isomeric state, which is currently studied by the nuClock collaboration, will make it usable for applications like a "nuclear clock" or quantum computing. The studies of the TACTICa collaboration are in the field of quantum logic spectroscopy and fundamental physics beyond the standard model. In addition to the production of monolayer recoil ion sources for TACTICa, a setup was developed for the electrostatic deceleration of daughter nuclei including ^{229m}Th coming from alpha-decaying sources like ^{233}U while maintaining their initial charge distribution and thus making them available for loading into a Paul trap.

Die vorliegende Arbeit befasst sich mit der Herstellung und Charakterisierung von dünnen anorganischen Schichten aus natürlichen Isotopen und exotischen Radionukliden mit verschiedenen Methoden. Diese Schichten werden in der Regel auf möglichst dünnen Substraten abgeschieden und werden z.B. für Targets in Beschleunigerexperimenten und anderen nuklearen Anwendungen für Kernreaktionsstudien und die Synthese superschwerer Elemente verwendet. Mit immer höheren Strahlintensitäten neuer Beschleunigeranlagen müssen die Targets der

steigenden Energiezufuhr standhalten. Zudem müssen sie auch mehr Material enthalten, da die Querschnitte für die Synthese der schwersten bekannten Elemente verschwindend klein sind. Für Off-Line-Studien der chemischen Reaktionen von Targets mit niederenergetischen Elektronen- und Ionenstrahlen wurde ein Pilotaufbau für "Off-line Deposit Irradiations" (ODIn) von dünnen Schichten aufgebaut, charakterisiert und mit Bleitargets in Betrieb genommen. Dieses Experiment wird dazu beitragen, eine Methode zur Konditionierung von Targets zu entwickeln, die für zukünftige Beschleunigerexperimente geeignet sind. Darüber hinaus wurden die Methoden dieser Arbeit für die Herstellung dünner radioaktiver Proben, so genannter Ionenrückstoßquellen, benutzt, die zur Erzeugung von Teilchenstrahlen ihrer emittierten Rückstoß-Ionen verwendet werden und daher im Gegensatz zu Targets andere Anforderungen haben. Das Ziel war die Herstellung idealer Ionenrückstoßquellen, die aus einzelnen Atomlagen (Monolagen) von alpha-zerfallenden Radionukliden bestehen. Sie werden für quantenlogische Spektroskopie-Experimente in der "Trapping And Cooling of Thorium Ions with Calcium" (TACTICa) Kollaboration verwendet. Ihr Ziel ist es, das Isomer ^{229m}Th zu untersuchen, das in einem Coulomb-Kristall aus $^{40}Ca^{+}$ Ionen in einer Paul-Falle gefangen wird. Das ^{229}Th ist ein Nuklid von hohem Interesse aufgrund seines niedrig liegenden isomeren Zustands bei (8.28 ± 0.17) eV. Die genau bekannte Energie und Halbwertszeit des isomeren Zustands, die derzeit von der nuClock Kollaboration untersucht wird, wird es für Anwendungen wie eine "Kern-Uhr" oder Quantenprozessoren nutzbar machen. Die Arbeiten der TACTICa-Kollaboration dienen zur quantenlogischen Spektroskopie und der Suche nach einer Physik jenseits des Standardmodells. Zusätzlich zur Herstellung der Monolagen-Rückstoßquellen wurde in dieser Arbeit ein Aufbau entwickelt, der die Tochterkerne aus den alpha-zerfallenden Quellen, darunter auch ^{229m}Th aus ^{233}U, unter Beibehaltung ihrer ursprünglichen Ladungsverteilung elektrostatisch abbremst und damit zum Einfangen in eine Paul-Falle zur Verfügung stellt.

"It is the great beauty of our science, chemistry, that advancement in it, whether in a degree great or small, instead of exhausting the subjects of research, opens the doors to further and more abundant knowledge, overflowing with beauty and utility, to those who will be at the easy personal pains of undertaking its experimental investigation."

– **Michael Faraday**, 1834

List of Abbreviations

ADC **A**nalog **D**igital **C**onverter

AFM **A**tomic **F**orce **M**icroscopy

DMF N,N-**D**i**M**methyl**F**ormamide

DoD **D**rop-**o**n-**D**emand

doF **d**egrees **o**f **F**reedom

EDX **E**nergy-**D**ispersive **X**-ray spectroscopy

FWHM **F**ull **W**idth at **H**alf **M**aximum

HPGe **H**igh **P**urity **Ge**rmanium detector

IB **I**so**B**utanol

IP **I**so**P**ropanol

MCA **M**ulti **C**hannel **A**nalyzer

MCP **M**icro**C**hannel **P**late detector

MP **M**olecular **P**lating

NAA **N**eutron **A**ctivation **A**nalysis

ODIn **O**ff-line **D**eposit **I**rradiatio**n**

PE **P**oly**E**thylene

PIPS **P**assivated **I**mplanted **P**lanar **S**ilicon detector

RI **R**adiographic **I**maging

SA **S**elf-**A**dsorption

SEM **S**canning **E**lectron **M**icroscopy

SHE **S**uper**H**eavy **E**lements

SHIP **S**eparator for **H**eavy **I**on reaction **P**roducts

TACTICa **T**rapping **A**nd **C**ooling of **T**horium **I**ons with **Ca**lcium

TRIGA **T**raining, **R**esearch, **I**sotopes, **G**enereal **A**tomics

Contributions

This thesis is based on four publications, which are listed below. The author is the main author of three publications [2-4]. Furthermore, the author provided mayor contributions to publication [1] in the form of method development, target production, target characterization as well as active coauthor of the text block in section II of the publication.

Publications

[1] T. Heftrich, et al., Thermal (n, γ) cross section and resonance integral of ^{171}Tm, Physical Review C 99 (2019) 065810.

[2] R. Haas, et al., ODIn — A setup for Off-line Deposit Irradiations of thin layers for nuclear physics applications, Nuclear Instruments and Methods in Physics Research Section A: Accelerators, Spectrometers, Detectors and Associated Equipment 957 (2020) 163366.

[3] R. Haas, et al., Alpha spectrometric characterization of thin ^{233}U sources for $^{229(m)}$Th production, Radiochimica Acta (2020) [accepted].

[4] R. Haas, et al., Development of a recoil ion source providing slow Th ions including $^{229(m)}$Th in a broad charge state distribution, Hyperfine Interactions 241 (25).

Contents

Chapter 1

Introduction

In 2017, the United Nations proclaimed the year 2019 as the International Year of the Periodic Table of Chemical Elements (IYPT 2019) [1]. It was the 150th anniversary of the first periodic table, which was created by Dmitry Mendeleev in 1869. Nowadays, 118 elements are known, of which 90 are natural elements consisting of 252 stable isotopes. Additionally, 3437 nuclides and 1318 isomeric states with half-lives longer than 100 ns have been discovered and are listed in the recent NUBASE evaluation [2]. And yet, there are still many chemical and physical properties unknown of some of these elements and their isotopes. Further insights in these properties as well as further new elements and isotopes to be discovered help to gain more fundamental knowledge and to complete the knowledge on the components of the periodic table. Recent examples are the investigations on the ionization energy of lawrencium [3], which helped to reconsider the position of the lanthanides inside the transition metals [4, 5], or the investigations on the chemical properties of flerovium [6, 7], which will help to determine its chemical behavior between metals and noble gases. A subject in nuclear physics is how all the natural elements found on earth are formed and if there also exist "stable" superheavy elements (SHE) in the universe, which is often referred as the "island of stability" [8–10]. Elements up to nickel are formed by nuclear fusion processes in stars [11], due to the released nuclear binding energy in the fusion process. Elements with higher proton numbers are mainly formed by two different astrophysical processes, called slow (s-) and rapid (r-) neutron capture process. In the s-process, stable isotopes of the elements iron up to nickel capture a single neutron to form β^--decaying isotopes, which stepwise leads to elements with higher proton numbers [12] up to polonium (Z = 84). The term "slow" is used because the capture of a single neutron is usually slower than the subsequent β^- decay process. The s-process occurs at lower neutron flux densities and star temperatures and originates from released neutrons of nuclear fusion reactions in the inner core of asymptotic giant branching stars [13, 14] (see section 1.3.1). On earth, this process can be imitated in high-flux nuclear reactors

to produce elements up to fermium (Z = 100) [15]. Heavier elements (including SHE) cannot be produced by single neutron capture, because it passes ^{258}Fm, which decays by spontaneous fission with a half-life of 370 µs. It is already known that elements heavier than polonium are produced by the r-process in the universe, which occurs at far higher neutron flux densities and temperatures in binary neutron star mergers [16] and in supernovae [17, 18]. To produce heavier actinides as well as the transactinides (SHE) on earth, fusion reactions are performed in particle accelerators [19]. These fusion reactions are classified as cold or hot fusions, depending on the excitation energy of compound nuclei E^* produced in them [20]. The excitation energy is below 20 MeV for compound nuclei produced in cold fusion reactions and above 30 MeV for those formed in hot fusion reactions. Nuclei like ^{54}Cr, ^{58}Fe, ^{62}Ni and ^{70}Zn are used as projectiles in cold fusion reactions for the production of elements up to Z = 112. Projectiles of nuclei with single or double magic nucleon numbers, e.g., ^{48}Ca are usually preferred for hot fusion reactions. In cold fusion reactions, lead and bismuth are used as target nuclei, whereas in hot fusions actinides starting with uranium up to californium are used [19, 20]. The production of these accelerator targets has a key role in the synthesis of the heaviest actinides and SHE for nuclear chemistry and nuclear physics experiments. Targets have to fulfill specific requirements in chemical purity, thickness, homogeneity of the material and its adherence to the substrate in dependence to the planned experiment. Due to the demand for higher production rates of SHE for more statistics in the experiments and due to the very small cross section for the synthesis of the heaviest known elements, the beam intensities of accelerators are increasing [21]. Targets must have to withstand these higher beam intensities and, therefore, the development of methods to produce targets in higher quality became important in recent years. A mayor problem of freshly produced targets is the chemical species of the actinides, which is sensible to humidity and thus the material deteriorates during long storage times. The state-of-the-art method, to transform the sensible target material into a more mechanically stable form, is to use beams of lower intensities to "bake-in" the targets [22]. The disadvantage of this method is that valuable accelerator beam time, which could be used for the actual experiment, is lost. Furthermore, the target production cannot be planned and executed far in advance before the actual experiment. Therefore, it is important to understand the chemical micro-processes involved in the "baking-in" procedure and to develop an accelerator-independent method to transform the fragile target material into a stable, storable form. For this purpose, a pilot experiment for "Off-line Deposit Irradiation" (ODIn) was designed, constructed and characterized as part of this work to perform electron and ion irradiations of thin layers at energies below 5 keV and at beam currents of maximum 2 mA. The experimental design, the beam characterization and first commissioning with lead targets is described in section 3. Besides the investigations of astrophysical processes and of SHE, experiments on the atomic and nuclear structure of exotic radionuclei and their isomers is important

for future applications in daily life. For example, the ^{229}Th, which can be obtained as daughter nuclide in the alpha decay of ^{233}U, has the lowest lying known isomeric nuclear state located at an excitation energy below 10 eV and has therefore been a nuclide of high interest in recent years [23]. The energy of this isomeric state is low enough, to reach it with modern laser systems. The knowledge of the exact energy and half-life, which is currently investigated by the nuClock collaboration [24–27], makes it applicable for the construction of a "nuclear clock" [28], an enhanced development of the atomic clock. An atomic clock uses the frequency of laser light that corresponds to a certain energy difference between atomic shell states for time measurement [29, 30]. In the nuclear clock, the atomic nucleus is about 5 magnitudes smaller than the atomic shell leading to reduced magnetic dipole and electric quadrupole moments and thus less perturbation by the environment and a higher precision [31, 32]. Furthermore, the ^{229m}Th isomer could be used as a qubit for quantum computing [28, 33]. On the theoretical site, high-precision quantum logic spectroscopy on ^{229m}Th could lead to new insights into physics beyond the standard model and the search for new particles by validation of the isotope shift using the non-linearity of the King plot [34, 35]. These motivations in the field of fundamental physics are the basis of the "Trapping And Cooling of Thorium Ions with Calcium" (TACTICa) collaboration and are further described in section 1.3.3. The aim of the TACTICa collaboration is to capture $^{229(m)}$Th^{n+} and further thorium isotopes inside a ^{40}Ca^{+} Coulomb ion crystal by sympathetic laser cooling in a Paul trap for high precision quantum logic spectroscopy [28]. The natural isotope ^{232}Th^{+} was already captured in previous experiments and verified as ^{232}Th by time-of-flight mass measurements [36, 37]. This isotope was loaded into the Paul trap by a laser ablation source. The same can be performed to capture further thorium isotopes like ^{229}Th in their ground states by laser ablation from bulk material. Since the exact excitation energy of the ^{229m}Th isomer is still currently unknown, this isomer is only available by i) internal conversion processes in the alpha decay of ^{233}U [38], ii) population in the β^{-}-decay of the artificial nuclide ^{229}Ac [39] and iii) synchrotron X-ray pumping to the second excited state of ^{229}Th at 29.19 keV [40]. As the alpha decay of ^{233}U is the easiest access due to the availability of ^{233}U as bulk material, it is the chosen ^{229m}Th production way for both, the nuClock and the TACTICa collaboration. The challenge is the deceleration of the emitted $^{229(m)}$Th recoil ions from a ^{233}U source to suitable trapping energies of a few hundred eV from the initial kinetic energy of 84 keV. In the nuClock collaboration, the deceleration of the recoil ions is performed by a buffer gas cell (see section 1.3.3). Thus, charge states above 3+ depopulate due to collisions with the buffer gas [24]. In the TACTICa collaboration the initial charge state distribution of the recoil ions has to be preserved, since ^{229m}Th^{n+} ions in higher charge states can be better captured in the Paul trap and are more interesting for precision spectroscopic investigations. The only way to both, decelerate the recoil ions and to preserve their initial charge state distribution, is to solely use electrostatic deceleration. The

design of such a source as well as ion flight simulations are given in section 5. Another crucial part of this recoil ion source is the fabrication of a ^{233}U source, which has both, a high recoil ion rate and a low broadening of the kinetic energy distribution of the recoil ions. An "ideal" source fulfilling these restrictions would only consist of a single layer of ^{233}U atoms. The fabrication of such a source with available methods as well as their full quantitative and qualitative characterization with focus on alpha spectrometric analysis is given in section 4.

1.1 Target fabrication techniques

A great variety of methods exist for the fabrication of targets and radioactive sources for different nuclear applications. Depending on the requirements, some specific methods are more suitable than others. Besides simple pipetting and extraction on filters, established conventional methods for the production of targets and radioactive sources are Molecular Plating [41], Pulsed Laser Deposition [42, 43], Polymer-Assisted Deposition which includes spin-coating [44], cold rolling [45], vacuum evaporation [46], painting/sedimentation [47], electrodeposition [48], die compaction [49] and Chemical Vapor Deposition [50]. Other methods including Drop-on-Demand inkjet printing (DoD) [51], chelation of ions from solution by sulfonic acid groups on silicon surfaces [52] and Self-Adsorption (SA) on metal oxide and fluorite surfaces [53, 54] are more suitable for the fabrication of thinner radioactive layers as needed for recoil ion sources. Four of these methods were used in this work for the production of targets and recoil ion sources and are introduced in sections 1.1.1 – 1.1.4.

1.1.1 Molecular Plating

The Molecular Plating (MP) technique is based on electrodeposition of a specific element in constant current mode and is the most widely applied method for the fabrication of targets with radionuclides or isotopically enriched material. It is performed in cells with two electrodes, where the cations are electrodeposited onto the working electrode, the cathode. The exact cell design depends on the geometry of the used substrate. In Mainz, two conventional cell designs exist for MP on different areas and substrates (see Fig. 1.1) [55, 56], which were also used in this work. Only small volumes of organic electrolytes (typically 10 mL to 35 mL with 0.2 % to 0.3 % of aqueous solution containing the isotope of interest) are needed. The method was developed by Parker and Falk [41] in 1962 as an alternative way for electrodepositions from aqueous solutions. At that time, it was thought that the material was deposited at the cathode as the original species dissolved in the electrolyte. The method was popular for its simplicity, because it requires only low currents of some mA cm^{-2} in contrast to ordinary electrodeposition and thus produces less hydrogen at the cathode, which disrupts the produced

layer [57]. Furthermore, another advantage is the high deposition yield (85 % to 95 %) of the method. Over decades, the original MP was applied in the way of Parker and Falk for radioactive reference samples [58], lanthanide [59] and actinide targets [55, 60–62]. The thereby produced targets were only characterized by their quantitative yields and the thickness, homogeneity and rigidity of the produced layers. For many years, the mayor qualitative finding about MP was that the produced layer did not consist of the originally used chemical compound [63], in contrast to the expectations of Parker and Falk. A full qualitative investigation of the electrochemical processes and the influence of several parameters on the resulting target layer was performed by A. Vascon et al. [56, 64–68] about 50 years after the first introduction by Parker and Falk. Major findings in these studies were the influence of the surface roughness of the substrate and ultrasonic stirring on the layer growth mechanism [56, 66], contaminants in the target layer from the organic solvents and the influence of the solvent on layer cracking [65, 66]. This led to the fabrication of smooth crack-free target layers [65] and advanced thin layers for α-particle sources [66]. The results set the basis for new targets and sources produced by MP [67, 68]. The optimal preparation parameters found by these investigations were also used for the target fabrication in section 3 and for the recoil ion source fabrication in section 4.

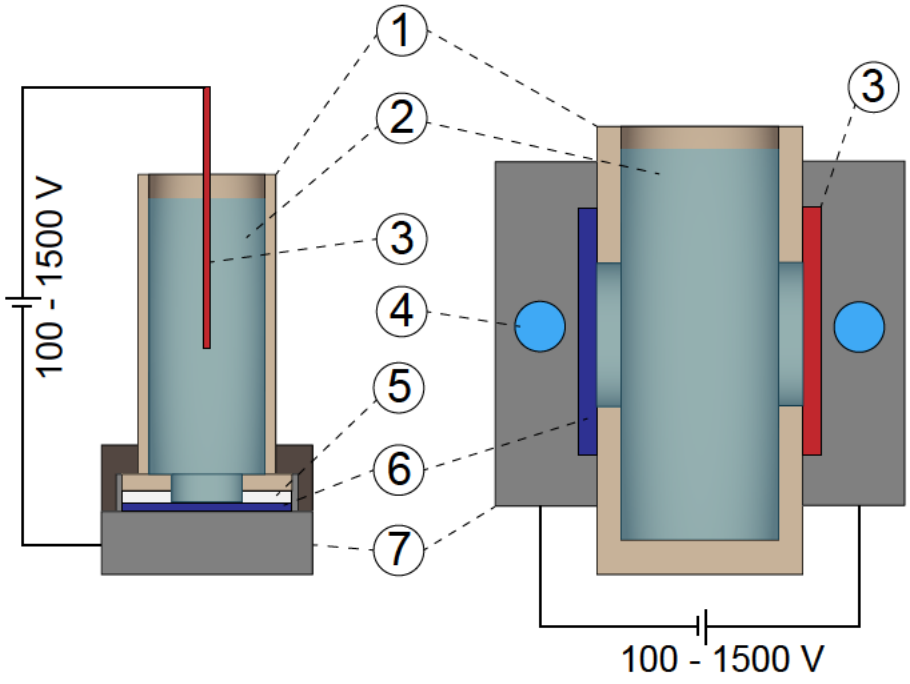

Figure 1.1: Schematic illustration of cells used for MP. Left: Vertical cell design for small depositions [55]. Right: Horizontal cell design by Vascon et al. [56] for large area depositions. 1) PEEK body, 2) electrolyte containing the radionuclides, 3) anode (palladium wire or disc), 4) water cooling, 5) spacer, 6) cathode (substrate), 7) base/holder (titanium) for mounting of electrodes. The dimensions are not to scale.

1.1.2 Drop-on-Demand inkjet printing

Overcoming the previously mentioned disadvantages of MP in section 1.1.1, such as the deposition of many different chemical compounds of a desired element as well as the deposition of organic impurities, the limitation to electrically conductive substrates and dimensional limitations due to cell design, required a fundamentally new method. This started with the development of an automated pipetting system by E. Maugeri et al. [69], who produced ^{7}Be targets for nuclear astrophysics research. The first inkjet printer system for target production was developed in 2017 [51], which allowed the investigation of the energy-dependent resolution limit of phosphor plates for radiographic imaging due to the high precision of the system and produced as a first application isotopically enriched ^{170}Er targets for nuclear astrophysics research [70, 71] (see section 1.3.1). The system is based on the Drop-on-Demand (DoD) principle [72] and can be divided into two ways of operation. In the first one, the fluid is kept inside a printer tip and droplets are released by pressure waves in the fluid. These are generated as a result of a rapid vaporization by a heating element, which is in contact with the fluid inside the printing head. A pulse current is passed trough the heating element causing an evaporation of the liquid and a subsequent collapse of the generated gas bubble, which causes a sudden volume change. This generates droplets at the lower end of the printer tip. The DoD operation mode with heating elements is commonly used in commercially available inkjet printers, but it is not feasible for application with substances used in nuclear chemistry since the evaporation of radioactive liquids may cause a high risk of contamination. The second way of operation consists of piezo elements and is depicted in Fig. 1.2.
The liquid is kept inside a flexible tip by its surface tension. A piezo-driven piston compresses the tip from the outside by a fast displacement. This displaces the liquid inside the tip in both directions. A droplet is generated at the lower end of the tip and falls off. New liquid refills the tip after a slow release of the piezo-driven piston. The way of displacement of the piston is proportional to the displaced volume of liquid and thus controls the generated drop volume. The minimum volume is limited by the inner diameter of the tip and the surface tension of the liquid. The length of the tip has an impact on the capillary forces on the liquid and has to be increased for liquids with small surface tensions to reduce unwanted drop generation. The velocity of the piston displacement controls the amount of transferred kinetic energy. A droplet is only ejected when this amount is larger than the surface energy needed to form a droplet [73]. The velocity is therefore usually increased for the generation of the smallest producible droplets and for liquids with a high viscosity.
Besides the adjustment of the printing parameters for a specific reproducible drop volume, also the evaporation behavior of the small droplets on different surfaces is important. D. Renisch et al. [74] found that deposits on super hydrophobic

surfaces are very small in diameter due to the high contact angle of evaporated droplets. The opposite effect can be achieved with droplets on super hydrophilic surfaces, where the evaporation generates thin deposits with greater diameters [75]. A similar effect may be achieved by adjustment of the liquids surface tension, which can be controlled by mixtures of aqueous solutions with alcohols. Small deposits of evaporated droplets have a higher thickness when compared with large deposits from droplets with the same volume and concentration. Therefore, small deposits are ideal for laser ablation targets [74], where a large amount of bulk material is needed within a small area. Larger deposits can be used for the generation of thin recoil ion sources to reduce the deceleration of emitted ions by the layer material. The DoD method was used in this work for the fabrication of isotopically enriched ^{170}Er targets described in section 2 and of recoil ion sources described in section 4.

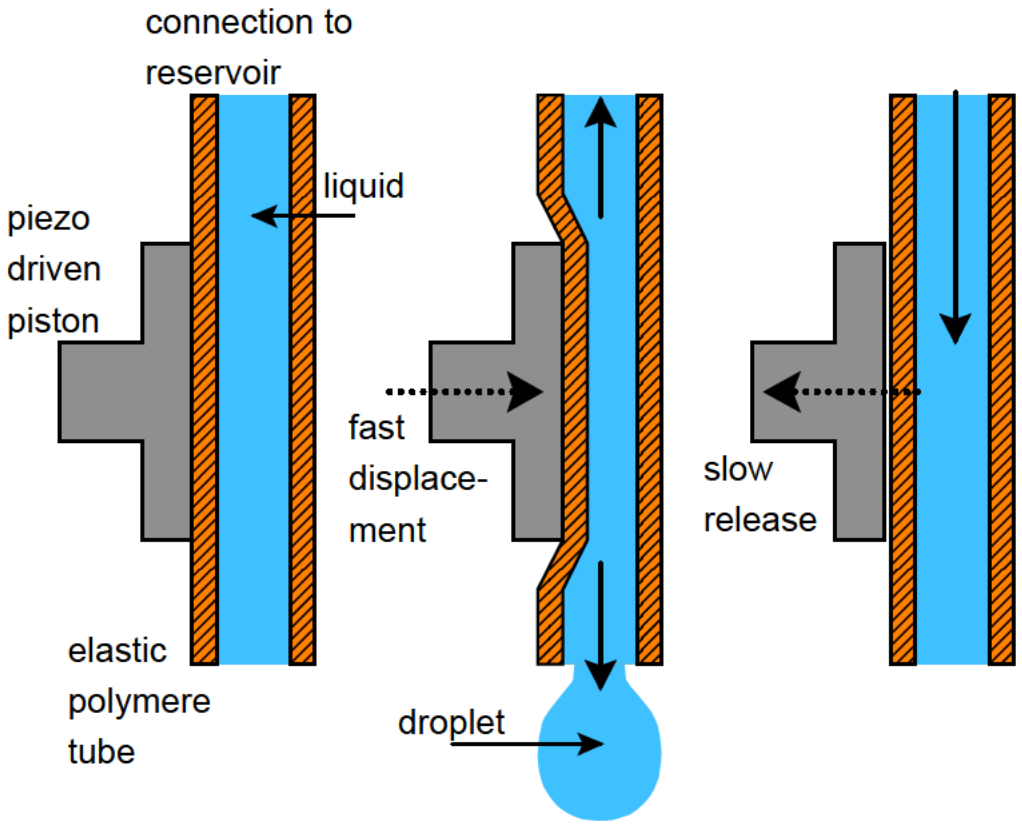

Figure 1.2: Illustration of the DoD working principle [76]. See text for details.

1.1.3 Chelation by sulfonic acid groups

High quality alpha spectrometry always consisted of the subsequent steps of chemical preparation of α-particle sources and the detection of the emitted particles. This requires technical equipment like a electrodeposition apparatus and detection systems including vacuum pumps, chemicals and time for both the chemical preparation and spectrometric measurement. For radionuclides with half-lives below minutes, radioanalytical investigations become difficult as a major amount of the radionuclides already decays during the chemical preparation of samples. To combine both steps for faster radioanalytical investigations, Krupp and Scherer developed prototypes of ion exchanging alpha detectors [52]. These ion exchangers are commonly used in columns to separate the different radioactive elements. The advantage of ion exchanging alpha detectors is that the steps of chemical processing and the analysis of the chemical components are combined, which saves a lot of time.

The principle of this development is the chemical functionalization of the passivated silicon surface of alpha detectors with sulfonic acid groups, which are well studied in their chelation behaviour with radionuclides like, e.g., uranyl cations UO_2^{2+} [77] and have equilibrium constants $K >> 1$ in weakly acidic aqueous solutions which leads to complete adsorption [78]. The procedure to produce these cation exchangers is a two-step reaction. The starting reagent is Mercaptopropyltrimethoxysilane (MPTMS), which is grafted onto the silicon surface and polymerized like in [79] and the thiol-groups are subsequently oxidized with hydrogen peroxide to sulfonic acid groups [80]. The reaction mechanism as well as a schematic illustration of a functionalized silicon detector are depicted in Fig. 1.3. During the polymerization of the thiol-functionalized silanes, multiple layers can be generated causing thicker polymer layers on the surface and different areal adsorption rates by inhomogeneous polymerization [52].

The thereby produced functionalized detectors can be placed in the solution to be investigated and a cation exchange reaction with the dissolved cationic species creates a single layer of the chelated ions on top of the polymer layer. This method to generate radionuclide monolayers is not limited to the alpha detector surfaces and can be processed to manufacture recoil ion sources with a single atomic layer of the radioactive material on many metal oxide surfaces. The best results though are carried out on silicon oxide surfaces. The method was used for recoil ion source production described in section 4.

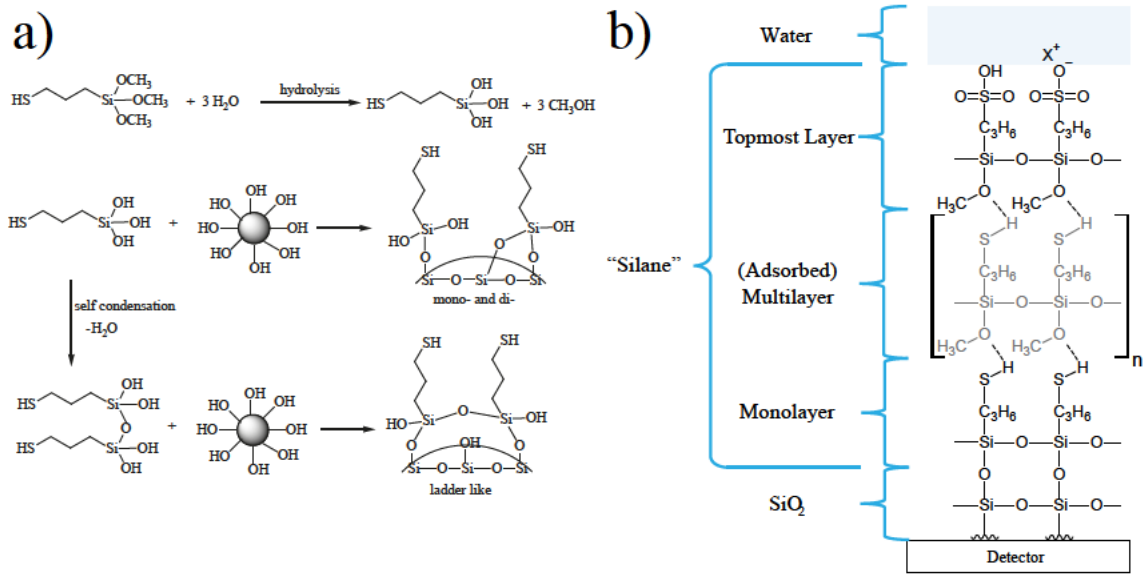

Figure 1.3: Schematic illustration (a) of the mechanism involved in the functionalization of silicon surfaces (shown here as silicon nanoparticles) with MPTMS [81] and (b) of a PIPS detector functionalized with multiple polymer layers in solution [52].

1.1.4 Self-adsorption

The investigation on the adsorption process of actinides on minerals, metal oxides, cement and concrete is a field of high importance in the search for a repository for the disposal of nuclear waste. Actinide speciation at different pH values is well studied in aquatic systems up to americium [82, 83]. These studies are usually performed with colloids of the substrate material and adsorption rates are therefore given in percentage by mass [54]. Studies on limited areas are more difficult to perform since the real chemical surface area of the substrate can only be measured, e.g., by the Brunauer–Emmett–Teller (BET) method [84], which is commonly used in materials science. Furthermore, it is important to know the speciation curves of both the dissolved actinide ion and the surface in solution for different pH values and in presence of anions like chlorides or carbonates. These anions change the coordination sphere of the cation in solution and have direct impact on the coordination sphere of the adsorbed cation [85]. A simple illustration of uranyl cation species and the corresponding TiO_2 species as adsorber at different pH values is depicted in Fig. 1.4.

Actinide mobility is very low in aquatic systems and therefore the chemisorption can be considered irreversible in water after the adjustment of the adsorption equilibrium [86, 87]. This process can be used excellently for preparing reference samples for alpha spectrometry and recoil ion sources with a single atomic layer of the radioactive material. A. Yamaguchi et al. [53] employed self-adsorption of dissolved $ThCl_4$ on fluorite substrates for the production of ^{229}Th targets for

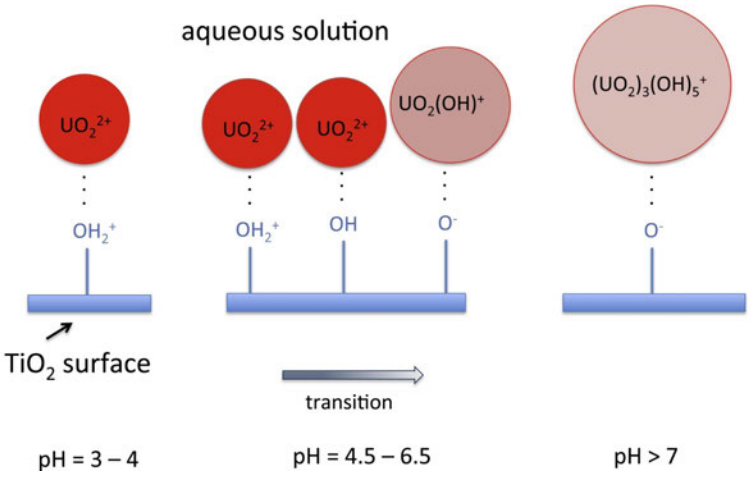

Figure 1.4: Illustration of the solution species of U(VI) adsorbing onto different TiO_2 species in solution at different pH values [54].

undulator irradiations. In this work, the knowledge of uranyl adsorption on TiO_2 in the field of nuclear waste disposal [54] is the foundation for the production of monolayer ^{233}U sources, which is further described in section 4.

1.2 Characterization methods

Several characterization methods are used to investigate targets and other radioactive sources with regards to their chemical composition, homogeneity, surface roughness, thickness and contaminants. Typical radioanalytical methods are gamma spectrometry, alpha spectrometry and radiographic imaging (RI). Other characterization methods, which can also be used on inactive materials, include neutron activation analysis (NAA), scanning electron microscopy (SEM), energy-dispersive X-ray spectroscopy (EDX), atomic force microscopy (AFM) and Raman spectrometry. The latter were used especially for sample characterization in section 3 and 4. This section gives the main theoretical and technical aspects of every method. The information on alpha spectrometry is kept here at a minimum, since this method and its limits for the characterization of recoil ion sources are discussed in great detail in section 4.

1.2.1 Neutron activation analysis and gamma spectrometry

Neutron activation analysis (NAA) is one of the most important methods in the field of radiometric trace analytics [88] and is usually performed in combination with gamma spectrometry [89]. Therefore, both methods are introduced together in this section. A variety of neutron sources exist to perform NAA, differing by the neutron flux and neutron energy. Experiments in this work were performed with the TRIGA (Training, Research, Isotopes, General Atomics) Mark II research

reactor in Mainz, Germany. Neutron energies of up to 10 MeV with different fluxes are generally produced and can be differentiated by thermal (<0.05 eV), epithermal (0.05 eV to 10^5 eV) and fast neutrons (10^5 eV to 10^7 eV). The TRIGA Mark II research reactor in Mainz delivers a thermal neutron flux of up to $4.2 \times 10^{12}\,\mathrm{cm^{-2}\,s^{-1}}$ in continuous mode (100 kW) and up to $1 \times 10^{16}\,\mathrm{cm^{-2}\,s^{-1}}$ in pulsed mode (250 MW peak, 30 ms) [90]. NAA uses the nuclear reaction (n,γ) of inactive material with mostly thermal neutrons to produce radioactive tracers. The isotope ${}^{A}_{Z}X_N$ with neutron number N+1 is produced in this process, which is, in most cases, converted into an element with a higher atomic number Z+1 via the β^- decay

$$ {}^{A}_{Z}X_N \;\rightarrow\; {}^{A}_{Z+1}X^{*}_{N-1} \;+\; e^- \;+\; \bar{\nu}_e \tag{1.1} $$

while maintaining the same mass number A. The β^- decay leads in general to nuclei in excited nuclear states. In the subsequent relaxation process into the nuclear ground state

$$ {}^{A}_{Z+1}X^{*}_{N-1} \;\rightarrow\; {}^{A}_{Z+1}X_{N-1} \;+\; \gamma \tag{1.2} $$

gamma rays with characteristic energies are emitted, which can be detected for the analysis. The produced activity A in the (n,γ) reaction can be calculated as a function of the irradiation duration t at a known neutron flux Φ via

$$ \begin{gathered} A\,(t) = \lambda\; N\,(t) = \sigma\; \Phi\; N_0\; \left[1 \;-\; \exp\left(-\lambda\; t\right)\right] \\ \lambda = \frac{\ln\,(2)}{t_{\frac{1}{2}}} \end{gathered} \tag{1.3} $$

where $N\,(t)$ is the number of produced radionuclei, N_0 is the initial number of irradiated nuclei, σ is the neutron capture cross section and λ is the decay constant, which can be calculated with the half-life $t_{\frac{1}{2}}$ of the produced radionuclei.
The produced activity can be used in absolute and relative activation analysis. For an absolute analysis, the epithermal and fast neutrons have to be moderated to thermal neutrons, since the exact cross section for non-thermal neutrons is often not well known. This leads to a decrease of the neutron flux. For a relative analysis, which is commonly used, the sample to be investigated and a standard sample of known mass with the same geometry and matrix as the unknown sample are irradiated together at the same neutron flux and for the same duration. The mass of the sample m_x can then easily be calculated via

$$ m_x = m_{St}\,\frac{A_x}{A_{St}} \tag{1.4} $$

where m_{St} is the mass of the standard sample and $\dfrac{A_x}{A_{St}}$ is the ratio of the activities. This simple way of instrumental activation analysis can be expanded by chemical

separation of elements before and after the irradiation to reduce the activity of nuclear reactions from other elements.
The detection of the activity can be performed by scintillation counters or semiconductor detectors. Scintillation counters are commonly used for yield determination because of their very high detection efficiency. In contrast to semiconductor detectors, they have a lower energy resolution and are therefore not suitable for nuclide identification. For the latter, high purity germanium (HPGe) detectors are commonly used, as in this work. The HPGe detector has a defect density of $<10^{-10}$ and can have different dopings (n-type or p-type). The coaxial p-type detector is used for the measurement of γ-radiation with energies of 40 keV to 3000 keV. The n-type detector is used for lower γ-energies and X-rays in the range of 3 keV to 3000 keV with thin windows of beryllium or carbon, which are transparent for this radiation. The HPGe detectors only need cooling with liquid nitrogen during the measurements and can be stored at room temperature. This is a great benefit in contrast to older gamma detectors (lithium drifted germanium), which had to be cooled permanently. The detector is kept in a lead shielding for reduction of background radiation during the measurements. It is operated at high voltage and the initial small signal is amplified by a preamplifier and a linear amplifier. The analog signal is then converted into a digital signal by an analog-digital-converter (ADC) and stored in digital form in a multi-channel analyzer (MCA). The resulting spectrum is a plot of the signal intensity (counts) against the channel number. Spectra are usually measured in 8192 channels. Energy calibrations as well as geometry-dependent efficiency calibrations are performed with certified standards, which contain a variety of isotopes of known activity and specific γ-lines in a wide energy range. The resulting channel spectra are fitted with the known energies and isotope quantities in Tailor polynomials to give the energy or efficiency as a function of the channel number.

1.2.2 Alpha spectrometry

Alpha spectrometry is another radioanalytical characterization method with a high importance in environmental science and nuclear safety [91]. Due to their charge and mass, alpha particles have a limited range in materials and in air, in contrast to, e.g., γ-radiation. The range in air at normal pressure can be approximated to about $1\,\mathrm{cm\,MeV^{-1}}$. Measurements are therefore performed under vacuum conditions of at least 1×10^{-3} mbar in small distance to the detector. Passivated implanted planar silicon (PIPS) detectors are commonly used semiconductor detectors for alpha spectrometry. They consist of an active volume (silicon) with a thickness of several hundreds of µm and of a boron implantation (dead layer) with about 50 µm thickness. The entrance window is ion-implanted and consists of a passivation (silicon dioxide) layer of <50 nm thickness. The active volume and the diameter of the entrance window influence the energy resolution of the PIPS detector.

The signal processing is analog to that of gamma spectrometry in section 1.2.1. Alpha spectrometry can be performed for both, quantitative and qualitative high-resolution measurements. The window size, source-detector-distance and number of channels is chosen depending on the kind of measurement. For quantitative yield determinations, 1024 channels, small distances of a few mm and large detector windows are usually chosen to maximize the geometric detection efficiency. For qualitative high-resolution measurements, more channels (2k to 8k) are necessary to determine peak parameters (tailing, FWHM) by suitable fit routines. Furthermore, the distance between source and detector has to be increased and apertures are used to reduce the detection of reflected alpha particles in the vacuum chamber. Energy and efficiency calibrations are usually performed with certified sources of ^{241}Am (432.6 a, 5.486 MeV) and ^{148}Gd (74.6 a, 3.183 MeV).

1.2.3 Radiographic imaging

Radiographic imaging (RI) is a purely qualitative radioanalytical characterization method to determine the areal distribution of radioactive material. The very first radiographic image of an uranium mineral sample was accidentally taken by Antoine Henri Becquerel with a photographic plate in 1896 [92]. The ionizing interaction of radiation with matter is still used for radiographic imaging. Nowadays, photographic plates are exchanged by imaging plates consisting of a thin inorganic fluorite matrix doped with europium [93]. Incoming radiation transfers energy to the electrons in the valence band and creates F-centers. The electrons in these anionic vacancies can be excited into the conduction band by a laser at 630 nm. The subsequent relaxation of the electrons transfers energy into the europium dopings and their relaxation emits fluorescence light, which can be detected by photomultipliers. By scanning the focused laser over the imaging plate, the areal distribution of radioactivity can be determined and digitized for later evaluations. The information is deleted by irradiation with intense light to reuse the plates. The working cycle is depicted in Fig. 1.5. The areal resolution of this method depends on the grain size, readout pixel size and decay energy of the radioactive sample. For β^--emitters, a linear dependency of areal resolution to decay energy was found [51, 94]. The areal resolution limit for, e.g., ^{198}Au (E_β =1.0 MeV, E_γ =412 keV) is $<$200 µm [95].

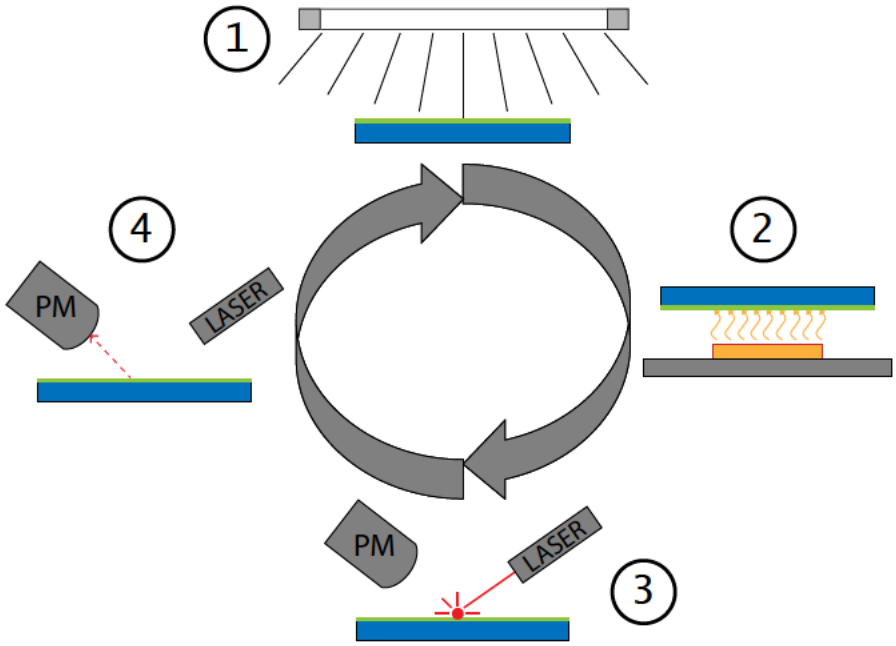

Figure 1.5: Schematic illustration of the working cycle of RI. (1) Deletion of the imaging plate by intense light, (2) irradiation with radioactive sample, (3) irradiation with laser light, (4) detection of fluorescence light with a photomultiplier (PM). See text for further details.

1.2.4 Scanning electron microscopy

Scanning electron microscopy (SEM) is used for topographic investigations of small samples on a nanometer to micrometer scale [96]. The device usually includes an X-ray detector for energy-dispersive X-ray spectroscopy (EDX) and thus both methods are summarized in this section. The microscopy with electrons is feasible as with light due to the electrons' wave characteristic, which can be described by the de-Broglie hypothesis for matter waves

$$\lambda = \frac{h}{p} \tag{1.5}$$

where λ denotes the electron wavelength, h is the Planck constant and p is the electron momentum. Since fast electrons of several keV have a much shorter wavelength than visible light, electron microscopes can reach much higher resolutions than light microscopes, since the resolution limit d (which is defined as the minimum visible distance between two objects) is linked to the numeric aperture NA and wavelength λ by Abbe's law:

$$d = \frac{\lambda}{2\mathrm{NA}} \tag{1.6}$$

In the electron microscope, electrons are thermoionically emitted from a negative biased wolfram cathode and accelerated towards an anode aperture. An electron

beam is generated with an energy equal to the potential difference between cathode and anode. The electron beam is then focused by several electromagnetic lenses (coils) and is deflected to scan over a specified area. The interaction of the primary electron beam with the sample material produces secondary electrons (SE), backscattered electrons (BSE) and X-rays (see Fig. 1.6). BSE and SE can be detected by Everhart-Thornley detectors, which are scintillation counters in a Faraday cage. BSE are high-energy beam electrons, which are reflected in the sample due to inelastic scattering with the atoms. Their energy loss, indicated by a color contrast in the BSE picture of the sample, gives information about the atomic masses in the sample. Therefore, heavier elements appear brighter in the BSE picture then lighter elements. SE are low-energy electrons (<50 eV) originating from inelastic scattering interactions of beam electrons with electrons in the outer shells of the elements in the sample. Since the SE detector has a tilted view, these electrons give information about the topography of the sample. Electrons coming from a surface facing the detector window appear brighter than electrons from the opposite surface or from cracks in the sample surface due to different intensities when they reach the detector. The induced characteristic X-rays emitted from the surface can be detected by a HPGe detector or a silicon drift detector and are used for spectroscopic investigations of the elements in the sample. Since the range of electrons into the material is increasing at higher energies (see section 3 for further details), non-visible regions of the sample can also be investigated by EDX.

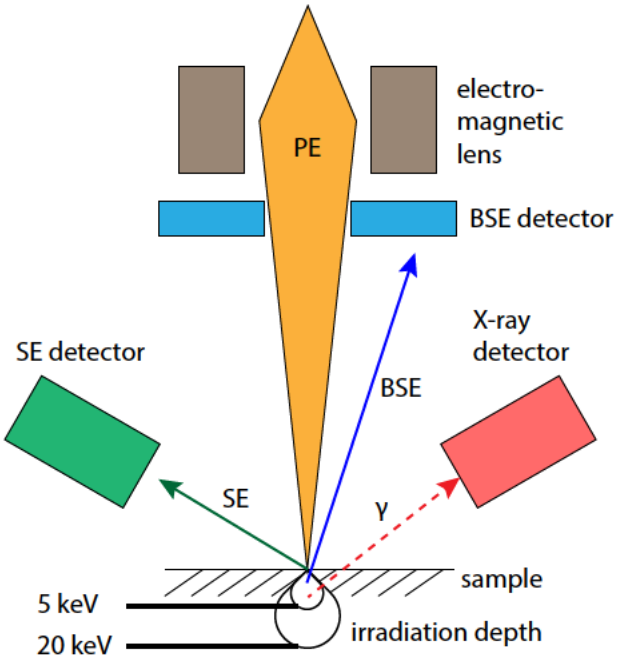

Figure 1.6: Schematic illustration of the principle of SEM. The primary electron (PE) beam is scanning over a sample and induces thereby the generation of backscattered electrons (BSE), secondary electrons (SE) and X-rays (γ), which can be detected by different detectors. The irradiation depth during the sample investigation is depending on the PE energy. See text for details.

1.2.5 Atomic force microscopy

Atomic force microscopy (AFM) is used for both topological and topographical investigations of surfaces in small areas, e.g., to determine surface roughnesses [97]. In the AFM, the main component for investigations is a small, piezo-driven tip (cantilever), which is scanning over a surface in different modes. The typical configuration of an AFM is depicted in Fig. 1.7. The main operation modes are the contact mode, where the tip is scanning in contact with the surface, and the non-contact mode, where the cantilever is oscillating at its eigenfrequency while scanning over the surface at a small distance. In the first mode, the distortion of the cantilever is recorded by a laser reflected on the backside of the cantilever and a position sensitive photodetector. A problem with this mode is that very rough surfaces may destroy the cantilever. In the non-contact mode, the change of amplitude and phase of the oscillation frequency is recorded. These are influenced by several forces acting between the tip of the cantilever and the surface, including Van-der-Waals force, Coulomb interactions, capillary forces, chemical bondings and Pauli repulsion. A complete scan of a surface gives therefore very precise informations on the topography and topology of a sample. Furthermore, by applying a small voltage between the cantilever and the sample, mainly the Coulomb forces are recorded and thus the work function of the surface can be measured. By this method, specific materials with known work functions can be identified. AFM was used in section 4 for the investigation of the surface roughness of thermally treated titanium foils.

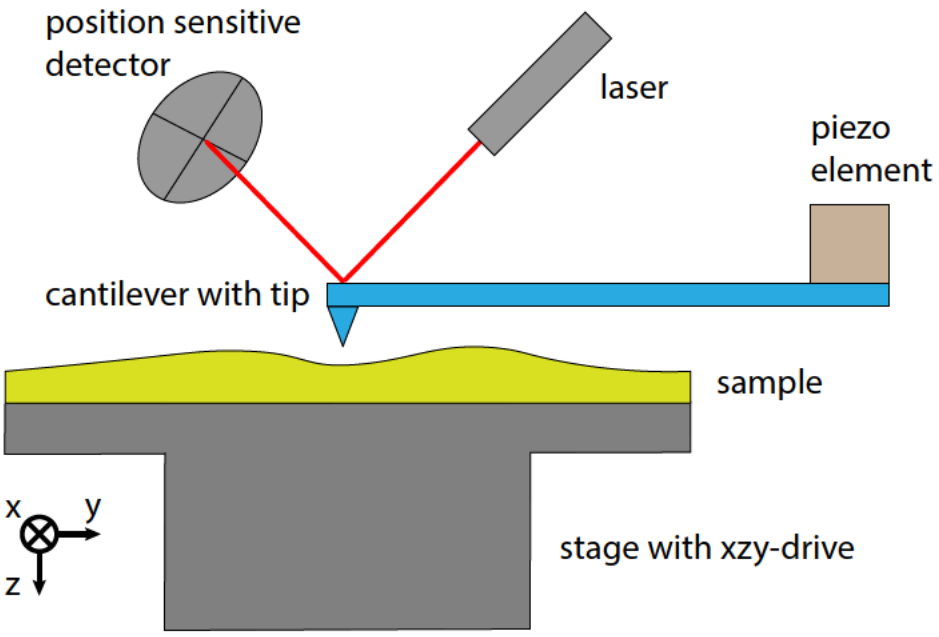

Figure 1.7: Schematic configuration of AFM. See text for details.

1.2.6 Raman spectrometry

Raman spectrometry is commonly used in chemistry for the identification of molecules and their bondings by investigation of their vibrational, rotational and low-frequency modes [98]. Monochromatic laser light is used to excite the modes. The inelastic scattered light from the sample molecules contains besides the excitation frequency (Rayleigh scattering) also further frequencies. The difference between these frequencies and the excitation frequency is called "Raman shift"

$$\Delta\tilde{\nu} = \left(\frac{1}{\lambda_{Excitation}} - \frac{1}{\lambda_{Spectrum}}\right) \tag{1.7}$$

and is usually reported in wavenumbers (cm^{-1}). The molecule is excited into a virtual energy state with a short lifetime and a photon is subsequently emitted. After this scattering process, the molecule is in a different rotational or vibrational state. Thus the Raman shifts correspond to the energy difference of initial and final state. If the final state is higher in energy than the initial state, the scattered photon is shifted to a lower frequency (Stokes shift). In the opposite case the scattered photon is shifted to a higher frequency (Anti-Stokes shift). The magnitude of the Raman effect, indicated by the line intensity, correlates with the polarizability of the electrons in the molecule. The Raman-scattered light is analyzed with an optical spectrometer or an interferometer by Fourier Transform (FT) methods. Charge-coupled device (CCD) or indium gallium arsenide (InGaAs) detectors are used for spectrum acquisition. Besides the chemical application, it can also be used in solid-state investigations to characterize materials by their composition, crystallographic orientation, mechanical stress due to temperature or pressure and crystallinity. Raman spectrometry was used in section 3 for the identification of different lead compounds of molecular plated targets before and after irradiation with electron beams.

1.3 Applications of thin layers in nuclear physics and nuclear chemistry

Samples of thin lanthanide or actinide layers are used as targets and recoil ion sources in different applications of nuclear physics and nuclear chemistry. Some of them are accelerator experiments for nuclear reaction studies or the synthesis of SHE, investigations of astrophysical processes and sources for the production of ion beams of specific isotopes. The latter can be divided in laser ablation sources and recoil ion sources. The main nuclear applications of this work are described in the following sections.

1.3.1 Targets of stable elements for investigations on the astrophysical s-process

In principle, all the stable trans-iron nuclides can be classified in three classes. These are s-nuclei at the bottom of the valley of stability, p-nuclei at the neutron-

deficient side and r-nuclei at the neutron-rich side. They are produced by three different astrophysical mechanisms, which are called s-, r- and p-process. The processes differ in their way of nuclide production. The p-nuclei are produced by "photo-erosion" of neutrons, α particles and protons involving heavy nuclei ($Z \geq 75$) previously formed in the s- and r-process, while the s- and r-process rely on neutron captures [99]. The main focus in this chapter will be on the s- and r-process.

Both, the s- and r-process, take place through (n, γ) reactions, by neutron capture and subsequent β-decay. A generic nucleus (Z, A) is thereby transformed into the heavier isotope (Z, A+1). If the isotope (Z, A+1) is stable against β-decay, an additional neutron capture takes place and leads to the isotope (Z, A+2). Otherwise, if the isotope is unstable, it decays into the isobar (Z+1, A+1) or captures an additional neutron. This process depends on the β-decay lifetime τ_β and the time between two successive neutron captures $\tau_{n\gamma}$. If the β-decays are faster than neutron captures ($\tau_\beta \gg \tau_{n\gamma}$), the phenomena is called s-process (s for "slow" neutron capture). Otherwise, if the neutron capture proceeds on a "rapid" time scale ($\tau_\beta \ll \tau_{n\gamma}$), it is called r-process [99, 100].

The main seed nucleus for both processes is ^{56}Fe. The s-process nucleosynthesis proceeds from $A \simeq 60$ up to ^{209}Bi closely to the valley of stability, as depicted in Fig. 1.8 a). Since the neutron capture is slow compared to the the β-decays, the neutron capture chain goes through the stable isotopes of an element until an unstable isotope is reached and the isobar is formed by β-decay. Then the neutron captures chain continues in the element with the next higher nuclear charge. The s-process ends at Z = 83, since α-decaying nuclides are formed by neutron capture, which reduce the obtained the nuclear charge again. The r-process moves along the far neutron-rich side of the valley of nuclear stability at the neutron drip line, where the neutron binding energy value approaches zero (see Fig. 1.8 a)). Therefore, a series of (n, γ) reactions is performed until an equilibrium is reached with the inverse (γ, n) reaction and β-decay occurs. A recurring sequence of neutron captures and subsequent β-decay starts, since a magic neutron number is reached. The r-process follows then a path along this magic neutron number back to the valley of nuclear stability until the neutron binding energy becomes sufficiently large enough to break through the cycle. Another neutron capture chain reaction follows then until the next magic neutron number is reached and the process of alternating neutron capture and subsequent β-decay repeats. After the synthesizing process, when the neutron irradiation aborts, the very neutron-rich unstable nuclides go through chains of β-decays and result in the most neutron-rich stable isobar for each value of A. By this process, very heavy elements even beyond Z = 83 can be formed.

As already mentioned for the s-process, the relation of $\tau_\beta \gg \tau_{n\gamma}$ is assumed for all unstable nuclides involved in the nucleosynthesis process. However, the s-process encounters also unstable nuclides, where $\tau_\beta \simeq \tau_{n\gamma}$ is given due to a very

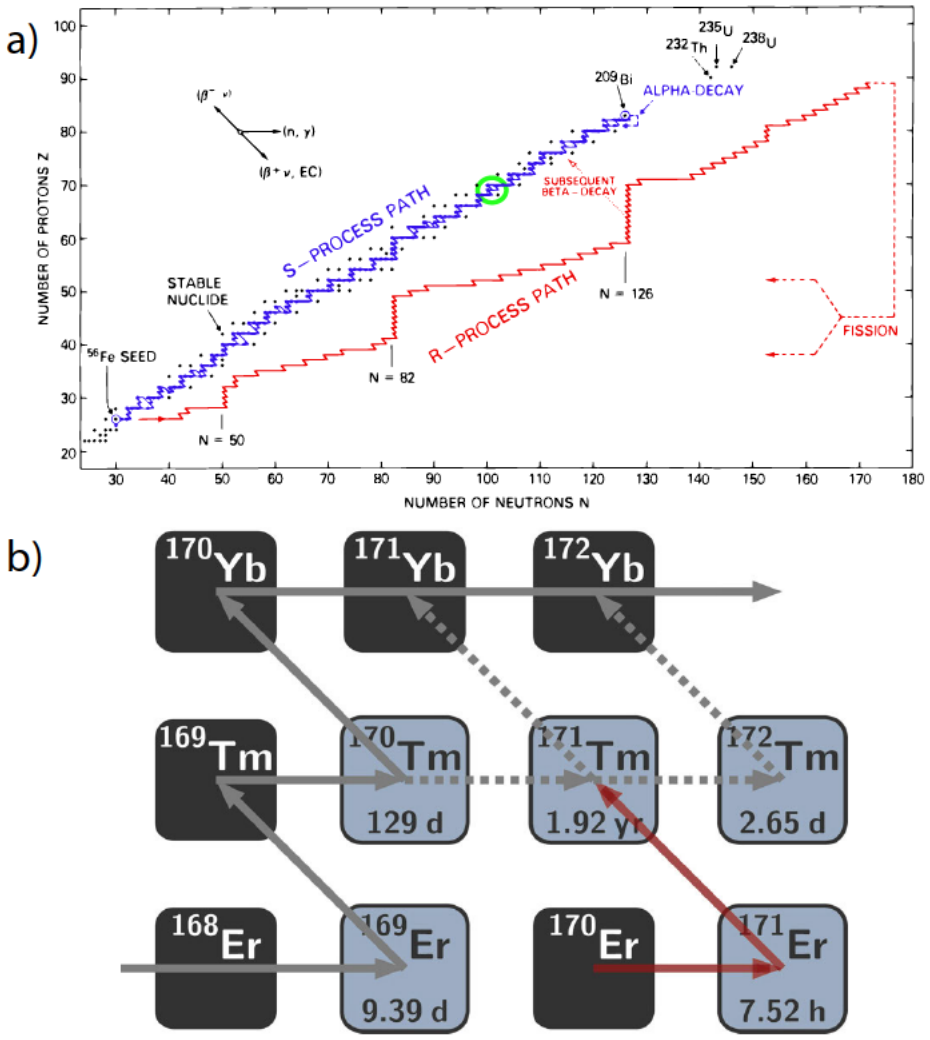

Figure 1.8: (a) Simple illustration of the s- and r-process paths in the chart of nuclides [101]. (b) Region, encircled in a), of the s-process path between Er and Yb, indicated by gray arrows [70]. ^{170}Tm and ^{171}Tm act as branching points in the s-process pathway, indicated by dashed arrows.

long half-life of the unstable nuclide. This leads to a splitting of the s-process pathway, which is called s-process branching, since one part of nuclides undergo β-decay and the other part captures an additional neutron. For example, lanthanide branchings occur at mass numbers A = 141, 151, 154, 163, 169, and 176 and are defined by the s-isotopes ^{142}Nd, ^{152}Gd, ^{154}Gd, ^{164}Er, ^{170}Tm and ^{176}Lu [100]. An excerpt of the branching point at mass number A = 170 from the chart of nuclides is given in Fig. 1.8 b). At a specific branching point the branching ratio R is defined as

$$R = \frac{1}{\tau_\beta \, N_n \, \langle \sigma v \rangle_A} \tag{1.8}$$

with the β-decay lifetime τ_β, the s-process neutron density N_n and the reaction

rate $\langle \sigma v \rangle_A$ of the capture reaction involving the isotope with mass number A. Under the assumption that the temperature is constant during neutron irradiation, the reaction rate $\langle \sigma v \rangle_A$ can be replaced with $\sigma_A v_T$, where σ_A is the Maxwellian-averaged neutron-capture cross section for the isotope with mass number A and v_T is the thermal velocity. The thermal velocity is given by

$$v_T \simeq \left(\frac{2\, k\, T}{M_n} \right) \tag{1.9}$$

where k and T are the Boltzmann constant and temperature and M_n is the neutron mass [101]. The comparison of abundances of nuclei reached at a specific branching point can give information about the physical conditions of the environment where the s-process takes place. If the β-decay lifetime τ_β is temperature-independent and $\langle \sigma v \rangle_A$ is known, the observed ratio R can provide information about the s-process neutron density N_n in a star. Otherwise, if the neutron density N_n is known, the ratio R can serve as a sensitive s-process "thermometer" or "barometer", when the dependence on the physical environment is critical for a branching point reaction [99, 101]. Therefore, the production of targets consisting of isotopically enriched material, e.g. ^{171}Tm, is needed for investigations of the neutron-capture cross section of these isotopes and thus is essential for further development of theoretical models of the astrophysical s-process.

1.3.2 Targets for the synthesis of the superheavy elements

In order to avoid misunderstandings around the terms "superheavy elements" (SHE) and "superheavy nuclei" (SHN), both, the International Union of Pure and Applied Chemistry (IUPAC) and the International Union of Pure and Applied Physics (IUPAP) defined the association of these terms more precisely [102]. Both terms are used for transactinides, in particular SHE is used when the properties of elements are discussed and SHN is used when the properties of nuclei are in focus. SHE can be produced only in accelerator facilities by nuclear fusion reactions. Elements up to nihonium, $Z = 113$, can be produced by cold fusion reactions with continuously decreasing cross sections down to 22 fb [103]. These are based on easily handleable targets of lead or bismuth and projectile beams of neutron rich isotopes of elements from calcium up to zinc. For the latter, isotopes with doubly magic nucleon numbers like, e.g., ^{48}Ca are preferred but the enrichment of the bulk material in large quantities is complex and expensive. Accelerators are therefore improved to deliver higher beam currents at lower material consumption and rotating target wheels were developed to withstand the high beam currents for longer time periods. Target material improvements during the fabrication are still a part of current research. The deposits produced by classic target fabrication methods are known to be quite sensitive to moisture, due to organic impurities and hygroscopic compounds, and deteriorate during long storage time periods. To

prevent these aging processes, targets are usually freshly produced short time before the actual use in accelerator experiments and are converted into a long-term stable compound by irradiation with heavy-ion beams. This kind of on-line conditioning is known as "baking-in" procedure. The process induces visual changes as well as a narrowing of the alpha lines in the spectrum (referring to [22]), which indicates a loss of material without a loss of activity. The changes of a ^{248}Cm target induced by irradiation with a 5.6 MeV u^{-1} ^{48}Ca beam are depicted in Fig. 1.9. These material transformations cannot be obtained thermally in, e.g., a muffle furnace under oxidizing or reducing atmosphere [104, 105] and are under current investigation, which is further discussed in section 3.

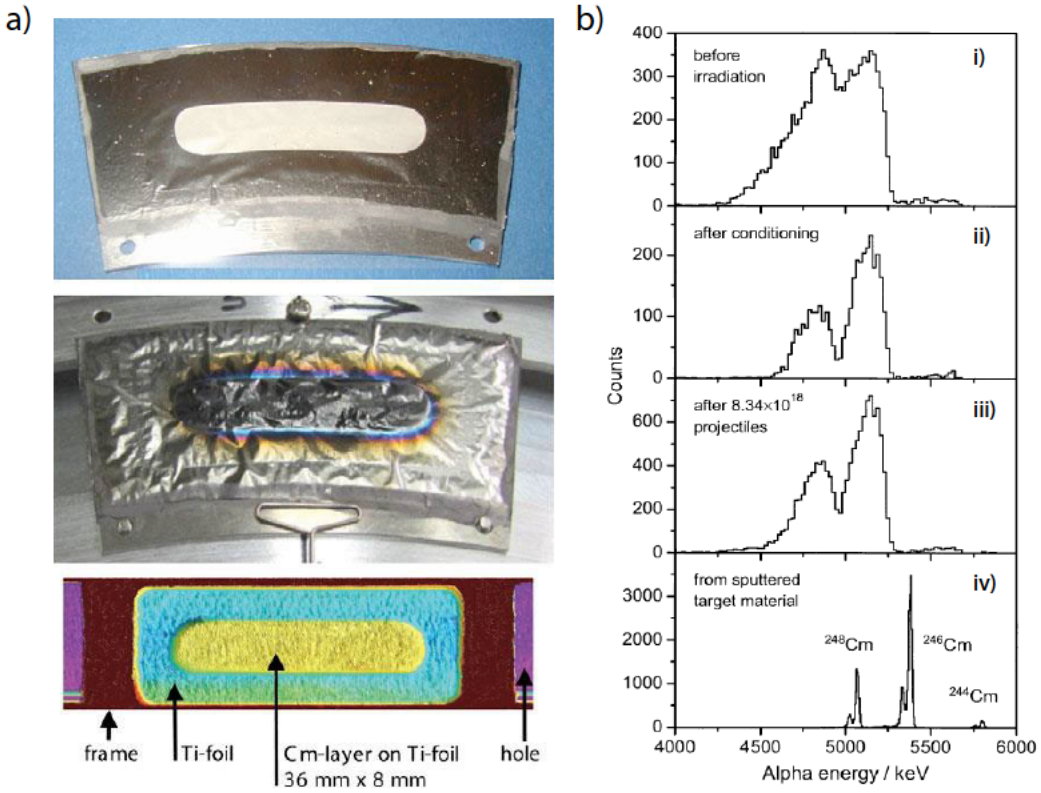

Figure 1.9: (a) Visual changes after irradiation of a ^{248}Cm target with 8.34×10^{18} ^{48}Ca beam particles. (b) Changes in the alpha spectra of ^{248}Cm after conditioning and after irradiation with 8.34×10^{18} projectiles. Alpha spectrum before irradiation and another alpha spectrum of sputtered material from the target are for reference. Figures are adapted from [22].

Also recoil ion separators and detection techniques are improved for higher detection efficiencies of short-lived reaction products. These improvements are necessary for more intensive studies of the SHE flerovium to oganesson, $Z = 114 - 118$, which are produced in hot fusion reactions. These are based on targets of highly radioactive, long-lived actinides up to californium, which are more complex to fabricate and are handled by special safety precautions. The success of a fusion process is determined by various factors, like the fusion barrier, the asymmetry of the reaction partners, the angular momentum, the reaction Q value and the ratio of ejectiles like neutron evaporation and γ-emission versus fission of the compound nucleus [19]. The fusion barrier defines the energy that is needed for the fusion process and is composed of the repulsive Coulomb barrier and the attractive nuclear potential. The fusion probability is depending on the ratio of surface tension versus Coulomb repulsion, which is influenced by the asymmetry of the reaction partners. The reaction Q value defines the excitation energy of the compound nucleus at a specific beam energy. A strongly excited compound nucleus has a higher chance for fission. The ratio of neutron evaporation and γ-emission versus the fission of the compound nucleus also determines its survival chance. The stability or fission probability of the SHE can be explained by the theoretical macroscopic-microscopic model invented by Strutinsky [106], which is based on the combination of the liquid drop model and nuclear shell effects. It shows that the fission barrier based on the liquid drop model vanishes with increasing Z and deformation for SHN but the nuclei are still stabilized by shell effects. Based on calculations with this model, the existence of an "island of stability" was revealed far beyond currently known nuclei [107] and this gives the motivation for further research on the SHE.

1.3.3 Recoil ion sources for ^{229m}Th production at NuClock and TACTICa

Relevance of ^{229m}Th in science

Most of the currently known nuclear isomeric states have energies far above 1 keV. There are only two nuclear isomeric states known at the moment with lower energies. These are the ^{235m}U with an energy of 76 eV and a half-life of 26 min and the ^{229m}Th with the lowest lying energy of (8.28 ± 0.17) eV [27] and a half-life of more than 60 s in the charge state 3+ [24]. Due to this low isomeric state, the ^{229m}Th is in the range for optical excitation with laser light (160 nm) and makes it a perfect candidate for the development of a nuclear clock, similar to existing optical ion clocks based on atomic shell transitions (see Fig. 1.10 a)).

The great advantage of a nuclear clock would the achievable relative inaccuracy. Various neutral and ionic atomic species already exist in metrology as shown in Fig. 1.10 a) and are utilized for frequency standards with inaccuracies down to 3.2×10^{-18} for $^{171}Yb^{+}$ [109]. These conventional clocks are sensitive to environmental perturbances and the most significant shifts arise due to magnetic fields, electric fields, and electric field gradients. Campbell et al. [108] have shown that the pair of

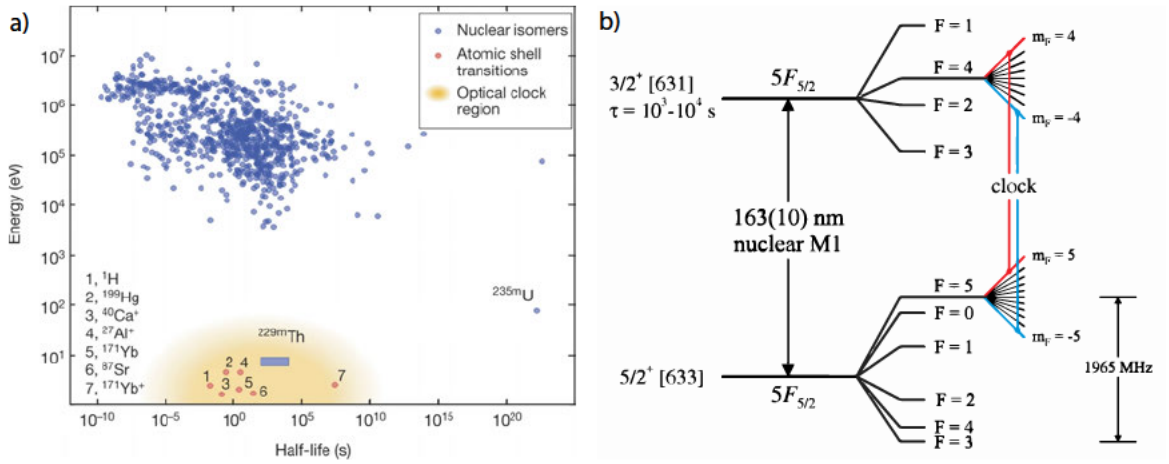

Figure 1.10: (a) Energy - half-life distribution of known nuclear isomers and atomic shell transitions for optical ion clocks and (b) estimated partial energy-level diagram for a ^{229m}Th single-ion nuclear clock. Figures adapted from [24] and [108].

stretched hyperfine states within the $5F_{5/2}$ electronic ground level of both nuclear ground and isomeric manifolds in $^{229m}Th^{3+}$, as depicted in Fig. 1.10 b), suppress all of the external field clock shifts and a total estimated inaccuracy of 1.5×10^{-19} could be achieved [108]. The nuclear clock could be established in two ways. One is based on $^{229m}Th^{3+}$ stored in a Paul trap [108] and the other one is based on ^{229m}Th embedded in a crystal lattice environment [28, 110, 111]. However, for a sufficient development of a nuclear clock, the exact energy of the isomeric state has to be measured very precisely. A promising concept of laser-based conversion electron Mössbauer spectroscopy could lead to a precise energy determination with 40 µeV resolution [112]. For this approach, a homogeneous $^{229}ThO_2$ target with 10 nm thickness will be needed, considering the VUV laser light penetration depth and the mean free path length of the internal conversion (IC) electrons. A promising way to produce these targets could be by self-adsorption (see section 4), which is currently under investigation.

As the ^{229m}Th is populated by IC in the alpha decay from ^{233}U and Auger electrons are released in this process, it can be assumed that a ^{233}U source will deliver ^{229m}Th recoil ions in high charge states. Gunter et al. [113] have found charge states up to 20+ in ^{222}Ra recoil ions from a ^{226}Th source and, therefore, it is likely to find also these high charge states in ^{229m}Th recoil ions [114]. Highly charged ions (HCI) of ^{229m}Th are useful for quantum logic spectroscopy (QLS) and testing fundamental physics like the variation of fundamental constants, quantum electrodynamic (QED) tests, isotope shift spectroscopy and validation of the non-linearity of King plots [23, 34, 35, 115]. They are also very useful for optical ion clocks, since many perturbing shifts like Stark shift, Zeeman shift, and electric quadrupole shift are suppressed [116].

An interesting application of HCI is the investigation of very weak forces, which are in the range of µeV up to eV. These forces have a strong charge state dependence, which is given in Table 1.1 [117]. This enables also the investigation of optical

Table 1.1: Charge state dependence of weak physical forces in HCI.

Physical force	Charge state dependence
Binding energy	Z^2
Hyperfine splitting	Z^3
QED effects	Z^4
Stark shifts	Z^{-6}

transitions in the fine structure and hyperfine structure of the HCI. Additionally, it enables the investigation of level crossing transitions. These level crossings emerge with rising charge state Z, when the energy levels of two electron orbitals cross each other in the change from a Madelung ordering, which is found in neutral atoms, to a Coulomb ordering, as in a hydrogen-like ion (see Fig. 1.11) [117–120].

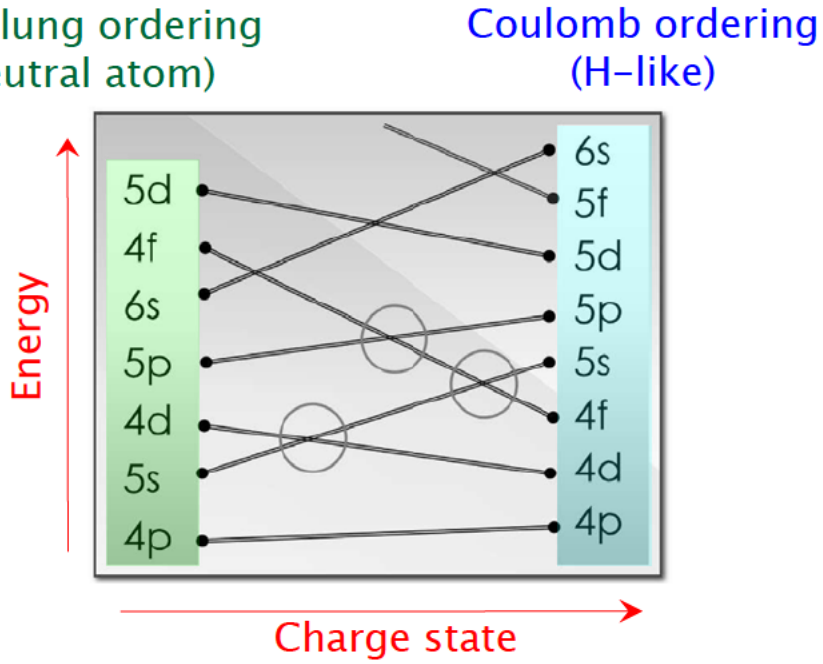

Figure 1.11: Scheme of level crossings depending on the charge state in HCI. Optical transitions can be observed in the encircled areas. Figure adapted from [117].

Furthermore, HCI are needed for performing QLS. Simple laser spectroscopy has typically no possibility for fast cycling transitions in HCI for state preparation, cooling and detection and is thus limited in accuracy to about 10^{-7} [121] in contrast to the high accuracy of singly charged atomic ions in, e.g., ion clocks with about 10^{-18} [109]. Therefore, QLS is needed for this high accuracy. In QLS, the ions,

HCI (spectroscopy ion) and logic ion, are captured in a linear Paul trap. The logic ions provide sympathetic cooling and the signal readout [122, 123]. In the TACTICa experiment, e.g., the logic ion will be $^{40}Ca^{+}$ [114]. In the Paul trap, both ions are coupled in their motional modes by a strong Coulomb interaction. Laser spectroscopy can then be performed on the spectroscopy ion and through a series of laser pulses, the internal state will be transferred from the spectroscopy ion onto the logic ion, where it can be detected. This quantum logic state transfer allows the investigation of a previously inaccessible species with a high accuracy [122, 123]. Furthermore, it allows to extract nuclear parameters from the observed atomic spectra and thus allows the investigation of isotope-shifts. In experiments, the isotope shifts can provide information about the nucleus in a King-plot analysis [124, 125]. King plots are a widely used method for systematic studies of isotope shifts of two atomic transitions in a chain of isotopes. For the construction of a King plot, two electronic transitions i and j of a chain of at least four isotopes of the same element are needed [115]. The transition i and j may also belong to different charge states of the same element. The isotope shift $\delta\nu_i^{A,A'}$ of the isotopes A and A' can be noted as

$$\delta\nu_i^{A,A'} = F_i\delta\left\langle r^2\right\rangle_{A,A'} + K_i\mu_{A,A'} \tag{1.10}$$

where the two terms represent the field shift and the mass shift, respectively. The $\delta\left\langle r^2\right\rangle_{A,A'}$ term is dominated by the difference in the charge radii of both nuclei and $\mu_{A,A'}$ is the reduced mass of the isotopes A and A'. Both terms are nuclear quantities and do not depend on the electronic transitions i and j, but F_i and K_i are isotope-independent, transition-dependent parameters. For two electronic transition i and j, the change in the nuclear charge radius $\delta\left\langle r^2\right\rangle_{A,A'}$ can be eliminated and a linear relation can be obtained [126]. Isotope-shift measurements can be used to determine the coupling strength of hypothetical new-physics (NP) boson fields to electrons and neutrons. The existence of a light boson particle with mass m_ϕ would cause a non-linearity in the King plot for the isotope shift of two atomic transitions of many isotopes of the same element and by this non-linearity the coupling constant α_{NP} could be investigated and new forces could be constrained [35, 115, 126]. This would add an additional term to the previous equation, which could then be noted as

$$\delta\nu_i^{A,A'} = F_i\delta\left\langle r^2\right\rangle_{A,A'} + K_i\mu_{A,A'} + \alpha_{NP}X_i\left(A - A'\right) \tag{1.11}$$

where X_i is the new-physics isotope shift constant. Furthermore, it allows the investigation of the variation of the fine-structure constant α, in which changes might be induced by interaction with dark matter [126].

Deceleration of ^{229m}Th recoil ions in a buffer gas cell

As previously explained, ^{229m}Th is a highly interesting nuclide in current nuclear physics research. The ^{229m}Th isomer is most easily populated by IC in the alpha decay from ^{233}U. However, the kinetic energy of this recoil ion is 84 keV (E_a = 4.824 MeV) due to the conservation of momentum in the alpha decay, which makes it not directly usable for physical measurements. Therefore, the ^{229m}Th ion must be decelerated. The nuClock collaboration uses the approach of buffer gas cooling [24, 127]. A recoil ion source, consisting of a purified thin ^{233}U deposit produced by molecular plating on a silicon wafer, is placed directly in the buffer gas cell with a low positive bias voltage. The buffer gas cell consists of a vacuum chamber filled with high purity helium gas at about 40 mbar, a DC cage, a radio frequency (RF) funnel with 180 ° phase difference between two adjacent electrodes and a supersonic Laval nozzle. The DC cage and funnel consist of electrodes with a DC gradient towards the nozzle. Inside the buffer gas cell, the emitted recoil ions are at first accelerated away from the source by the positive voltage offset, leading to a kinetic energy of about 84.3 keV. By this, less recoil ions of the 2π distribution are lost due to interaction with the source. The recoil ions subsequently interact in inelastic collisions with the buffer gas and are thereby cooled down. The DC gradient leads the scattered recoil ions in the cell towards the nozzle. In the RF funnel, the phase variation causes a repelling force on the ions, which prevents them from charge exchange at the electrodes. The recoil ions are then extracted in charge states up to 3+ together with helium as carrier gas and enter a radio frequency quadrupole (RFQ) ion guide and buncher system. In there the ions can be further extracted by a DC gradient and are shape-phase cooled by interaction with the residual buffer gas at a pressure of 10^{-2} mbar. The ions can also be stored and sent out in small bunches. At the RFQ exit a sub-millimeter recoil-ion beam is extracted. The beam is sent into a quadrupole mass separator, where other nuclides like contaminants from daughter nuclides from the source can be separated from the recoil-ion beam. By the buffer gas cooling method, the $^{229(m)}$Th recoil ions are not just decelerated, but efficiently shape-phase cooled and, therefore, a smooth recoil ion beam can be produced. Furthermore, the extraction efficiency is quite high. However, only ions in charge states up to 3+ are extracted and higher charge states are lost due to the collisions with the buffer gas. Therefore, the method is not suitable to deliver decelerated $^{229(m)}$Th recoil ions for high precision spectroscopy experiments, where also ions in higher charge states are needed.

1.4 References

[1] International Union of Pure and Applied Chemistry, The United Nations proclaims the International Year of the Periodic Table of Chemical Elements, https://iupac.org/wp-content/uploads/2017/12/Press-Release-International-Year-of-the-Periodic-Table_UN-Proclamation_21-December-2017.pdf, [Press release online; accessed 23-March-2020] (2017).

[2] G. Audi, F. G. Kondev, M. Wang, W. J. Huang, S. Naimi, The NUBASE2016 evaluation of nuclear properties, Chinese Physics C 41 (2017) 030001.

[3] T. K. Sato, M. Asai, A. Borschevsky, T. Stora, N. Sato, Y. Kaneya, K. Tsukada, Ch. E. Düllmann, K. Eberhardt, E. Eliav, S. Ichikawa, U. Kaldor, J. V. Kratz, S. Miyashita, Y. Nagame, K. Ooe, A. Osa, D. Renisch, J. Runke, N. Trautmann, Measurement of the first ionization potential of lawrencium, element 103, Nature 520 (2015) 209–11.

[4] B. Mole, Matter & energy: Debate continues over 103's place in periodic table: New data on lawrencium rekindle an old argument, Science News 187 (2015) 6–7.

[5] V. Tsimmerman, Using Atomic Microstates and Atomic Number Parity in Support of Lutetium and Lawrencium Classification as Transition Metals, J. Chem 12 (2018) 92–95.

[6] A. Yakushev, J. M. Gates, A. Türler, M. Schädel, Ch. E. Düllmann, D. Ackermann, L.-L. Andersson, M. Block, W. Brüchle, J. Dvorak, K. Eberhardt, H. G. Essel, J. Even, U. Forsberg, A. Gorshkov, R. Graeger, K. E. Gregorich, W. Hartmann, R.-D. Herzberg, F. P. Heßberger, D. Hild, A. Hübner, E. Jäger, J. Khuyagbaatar, B. Kindler, J. V. Kratz, J. Krier, N. Kurz, B. Lommel, L. J. Niewisch, H. Nitsche, J. P. Omtvedt, E. Parr, Z. Qin, D. Rudolph, J. Runke, B. Schausten, E. Schimpf, A. Semchenkov, J. Steiner, P. Thörle-Pospiech, J. Uusitalo, M. Wegrzecki, N. Wiehl, Superheavy Element Flerovium (Element 114) Is a Volatile Metal, Inorganic Chemistry 53 (2014) 1624–1629.

[7] A. Yakushev, R. Eichler, Gas-phase chemistry of element 114, flerovium, EPJ Web of Conferences 131 (2016) 07003.

[8] W. H. Bassichis, A. K. Kerman, Self-Consistent Calculations of Shell Effects Including the Proposed Island of Stability, Phys. Rev. C 2 (1970) 1768–1776.

[9] A. Sobiczewski, K. Pomorski, Description of structure and properties of superheavy nuclei, Progress in Particle and Nuclear Physics 58 (2007) 292–349.

[10] Y. Oganessian, Nuclei in the "Island of Stability" of Superheavy Elements, Journal of Physics: Conference Series 337 (2012) 012005.

[11] E. M. Burbidge, G. R. Burbidge, W. A. Fowler, F. Hoyle, Synthesis of the Elements in Stars, Rev. Mod. Phys. 29 (1957) 547–650.

[12] J. W. Truran, I. Iben Jr, On s-process nucleosynthesis in thermally pulsing stars, The Astrophysical Journal 216 (1977) 797–810.

[13] M. Busso, R. Gallino, G. J. Wasserburg, Nucleosynthesis in Asymptotic Giant Branch Stars: Relevance for Galactic Enrichment and Solar System Formation, Annual Review of Astronomy and Astrophysics 37 (1999) 239–309.

[14] A. I. Boothroyd, Heavy Elements in Stars, Science 314 (2006) 1690–1691.

[15] G. T. Seaborg, Elements beyond 100, present status and future prospects, Annual review of nuclear science 18 (1968) 53–152.

[16] B. P. Abbott et al. (LIGO Scientific Collaboration and Virgo Collaboration), Gw170817: Observation of gravitational waves from a binary neutron star inspiral, Phys. Rev. Lett. 119 (2017) 161101.

[17] F.-K. Thielemann, A. Arcones, R. Käppeli, M. Liebendörfer, T. Rauscher, C. Winteler, C. Fröhlich, I. Dillmann, T. Fischer, G. Martinez-Pinedo, K. Langanke, K. Farouqi, K.-L. Kratz, I. Panov, I. Korneev, What are the astrophysical sites for the r-process and the production of heavy elements?, Progress in Particle and Nuclear Physics 66 (2011) 346 – 353.

[18] A. A. Lutovinov, Chemical Elements in Space, Herald of the Russian Academy of Sciences 90 (2020) 239–244.

[19] S. Hofmann, Synthesis and properties of isotopes of the transactinides, Radiochimica Acta 107 (2019) 879–915.

[20] A. Nasirov, A. Muminov, G. Giardina, G. Mandaglio, Basic distinctions between cold-and hot-fusion reactions in the synthesis of superheavy elements, Physics of Atomic Nuclei 77 (2014) 881–889.

[21] G. Münzenberg, H. Devaraja, T. Dickel, H. Geissel, M. Gupta, S. Heinz, S. Hofmann, W. Plass, C. Scheidenberger, J. Winfield, et al., SHE research with rare-isotope beams, challenges and perspectives, and the new generation of SHE factories, in: New Horizons in Fundamental Physics, Springer, 2017, pp. 81–90.

[22] S. Hofmann, S. Heinz, R. Mann, J. Maurer, J. Khuyagbaatar, D. Ackermann, S. Antalic, W. Barth, M. Block, H. Burkhard, V. F. Comas, L. Dahl, K. Eberhardt,

J. Gostic, R. A. Henderson, J. A. Heredia, F. P. Heßberger, J. M. Kenneally, B. Kindler, I. Kojouharov, J. V. Kratz, R. Lang, M. Leino, B. Lommel, K. J. Moody, G. Münzenberg, S. L. Nelson, K. Nishio, A. G. Popeko, J. Runke, S. Saro, D. A. Shaughnessy, M. A. Stoyer, P. Thörle-Pospiech, K. Tinschert, N. Trautmann, J. Uusitalo, P. A. Wilk, A. V. Yeremin, The reaction 48 Ca+ 248 Cm→ 296 116* studied at the GSI-SHIP, The European Physical Journal A 48 (2012) 62.

[23] M. S. Safronova, D. Budker, D. DeMille, D. F. J. Kimball, A. Derevianko, C. W. Clark, Search for new physics with atoms and molecules, Rev. Mod. Phys. 90 (2018) 025008.

[24] L. v. d. Wense, B. Seiferle, M. Laatiaoui, J. B. Neumayr, H.-J. Maier, H.-F. Wirth, C. Mokry, J. Runke, K. Eberhardt, Ch. E. Düllmann, N. G. Trautmann, P. G. Thirolf, Direct detection of the ^{229}Th nuclear clock transition, Nature 533 (2016) 47–51.

[25] B. Seiferle, L. von der Wense, P. G. Thirolf, Lifetime Measurement of the ^{229}Th Nuclear Isomer, Phys. Rev. Lett. 118 (2017) 042501.

[26] J. Thielking, M. Okhapkin, P. Głowacki, D. Meier, L. v. d. Wense, B. Seiferle, Ch. E. Düllmann, P. Thirolf, E. Peik, Laser spectroscopic characterization of the nuclear clock isomer ^{229m}Th, Nature 556 (2018) 321–325.

[27] B. Seiferle, L. v. d. Wense, P. V. Bilous, I. Amersdorffer, C. Lemell, F. Libisch, S. Stellmer, T. Schumm, Ch. E. Düllmann, A. Palffy, P. G. Thirolf, Energy of the ^{229}Th nuclear clock transition, Nature 573 (2019) 243–246.

[28] E. Peik, Chr. Tamm, Nuclear laser spectroscopy of the 3.5 eV transition in Th-229, Europhysics Letters (EPL) 61 (2003) 181–186.

[29] P. Forman, Atomichron: The atomic clock from concept to commercial product, ieee ultrasonics, Ferroelectrics and Frequency Control Society (1998).

[30] A. D. Ludlow, M. M. Boyd, J. Ye, E. Peik, P. O. Schmidt, Optical atomic clocks, Rev. Mod. Phys. 87 (2015) 637–701.

[31] E. Peik, M. Okhapkin, Nuclear clocks based on resonant excitation of gamma-transitions, Comptes Rendus Physique 16 (2015) 516 – 523.

[32] L. von der Wense, B. Seiferle, P. G. Thirolf, Towards a ^{229}Th-based nuclear clock, Measurement Techniques 60 (2018) 1178–1192.

[33] S. Raeder, V. Sonnenschein, T. Gottwald, I. Moore, M. Reponen, S. Rothe, N. Trautmann, K. Wendt, Resonance ionization spectroscopy of thorium isotopes–towards a laser spectroscopic identification of the low-lying 7.6 eV

isomer of ^{229}Th, Journal of Physics B: Atomic, Molecular and Optical Physics 44 (2011) 165005.

[34] V. V. Flambaum, Enhanced Effect of Temporal Variation of the Fine Structure Constant and the Strong Interaction in ^{229}Th, Phys. Rev. Lett. 97 (2006) 092502.

[35] V. V. Flambaum, A. J. Geddes, A. V. Viatkina, Isotope shift, nonlinearity of King plots, and the search for new particles, Phys. Rev. A 97 (2018) 032510.

[36] K. Groot-Berning, F. Stopp, G. Jacob, D. Budker, R. Haas, D. Renisch, J. Runke, P. Thörle-Pospiech, Ch. E. Düllmann, F. Schmidt-Kaler, Trapping and sympathetic cooling of single thorium ions for spectroscopy, Phys. Rev. A 99 (023420) (2019).

[37] F. Stopp, K. Groot-Berning, G. Jacob, D. Budker, R. Haas, D. Renisch, J. Runke, P. Thörle-Pospiech, Ch. E. Düllmann, F. Schmidt-Kaler, Catching, trapping and in-situ-identification of thorium ions inside Coulomb crystals of $^{40}Ca^{+}$ ions, Hyperfine Interact. 240 (33) (2019).

[38] V. Barci, G. Ardisson, G. Barci-Funel, B. Weiss, O. El Samad, R. K. Sheline, Nuclear structure of ^{229}Th from γ-ray spectroscopy study of ^{233}U α-particle decay, Phys. Rev. C 68 (2003) 034329.

[39] Y. Shigekawa, Y. Kasamatsu, E. Watanabe, H. Ninomiya, S. Hayami, N. Kondo, Y. Yasuda, H. Haba, A. Shinohara, Observation of internal-conversion electrons emitted from ^{229m}Th produced by β decay of ^{229}Ac, Phys. Rev. C 100 (2019) 044304.

[40] T. Masuda, A. Yoshimi, F. Akira, H. Fujimoto, H. Haba, H. Hara, T. Hiraki, H. Kaino, Y. Kasamatsu, S. Kitao, K. Konashi, Y. Miyamoto, K. Okai, S. Okubo, N. Sasao, M. Seto, T. Schumm, Y. Shigekawa, K. Suzuki, K. Yoshimura, X-ray pumping of the Th nuclear clock isomer, Nature 573 (2019) 238–242.

[41] W. Parker, R. Falk, Molecular plating: A method for the electrolytic formation of thin inorganic films, Nuclear Instruments and Methods 16 (1962) 355–357.

[42] P. Maier-Komor, Preparation of isotope targets using laser beam evaporation techniques, Nuclear Instruments and Methods 167 (1979) 73 – 76.

[43] A. Mitu, M. Dumitru, R. Suvăilă, A. Oprea, I. Gheorghe, P. Mereută, S. Brajnicov, I. Burducea, N. M. Florea, N. Mărginean, T. Glodariu, M. Dinescu, G. C. –. Danil, Refractory osmium targets for accelerator based nuclear activation experiments prepared by Pulsed Laser Deposition technique, Vacuum 161 (2019) 162–167.

[44] M. A. Garcia, M. N. Ali, N. N. Chang, T. Parsons-Moss, P. D. Ashby, J. M. Gates, L. Stavsetra, K. E. Gregorich, H. Nitsche, Metal oxide targets produced by the polymer-assisted deposition method, Nuclear Instruments and Methods in Physics Research Section A: Accelerators, Spectrometers, Detectors and Associated Equipment 613 (2010) 396–400.

[45] S. Clifford, X. Guo-ji, C. Ingelbrecht, M. J. Pomeroy, Processes for the production of ultra-pure metals from oxide and their cold rolling to ultra-thin foils for use as targets and as reference materials, Nuclear Instruments and Methods in Physics Research Section A: Accelerators, Spectrometers, Detectors and Associated Equipment 480 (2002) 29 – 35.

[46] R. Grossmann, H. J. Maier, H. U. Friebel, D. Frischke, Preparation of radioactive targets for tandem accelerator experiments by high vacuum evaporation–condensation, Nuclear Instruments and Methods in Physics Research Section A: Accelerators, Spectrometers, Detectors and Associated Equipment 480 (2002) 209 – 213.

[47] L. V. Drapchinsky, T. E. Kuzmina, S. M. Soloviev, Practice of using the multiple painting method, Nuclear Instruments and Methods in Physics Research Section A: Accelerators, Spectrometers, Detectors and Associated Equipment 438 (1999) 116 – 118.

[48] S. Chakrabarty, B. S. Tomar, A. Goswami, V. A. Raman, S. B. Manohar, Preparation of thin osmium targets by electrodeposition, Nuclear Instruments and Methods in Physics Research Section B: Beam Interactions with Materials and Atoms 174 (2001) 212 – 214.

[49] K. M. Glover, F. J. G. Rogers, T. A. Tuplin, Techniques used at Harwell in the preparation of stable and active nuclide targets, Nuclear Instruments and Methods 102 (1972) 443 – 450.

[50] Y. Shiokawa, R. Amano, A. Nomura, M. Yagi, Preparation of lanthanide, thorium and uranium oxide films by chemical vapor deposition using beta-diketone chelates, Journal of radioanalytical and nuclear chemistry 152 (1991) 373–380.

[51] R. Haas, S. Lohse, Ch. E. Düllmann, K. Eberhardt, C. Mokry, J. Runke, Development and characterization of a Drop-on-Demand inkjet printing system for nuclear target fabrication, Nuclear Instruments and Methods in Physics Research Section A: Accelerators, Spectrometers, Detectors and Associated Equipment 874 (2017) 43–49.

[52] D. Krupp, U. W. Scherer, Prototype development of ion exchanging alpha detectors, Nuclear Instruments and Methods in Physics Research Section A:

Accelerators, Spectrometers, Detectors and Associated Equipment 897 (2018) 120–128.

[53] A. Yamaguchi, M. Kolbe, H. Kaser, T. Reichel, A. Gottwald, E. Peik, Experimental search for the low-energy nuclear transition in ^{229}Th with undulator radiation, New Journal of Physics 17 (2015) 053053.

[54] A. C. M. Lamb, F. Grieser, T. Healy, The adsorption of uranium (VI) onto colloidal TiO_2, SiO_2 and carbon black, Colloids and Surfaces A: Physicochemical and Engineering Aspects 499 (2016) 156–162.

[55] N. Trautmann, H. Folger, Preparation of actinide targets by electrodeposition, Nuclear Instruments and Methods in Physics Research Section A: Accelerators, Spectrometers, Detectors and Associated Equipment 282 (1989) 102 – 106.

[56] A. Vascon, S. Santi, A. Isse, T. Reich, J. Drebert, H. Christ, Ch. E. Düllmann, K. Eberhardt, Elucidation of constant current density molecular plating, Nuclear Instruments and Methods in Physics Research Section A: Accelerators, Spectrometers, Detectors and Associated Equipment 696 (2012) 180 – 191.

[57] C. Ingelbrecht, A. Moens, R. Eykens, A. Dean, Improved electrodeposited actinide layers, Nuclear Instruments and Methods in Physics Research Section A: Accelerators, Spectrometers, Detectors and Associated Equipment 397 (1997) 34 – 38.

[58] W. Parker, H. Bildstein, N. Getoff, Molecular plating III the rapid preparation of radioactive reference samples, Nuclear Instruments and Methods 26 (1964) 314 – 316.

[59] W. Parker, H. Bildstein, N. Getoff, H. Fischer-Colbrie, H. Regal, Molecular plating II a rapid and quantitative method for the electrodeposition of the rare-earth elements, Nuclear Instruments and Methods 26 (1964) 61 – 65.

[60] W. Parker, H. Bildstein, N. Getoff, Molecular plating I, a rapid and quantitative method for the electrodeposition of thorium and uranium, Nuclear Instruments and Methods 26 (1964) 55 – 60.

[61] N. Getoff, H. Bildstein, Molecular plating, IV a rapid method for the electrodeposition of plutonium, Nuclear Instruments and Methods 36 (1965) 173 – 175.

[62] N. Getoff, H. Bildstein, Molecular plating: VI. Quantitative electrodeposition of americium, Nuclear Instruments and Methods 70 (1969) 352 – 354.

[63] M. V. Ramaniah, R. J. Singh, S. K. Awasthi, S. Prakash, Studies on electrodeposition of actinide elements from non-aqueous medium, The International Journal of Applied Radiation and Isotopes 26 (1975) 648 – 650.

[64] A. Vascon, Ch. E. Düllmann, K. Eberhardt, B. Kindler, B. Lommel, J. Runke, Toward large-area targets for "TRAKULA", Nuclear Instruments and Methods in Physics Research Section A: Accelerators, Spectrometers, Detectors and Associated Equipment 655 (2011) 72 – 79.

[65] A. Vascon, S. Santi, A. Isse, A. Kühnle, T. Reich, J. Drebert, K. Eberhardt, Ch. E. Düllmann, Smooth crack-free targets for nuclear applications produced by molecular plating, Nuclear Instruments and Methods in Physics Research Section A: Accelerators, Spectrometers, Detectors and Associated Equipment 714 (2013) 163 – 175.

[66] A. Vascon, N. Wiehl, T. Reich, J. Drebert, K. Eberhardt, Ch. E. Düllmann, The performance of thin layers produced by molecular plating as alpha-particle sources, Nuclear Instruments and Methods in Physics Research Section A: Accelerators, Spectrometers, Detectors and Associated Equipment 721 (2013) 35 – 44.

[67] A. Vascon, S. Santi, A. Isse, T. Reich, J. Drebert, H. Christ, K. Eberhardt, Ch. E. Düllmann, Fundamental aspects of molecular plating and production of smooth crack-free Nd targets, Journal of Radioanalytical and Nuclear Chemistry 299 (2014) 1085–1091.

[68] A. Vascon, J. Runke, N. Trautmann, B. Cremer, K. Eberhardt, Ch. E. Düllmann, Quantitative molecular plating of large-area ^{242}Pu targets with improved layer properties, Applied Radiation and Isotopes 95 (2015) 36 – 43.

[69] E. A. Maugeri, S. Heinitz, R. Dressler, M. Barbagallo, N. Kivel, D. Schumann, M. Ayranov, A. Musumarra, M. Gai, N. Colonna, M. Paul, S. Halfon, L. Cosentino, P. Finocchiaro, A. Pappalardo, Preparation of ^{7}Be targets for nuclear astrophysics research, Journal of Instrumentation 12 (2017) P02016.

[70] M. Weigand, T. Heftrich, Ch. E. Düllmann, K. Eberhardt, S. Fiebiger, J. Glorius, K. Göbel, R. Haas, C. Langer, S. Lohse, 66.7-keV γ-line intensity of ^{171}Tm determined via neutron activation, Physical Review C 97 (2018) 035803.

[71] T. Heftrich, M. Weigand, C. E. Düllmann, K. Eberhardt, S. Fiebiger, J. Glorius, K. Göbel, C. Guerrero, R. Haas, S. Heinitz, J. Lerendegui-Marco, F. Käppeler, J. D. Kaiser, U. Köster, C. Langer, S. Lohse, F. Ludwig, R. Reifarth, D. Renisch, K. Scheutwinkel, D. Schumann, N. Wiehl, C. Wolf, Thermal (n, γ) cross section and resonance integral of ^{171}Tm, Phys. Rev. C 99 (2019) 065810.

[72] B. Derby, Inkjet Printing of Functional and Structural Materials: Fluid Property Requirements, Feature Stability, and Resolution, Annual Review of Materials Research 40 (2010) 395–414.

[73] E. Tekin, P. J. Smith, U. S. Schubert, Inkjet printing as a deposition and patterning tool for polymers and inorganic particles, Soft Matter 4 (2008) 703–713.

[74] D. Renisch, T. Beyer, K. Blaum, M. Block, Ch. E. Düllmann, K. Eberhardt, M. Eibach, S. Nagy, D. Neidherr, W. Nörtershäuser, C. Smorra, Targets on superhydrophobic surfaces for laser ablation ion sources, Nuclear Instruments and Methods in Physics Research Section A: Accelerators, Spectrometers, Detectors and Associated Equipment 676 (2012) 84–89.

[75] R. Abrosimov, Herstellung und Charakterisierung superhydrophiler Ti-Oberflächen für kernchemische Anwendungen, Bachelor's thesis, Johannes Gutenberg-Universität Mainz (2020).

[76] BioFluidix GmbH, PipeJet P9 Nanodispenser Datasheet, www.biofluidix.com, [Online; accessed March 2020] (2014).

[77] International Atomic Energy Agency, Ion Exchange Technology in the nuclear fuel cycle, Vienna (Austria) (1986).

[78] R. M. Diamond, K. Street Jr, G. T. Seaborg, An ion-exchange study of possible hybridized 5f bonding in the actinides1, Journal of the American Chemical Society 76 (1954) 1461–1469.

[79] D. K. Aswal, S. Lenfant, D. Guerin, J. V. Yakhmi, D. Vuillaume, Self assembled monolayers on silicon for molecular electronics, Analytica Chimica Acta 568 (2006) 84 – 108.

[80] W. M. Van Rhijn, D. E. De Vos, B. F. Sels, W. D. Bossaert, Sulfonic acid functionalised ordered mesoporous materials as catalysts for condensation and esterification reactions, Chemical communications 3 (1998) 317–318.

[81] J. Wu, L. Ling, J. Xie, G. Ma, B. Wang, Surface modification of nanosilica with 3-mercaptopropyl trimethoxysilane: Experimental and theoretical study on the surface interaction, Chemical Physics Letters 591 (2014) 227 – 232.

[82] G. R. Choppin, Actinide speciation in aquatic systems, Marine Chemistry 99 (2006) 83 – 92.

[83] G. R. Choppin, Actinide speciation in the environment, Journal of Radioanalytical and Nuclear Chemistry 273 (2007) 695–703.

[84] S. Brunauer, P. H. Emmett, E. Teller, Adsorption of gases in multimolecular layers, Journal of the American chemical society 60 (1938) 309–319.

[85] N. Jaffrezic-Renault, H. Poirier-Andrade, D. H. Trang, Models for the adsorption of uranium on titanium dioxide, Journal of Chromatography A 201 (1980) 187–192.

[86] B. Grambow, Mobile fission and activation products in nuclear waste disposal, Journal of Contaminant Hydrology 102 (2008) 180 – 186.

[87] H. Geckeis, T. Rabung, Actinide geochemistry: From the molecular level to the real system, Journal of Contaminant Hydrology 102 (2008) 187 – 195.

[88] D. De Soete, R. Gijbels, J. Hoste, in: Neutron activation analysis, Vol. first edition, Wiley London, 1972.

[89] G. F. Knoll, Radiation detection and measurement second edition (1989).

[90] TRIGA Mark II technical data, https://www.kernchemie.uni-mainz.de/reaktor/technische-daten/, [Online; accessed 09-April-2020].

[91] S. Aggarwal, Alpha-particle spectrometry for the determination of alpha emitting isotopes in nuclear, environmental and biological samples: Past, Present and Future, Anal. Methods 8 (2016) 5353–5371.

[92] A. H. Becquerel, Sur les radiations invisibles émises par les sels d'uranium, CR Acad. Sci. Paris 122 (1896) 689–694.

[93] H. von Seggern, Photostimulable x-ray storage phosphors: A review of present understanding, Brazilian Journal of Physics 29 (1999) 254–268.

[94] R. F. Johnston, S. C. Pickett, D. L. Barker, Autoradiography using storage phosphor technology, Electrophoresis 11 (1990) 355–360.

[95] D. Liebe, K. Eberhardt, W. Hartmann, T. Häger, A. Hübner, J. V. Kratz, B. Kindler, B. Lommel, P. Thörle, M. Schädel, J. Steiner, The application of neutron activation analysis, scanning electron microscope, and radiographic imaging for the characterization of electrochemically deposited layers of lanthanide and actinide elements, Nuclear Instruments and Methods in Physics Research Section A: Accelerators, Spectrometers, Detectors and Associated Equipment 590 (2008) 145–150.

[96] W. Zhou, R. Apkarian, Z. L. Wang, D. Joy, Fundamentals of scanning electron microscopy (SEM), in: Scanning microscopy for nanotechnology, Springer, 2006, pp. 1–40.

[97] E. Meyer, Atomic force microscopy, Progress in surface science 41 (1992) 3–49.

[98] J. M. Chalmers, H. G. M. Edwards, M. D. Hargreaves, Infrared and Raman spectroscopy in forensic science, John Wiley & Sons, 2012.

[99] M. L. Pumo, The s-process nucleosynthesis in massive stars: current status and uncertainties due to convective overshooting, Astrophysics (2012) 41.

[100] F. Käppeler, The origin of the heavy elements: The s process, Progress in Particle and Nuclear Physics 43 (1999) 419–483.

[101] C. E. Rolfs, W. S. Rodney, W. S. Rodney, Cauldrons in the cosmos: Nuclear astrophysics, University of Chicago press, 1988.

[102] S. Hofmann, S. N. Dmitriev, C. Fahlander, J. M. Gates, J. B. Roberto, H. Sakai, On the discovery of new elements (IUPAC/IUPAP Provisional Report), Pure and Applied Chemistry 90 (2018) 1773–1832.

[103] P. J. Karol, R. C. Barber, B. M. Sherrill, E. Vardaci, T. Yamazaki, Discovery of the elements with atomic numbers Z= 113, 115 and 117 (IUPAC Technical Report), Pure and Applied Chemistry 88 (2016) 139–153.

[104] J. D. Burns, K. G. Myhre, N. J. Sims, D. W. Stracener, R. A. Boll, Effects of annealing temperature on morphology and thickness of samarium electrodeposited thin films, Nuclear Instruments and Methods in Physics Research Section A: Accelerators, Spectrometers, Detectors and Associated Equipment 830 (2016) 95–101.

[105] D. A. Mayorov, E. E. Tereshatov, T. A. Werke, M. M. Frey, C. M. Folden III, Heavy-ion beam induced effects in enriched gadolinium target films prepared by molecular plating, Nuclear Instruments and Methods in Physics Research Section B: Beam Interactions with Materials and Atoms 407 (2017) 256–264.

[106] V. M. Strutinsky, Shell effects in nuclear masses and deformation energies, Nuclear Physics A 95 (1967) 420–442.

[107] A. Sobiczewski, Review of recent SHE predictions, Physica Scripta 10 (1974) 47.

[108] C. J. Campbell, A. G. Radnaev, A. Kuzmich, V. A. Dzuba, V. V. Flambaum, A. Derevianko, Single-Ion Nuclear Clock for Metrology at the 19th Decimal Place, Phys. Rev. Lett. 108 (2012) 120802.

[109] N. Huntemann, C. Sanner, B. Lipphardt, C. Tamm, E. Peik, Single-ion atomic clock with 3×10^{-18} systematic uncertainty, Physical review letters 116 (2016) 063001.

[110] S. Stellmer, M. Schreitl, T. Schumm, Radioluminescence and photoluminescence of Th:CaF_2 crystals, Scientific reports 5 (2015) 1–10.

[111] J. Jeet, C. Schneider, S. T. Sullivan, W. G. Rellergert, S. Mirzadeh, A. Cassanho, H. Jenssen, E. V. Tkalya, E. R. Hudson, Results of a Direct Search Using Synchrotron Radiation for the Low-Energy Th 229 Nuclear Isomeric Transition, Physical review letters 114 (2015) 253001.

[112] L. C. v. d. Wense, B. Seiferle, C. Schneider, J. Jeet, I. Amersdorffer, N. Arlt, F. Zacherl, R. Haas, D. Renisch, P. Mosel, et al., The concept of laser-based conversion electron Mössbauer spectroscopy for a precise energy determination of ^{229m}Th, Hyperfine Interactions 240 (2019) 23.

[113] K. Gunter, F. Asaro, A. C. Helmholz, Charge and Energy Distributions of Recoils from ^{226}Th Alpha Decay, Phys. Rev. Lett. 16 (1966) 362–364.

[114] R. Haas, T. Kieck, D. Budker, C. E. Düllmann, K. Groot-Berning, W. Li, D. Renisch, F. Schmidt-Kaler, F. Stopp, A. Viatkina, Development of a recoil ion source providing slow Th ions including $^{229(m)}$Th in a broad charge state distribution, Hyperfine Interactions 241 (2020) 25.

[115] V. A. Yerokhin, R. A. Müller, A. Surzhykov, P. Micke, P. O. Schmidt, Nonlinear isotope-shift effects in Be-like, B-like, and C-like argon, Physical Review A 101 (2020) 012502.

[116] J. Berengut, V. Flambaum, A. Ong, Testing spatial α-variation with optical atomic clocks based on highly charged ions, in: EPJ Web of Conferences, Vol. 57, EDP Sciences, 2013, p. 02001.

[117] M. Kozlov, M. Safronova, J. C. López-Urrutia, P. Schmidt, Highly charged ions: Optical clocks and applications in fundamental physics, Reviews of Modern Physics 90 (2018) 045005.

[118] J. Berengut, V. Dzuba, V. Flambaum, Enhanced laboratory sensitivity to variation of the fine-structure constant using highly charged ions, Physical review letters 105 (2010) 120801.

[119] J. Berengut, V. Dzuba, V. Flambaum, A. Ong, Electron-hole transitions in multiply charged ions for precision laser spectroscopy and searching for variations in α, Physical review letters 106 (2011) 210802.

[120] J. Berengut, V. Dzuba, V. Flambaum, A. Ong, Highly charged ions with E 1, M 1, and E 2 transitions within laser range, Physical Review A 86 (2012) 022517.

[121] V. Mäckel, R. Klawitter, G. Brenner, J. C. López-Urrutia, J. Ullrich, Laser spectroscopy on forbidden transitions in trapped highly charged Ar^{13+} ions, Physical review letters 107 (2011) 143002.

[122] D. Wineland, J. Bergquist, J. Bollinger, R. Drullinger, W. Itano, Quantum computers and atomic clocks, in: Frequency Standards And Metrology, World Scientific, 2002, pp. 361–368.

[123] P. O. Schmidt, T. Rosenband, C. Langer, W. M. Itano, J. C. Bergquist, D. J. Wineland, Spectroscopy using quantum logic, Science 309 (2005) 749–752.

[124] W. King, Comments on the article "Peculiarities of the isotope shift in the samarium spectrum", JOSA 53 (1963) 638–639.

[125] W. King, Isotope Shifts in Atomic Spectra, Plenum Press (1984).

[126] J. C. Berengut, D. Budker, C. Delaunay, V. V. Flambaum, C. Frugiuele, E. Fuchs, C. Grojean, R. Harnik, R. Ozeri, G. Perez, Y. Soreq, Probing New Long-Range Interactions by Isotope Shift Spectroscopy, Phys. Rev. Lett. 120 (2018) 091801.

[127] L. v. d. Wense, P. G. Thirolf, D. Kalb, M. Laatiaoui, Towards a direct transition energy measurement of the lowest nuclear excitation in ^{229}Th, Journal of Instrumentation 8 (2013) P03005.

Chapter 2

Publication I: Investigations on the astrophysical s-process

The following article entitled "66.7-keV γ-line intensity of ^{171}Tm determined via neutron activation" was published in *Physical Review C*, volume 97, 035803 by M. Weigand et al. in 2018, as a collaborative work of physicists from the Goethe-Universität Frankfurt and of the group of Prof. Düllmann from the Johannes Gutenberg-Universität (JGU) Mainz. The experiments were performed at the TRIGA Mark II research reactor at the former Institute of Nuclear Chemistry, JGU Mainz. In the experiment described in this publication, a target of enriched ^{170}Er was produced by the DoD method, irradiated with neutrons and the 66.7 keV γ-line intensity of ^{171}Tm, the β^--daughter nuclide of the produced ^{171}Er, was investigated. The obtained data of this experiment were used for further experiments with enriched ^{171}Tm samples. This was published by T. Heftrich et al. in *Physical Review C*, 99 (2019) 065810. The copyright of the following article belongs to American Physical Society (APS).

2.1 Own contributions

A method was developed based on the DoD method to produce ^{170}Er targets according to the requirements of the experiment. The DoD method was used for the first time for the fabrication of a target with a closed layer consisting of isotopically enriched ^{170}Er. The homogeneous layer was achieved by stepwise drying under IR light and adding further material by printing onto the dried deposits. The homogeneity of the produced layer was investigated and verified by SEM measurements. Furthermore, the text block of the sample preparation was written in this publication.

PHYSICAL REVIEW C **97**, 035803 (2018)

66.7-keV γ-line intensity of ^{171}Tm determined via neutron activation

M. Weigand,[1,*] T. Heftrich,[1] Ch. E. Düllmann,[2,3,4] K. Eberhardt,[2] S. Fiebiger,[1] J. Glorius,[1,3] K. Göbel,[1] R. Haas,[2,4] C. Langer,[1] S. Lohse,[2,4] R. Reifarth,[1] D. Renisch,[2,4] and C. Wolf[1]

[1]*Goethe-Universität Frankfurt, 60438, Frankfurt a.M., Germany*
[2]*Johannes Gutenberg-Universität Mainz, 55122, Mainz, Germany*
[3]*GSI Helmholtzzentrum für Schwerionenforschung, 64291, Darmstadt, Germany*
[4]*HIM Helmholtz-Institut Mainz, 55128, Mainz, Germany*

(Received 12 February 2018; published 16 March 2018)

Background: About 50% of the heavy elements are produced in stars during the slow neutron capture process. The analysis of branching points allows to set constraints on the temperature and the neutron density in the interior of stars. The temperature dependence of the branch point ^{171}Tm is weak. Hence, the ^{171}Tm neutron capture cross section can be used to constrain the neutron density during the main component of the s process in thermally pulsing asymptotic giant branch stars.
Purpose: In order to perform neutron capture experiments on ^{171}Tm, sample material has to be produced and characterized. The characterization is done by γ spectroscopy, relying on the intensities of the involved γ lines. Only the 66.7-keV γ line can be observed whose intensity was uncertain so far.
Method: An enriched ^{170}Er sample was activated with thermal neutrons at the TRIGA (Training, Research, Isotopes, General Atomics) research reactor at the Johannes Gutenberg-Universität Mainz. The activation resulted in an easily quantifiable number of ^{171}Er nuclei that subsequently decayed to ^{171}Tm.
Result: The intensity of the 66.7-keV γ line of the ^{171}Tm decay was measured to $I_\gamma = (0.144 \pm 0.010)\%$.
Conclusions: Our result is in good agreement with the value found in the literature.

DOI: 10.1103/PhysRevC.97.035803

I. ASTROPHYSICAL BACKGROUND

The observed abundances of elements heavier than iron are almost entirely formed by neutron capture processes in different scenarios. A distinction is made between the slow neutron capture in thermally pulsing asymptotic giant branch stars (s process) and its rapid counterpart in explosive scenarios (r process). The specific s process path along the valley of stability depends on temperatures and neutron densities in stars, neutron capture cross sections, and half-lives in the case of unstable isotopes. The s process path in the region of mass number $A = 171$ is depicted in Fig. 1 (gray arrows). It follows the chain of stable isotopes via neutron captures, interrupted by β decays at unstable isotopes. Only at nuclei with longer half-lives is another neutron capture probable during the s process (dashed lines). These isotopes act as branching points and are useful to constrain s-process models [1]. In the scope of Fig. 1 this applies for ^{170}Tm and ^{171}Tm.

In order to study the branching at ^{171}Tm, only one neutron capture experiment has been performed in the past [2], but more are currently in the process of analysis and results will soon be published [3,4]. The number of ^{171}Tm nuclei in the sample material is determined via its decay γ line at 66.7 keV. For its intensity I_γ, the literature gives a value of 0.143% [5], which results from one single publication and no uncertainty is provided. Therefore, a new measurement was performed at the TRIGA (Training, Research, Isotopes, General Atomics) type research reactor at the Institute of Nuclear Chemistry, Johannes Gutenberg-Universität, Mainz, Germany [6,7].

Our approach is based on the production of a well-quantified amount of ^{171}Tm via neutron activation of ^{170}Er producing ^{171}Er, which eventually decays to ^{171}Tm with a known half-life (Fig. 1). Subsequently, the I_γ could simply be determined by measuring the γ activity of the known number of ^{171}Tm nuclei.

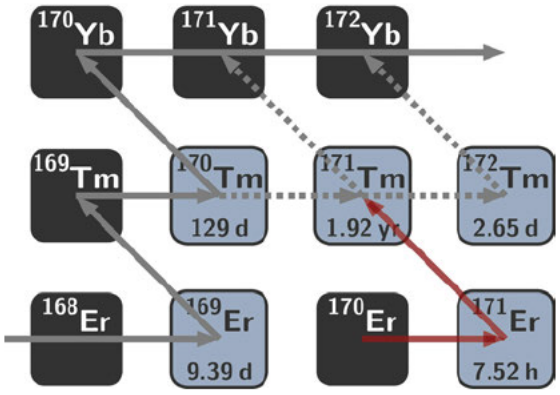

FIG. 1. The s-process region between Er and Yb with the mass flow path depicted by gray arrows. Secondary paths are represented by dashed lines. The radioactive isotopes ^{170}Tm and ^{171}Tm act as branching points. The red arrows depict the activation of ^{170}Er, which leads to ^{171}Er. Counting its γ emission allows to determine the number of nuclei that finally decay to ^{171}Tm.

*m.weigand@gsi.de

2469-9985/2018/97(3)/035803(4)

TABLE I. Data on the contaminants of the acquired Er_2O_3 powder as stated by the supplier. As a survey of all relevant decay data showed, none of the contaminants interfered at the targeted energy of 66.7 keV.

Er isotopes (% at.)					
^{162}Er	^{164}Er	^{166}Er	^{167}Er	^{168}Er	^{170}Er
0.006	0.033	0.54	0.38	0.94	98.1
Chemical admixtures (ppm)					
Fe	Si	Al	Cu	W	Ti
<400	<100	150	<30	<30	<40
Ca	Mn	Mg	Ni	Zr	Cr
250	<40	<300	<250	<100	<50
Pb	Mo	V	Sn	Bi	Co
<80	<40	<30	<30	<30	<50
Yb	Ce	Sm	Gd	Dy	Tm
90	160	40	400	100	400

II. PREPARATION OF THE ^{170}Er SAMPLE

Neutron activation of contaminants with higher Z may lead to x-ray background in the energy region around 66.7 keV. Therefore, isotopically enriched ^{170}Er (98.1%) in the form of Er_2O_3 (ISOFLEX) was chosen as a sample material. The isotopic composition and the content of contaminants as stated by the supplier are given in Table I. Since Er is a high-Z element, self-absorption of the emitted x rays with relatively low energy has to be considered. Therefore, the drop-on-demand technique was used for the preparation of a thin target layer [8]. An amount of 92.7 mg of ^{170}Er (in form of $^{170}Er_2O_3$) was dissolved in concentrated HNO_3. The solution was evaporated to dryness under an IR lamp, yielding $^{170}Er(NO_3)_3$ residue. This was dissolved in 400 µl distilled water, yielding a solution with a concentration of 230 mg/ml with regard to ^{170}Er. This solution was printed onto a polycrystalline graphene foil (thickness 12 µm, Applied Nanotech Inc.) in a circular area 20 mm in diameter. In total, 6225 individual drops were deposited on the graphene foil in five layers, the individual deposits of which overlapped to create a homogeneous target layer. After printing, the target was dried under an IR lamp for a few minutes to remove crystal water and was covered on both sides with self-adhesive 40-µm-thick Kapton foil to prevent any damage to the salt layer during the irradiation and to keep the hygroscopic salt layer dry.

A. γ-line absorption in the sample

As mentioned, the absorption of the emitted relatively low-energy γ rays in the sample itself has to be considered. The preparation of the sample material resulted in an areal density of Er atoms of $n_A = (2.44 \pm 0.07) \times 10^{19}$ cm^{-2}. The γ-ray transmission τ can be calculated with the relationship

$$\tau = \frac{1 - \exp(-\sigma n_A)}{\sigma n_A}, \quad (1)$$

where σ denotes the photon absorption cross section obtained from the XCOM database [9]. For our sample material, the calculation results in a transmission of 96.55%. The dominant absorber is the Er layer itself because the photon absorption cross sections of the supporting graphene and Kapton foils are several orders of magnitude smaller. The resulting self-absorption correction factor for 66.7 keV is thus

$$\tau = 0.9655 \pm 0.010. \quad (2)$$

The uncertainty originates from the Er areal density.

III. REACTOR ACTIVATION

The Er sample was exposed to the thermalized neutron field of the TRIGA reactor in Mainz for about 3 h at a neutron flux of about 7×10^{11} s^{-1}cm^{-2}. The reactor power was monitored every 10 s and showed only minor fluctuations in the order of 0.5% and hence was treated as constant.

Neutron captures on ^{170}Er produced the unstable ^{171}Er, which decays to ^{171}Tm with a half-life of (7.516 ± 0.002) h [5]. The total activity of the sample was in the order of 100 MBq at the end of the neutron irradiation. After 2 days of waiting, the γ-ray emissions of ^{171}Er at 308 keV and 295 keV were investigated with a HPGe detector with a length of 67 mm, a diameter of 69 mm, and a relative efficiency of 60%. The obtained spectrum is shown in Fig. 2.

Since both γ lines are emitted in γ cascades with other, weaker transitions, and because of the still high activity of the sample, a large distance of 43 cm between detector and the Er sample was chosen. The remaining cascade effects were investigated by means of GEANT3 [10] simulations and were found to be negligible (<0.1%).

The efficiency calibration of the detector was performed with a calibrated solution of ^{241}Am, ^{109}Cd, ^{57}Co, ^{60}Co, ^{85}Sr, ^{88}Y, ^{113}Sn, ^{137}Cs, ^{139}Ce, and ^{203}Hg, providing a wealth of γ lines over a broad energy range. The uncertainties of the source activities were in the range of 2.3% to 3.1%. Efficiencies and line intensities relevant for the Er counting are presented in Table II.

The relationship between the γ-ray counts and the number of produced ^{171}Er nuclei is given by

$$N(^{A+1}X) = \frac{C_\gamma}{\epsilon_\gamma I_\gamma f_a f_w f_m f_{dt}}, \quad (3)$$

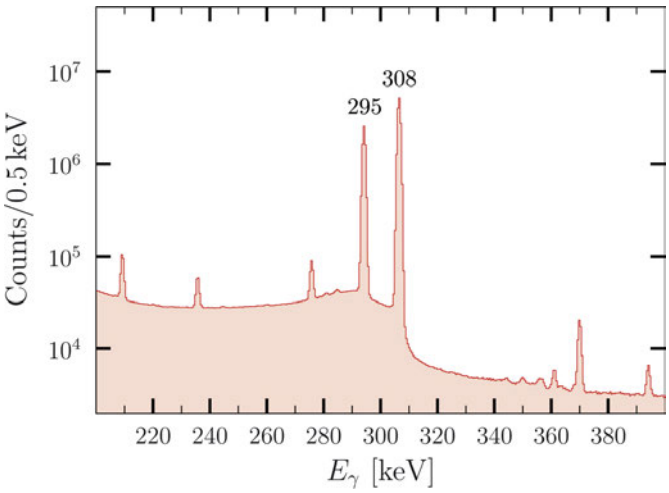

FIG. 2. The most prominent γ-ray emission lines of ^{171}Er at 308 keV and 295 keV after a counting time of 3 h.

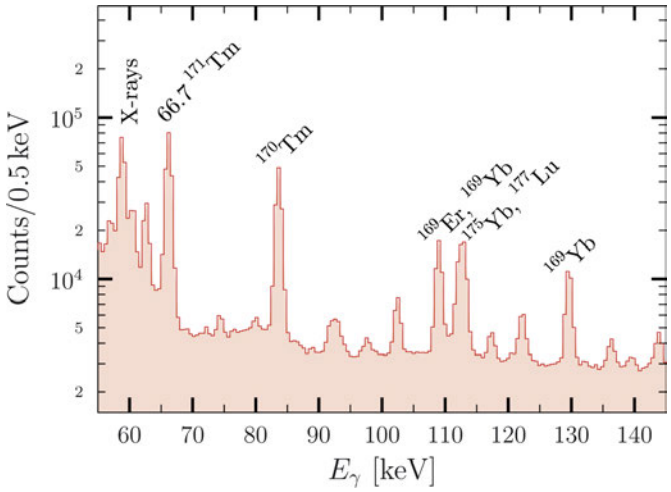

FIG. 3. Resulting spectrum from the same sample as in Fig. 2 after about 6 days of the ^{171}Tm counting. Besides ^{171}Tm at 66.7 keV, γ lines of other constituents of the sample material are visible, most notably isotopes of Tm, Er, and Yb. Below 65 keV x rays from various species overlap. No contributions by isotopes other than listed in Table I could be identified via spectroscopic analysis.

where

$$f_a = \frac{1-\exp(-\lambda_i t_a)}{\lambda_i t_a}, \quad (4)$$

$$f_w = \exp(-\lambda_i t_w), \quad (5)$$

$$f_m = 1-\exp(-\lambda_i t_m) \quad (6)$$

are the corrections for the decay during the activation f_a, during the waiting time between activation and measurement f_w, and during the measurement f_m. The small correction for the dead time of the detection system is represented by f_{dt}.

The counting was performed in 3-h intervals over 3 days. The dead time of the detection system gradually declined over the course of the measurement from about 9% at the beginning to 1.8% at the end. The number of ^{171}Er atoms produced in the reactor on October 4, 2017, hence the number of produced ^{171}Tm atoms, was determined as

$$N(^{171}\mathrm{Er}) = (3.31 \pm 0.16) \times 10^{12} = N(^{171}\mathrm{Tm}). \quad (7)$$

TABLE II. Data for the relevant γ-ray emissions following the decay of ^{171}Tm and ^{171}Er, and the corresponding detection efficiencies ϵ_γ of the used HPGe detector. Values for E_γ and $I_\gamma = I_{rel} I_{abs}$ were obtained from Ref. [5].

Isotope	^{171}Tm	^{171}Er	^{171}Er
E_γ	66.7 keV	295.90 keV	308.29 keV
I_{rel}	0.0014286	289	644
ΔI_{rel}	—	±8	±16
I_{abs}	1	0.100	0.100
ΔI_{abs}	—	±0.003	±0.003
ϵ_γ	0.00749	0.000966	0.000942
$\Delta\epsilon_\gamma$	±0.00034	±0.000014	±0.000014

IV. I_γ DETERMINATION

The activation of the erbium sample had to be strong to achieve a measurable decay rate of the produced ^{171}Tm in the next step, which has a much longer half-life and a very low γ-ray intensity. After 5 days which corresponds to about 16 half-life times, basically all of the produced ^{171}Er nuclei had decayed to ^{171}Tm and its γ-rays were observed over the course of 6 days in 24 hour intervals (Fig. 3). Subsequently, the intensity of the 66.7-keV line could be calculated via

$$I_\gamma(66.7\,\mathrm{keV}) = \frac{C}{A(t)\epsilon_\gamma t_m f_w f_m f_{dt} \tau}, \quad (8)$$

where $A(t)$ is the Tm activity during the measurement determined from the number of produced ^{171}Er nuclei and C the number of counts in the 66.7-keV line. We found:

$$I_\gamma(66.7\,\mathrm{keV}) = (0.1442 \pm 0.0040_{stat} \pm 0.0089_{sys})\%. \quad (9)$$

The previously recommended value of 0.14286 [5] agrees with our measurement within the uncertainties of our measurement.

A. Uncertainties

The main contributors to the total systematic uncertainty are the γ-line intensities of ^{171}Er and the detector efficiencies. Uncertainties resulting from dead-time and cascade corrections, and from the decay constants of ^{171}Er and ^{171}Tm are negligible. All sources for uncertainties are presented in Table III. The statistical uncertainties from the Er and Tm counting are as small as 0.02% and 0.26%. All parameters that were used for weighted averaging had to be treated as statistical uncertainties, hence the larger final statistical uncertainty.

TABLE III. All sources of uncertainties for the measured 66.7 keV I_γ of ^{171}Tm.

Source of uncertainty	Uncertainty / %
Er counting	
γ-intensity I_{rel}, 295 keV (*)	2.8
γ-intensity I_{rel}, 308 keV (*)	2.5
γ-intensity normalization I_{abs}	3.0
Detection efficiency ϵ_γ (*)	1.4
Factors f_a, f_w, and f_m	<0.1
γ-counting statistics (*)	<0.1
Statistical uncertainty for $N(^{171}\mathrm{Tm})$	2.7
Systematic uncertainty for $N(^{171}\mathrm{Tm})$	3.3
Total uncertainty for $N(^{171}\mathrm{Tm})$	4.3
Tm counting	
Detection efficiency ϵ_γ	4.5
Factors f_w and f_m	<0.1
Transmission τ	1.0
γ-counting statistics	0.3
Statistical uncertainty for I_γ (66.7 keV)	2.8
Systematic uncertainty for I_γ (66.7 keV)	6.2
Total uncertainty for I_γ (66.7 keV)	6.8

*Used for weighted averaging to consider the different uncertainties of the two Er lines and the runs.

V. SUMMARY AND DISCUSSION

To study the *s*-process reaction path, branching points are very important, since they allow us to constrain the conditions in the interior of stars [11,12]. The analysis of the interesting branching point ^{171}Tm is currently hampered by the insufficient knowledge of the corresponding nuclear data. We report on new results for the intensity of the 66.7-keV γ line. It was measured via activation of isotopically enriched ^{170}Er. The produced ^{171}Er decays to ^{171}Tm with a half-life of 7.5 h. The number of produced ^{171}Er nuclei and, as a result also the number of ^{171}Tm nuclei, was determined via γ counting. In a second step, γ spectroscopy of ^{171}Tm of the 66.7-keV γ line was performed. The resulting γ intensity is

$$I_\gamma = (0.144 \pm 0.010)\%, \quad (10)$$

in agreement with the value found in the literature. This now allows for reliable characterizations of ^{171}Tm samples and neutron capture cross-section experiments. Further improvement of this value could be achieved by remeasuring the γ intensities of the ^{171}Er γ lines with higher precision.

ACKNOWLEDGMENTS

We are very grateful for the excellent support by the entire team of the TRIGA reactor in Mainz. This work was partly supported by the BMBF Projects No. 05P12RFFN6 and No. 05P15RFFN1, the Helmholtz International Center for FAIR and HGS-HIRe, the DFG project RE 3461/4-1, and the European Research Council under the European Unions's Seventh Framework Programme (FP/2007-2013) / ERC Grant Agreement No. 615126.

[1] R. Reifarth, C. Lederer, and F. Käppeler, J. Phys. G **41**, 053101 (2014).
[2] R. Reifarth, R. Haight, M. Heil, M. Fowler, F. Käppeler, G. Miller, R. Rundberg, J. Ullmann, and J. Wilhelmy, Nucl. Phys. A **718**, 478 (2003).
[3] C. Guerrero *et al.* The n_TOF Collaboration and the SARAF Team (unpublished).
[4] T. Heftrich *et al.* (unpublished).
[5] C. M. Baglin, Nucl. Data Sheets **96**, 399 (2002).
[6] K. Eberhardt and A. Kronenberg, Kerntechnik **65**, 269 (2000).
[7] G. Hampel, K. Eberhardt, and N. Trautmann, Atw. Internationale Zeitschrift fuer Kernenergie **51**, 328 (2006).
[8] R. Haas, S. Lohse, C. Düllmann, K. Eberhardt, C. Mokry, and J. Runke, Nucl. Instrum. Methods Phys. Res., Sect. A **874**, 43 (2017).
[9] M. J. Berger, J. H. Hubbell, S. M. Seltzer, J. Chang, J. S. Coursey, R. Sukumar, D. S. Zucker, and K. Olsen, XCOM: Photon Cross Section Database (version 1.5) (2010).
[10] J. Apostolakis, Tech. Rep., CERN, GEANT library (1993) https://www.nist.gov/pml/xcom-photon-cross-sections-database.
[11] R. Reifarth, C. Arlandini, M. Heil, F. Käppeler, P. Sedychev, A. Mengoni, M. Herman, T. Rauscher, R. Gallino, and C. Travaglio, Astrophys. J. **582**, 1251 (2003).
[12] R. Reifarth, F. Käppeler, F. Voss, K. Wisshak, R. Gallino, M. Pignatari, and O. Straniero, Astrophys. J. **614**, 363 (2004).

Chapter 3

Publication II: ODIn - A setup for Off-line Deposit Irradiations

The following article was published as full article in *Nuclear Instruments and Methods in Physics Research Section A: Accelerators, Spectrometers, Detectors and Associated Equipment*, volume 957, pages 163366 in 2020. It describes the design, characterization and first commissioning of a pilot experiment for Off-line Deposit Irradiations (ODIn), which will help to investigate the radiation induced processes of electron and ion beams with thin layer samples.

3.1 Own contributions

The experiment for off-line irradiations was designed and constructed. A remote control was developed for the ion source and the experimental infrastructure was built up. The produced electron and ion beams were fully characterized. Theoretical calculations of stopping powers, deposited energies and irradiation depths were performed. The first commissioning of electron beams with molecular plated lead samples was performed and the induced changes were visually identified. At last, the paper was written completely self-directed.

ODIn - A setup for Off-line Deposit Irradiations of thin layers for nuclear physics applications

R. Haas[1,2,3], C.-C. Meyer[1,2], S. Böhland[1], Ch. E. Düllmann[1,2,3], J. Mäder[3], K. Tinschert[3]

3.2 Abstract

A table top setup was developed for the irradiation of thin layers with low-energy electrons and ions of gaseous species. This serves to gain a better understanding of the chemical microprocesses involved during irradiations. The gained insights will complement the understanding of heavy-ion beam induced transformations at on-line facilities and will be used to develop an accelerator-independent method to transform freshly produced targets into a long-term stable form. The pilot experiment for these Off-line Deposit Irradiations (ODIn) is installed at the Helmholtz Institute Mainz. The setup, beam characterization and first commissioning are described.

3.3 Introduction

Thin films of radionuclides are a key element in many nuclear physics applications. These include applications as nuclear targets in accelerator-based experiments, e.g., in the production of superheavy elements in heavy-ion fusion reactions. With ever increasing beam intensities of new and more powerful accelerators, the targets have to withstand ever more intense heavy-ion bombardments over long time periods. For the synthesis of the heaviest elements, actinide targets are used, which are frequently produced using the well established "Molecular Plating" technique [1, 2]. This method is also applied for the production of radionuclide samples, e.g., serving as recoil ion sources providing α-decay daughters [3] or fission fragments. A. Vascon et al. characterized this method in more detail for lanthanides [4], which served as homologs of actinides, and found ideal parameters to produce crack-free large area targets [5]. The performance as α-particle source was characterized as well [6]. An important finding was the additional deposition of organic solvent material as well as the speciation of the deposited lanthanide on the produced targets. The latter indicated that the material is deposited as hydroxides and carboxylates, but not in the originally provided chemical form, e.g, the nitrate [5]. The deposits are known to often be quite sensitive to moisture and oxygen and deteriorate during long storage time periods at air. Furthermore, the deposit was found to be

[1]Department Chemie, Johannes Gutenberg-Universität Mainz, 55128 Mainz, Germany
[2]Helmholtz-Institut Mainz, 55128 Mainz, Germany
[3]GSI Helmholtzzentrum für Schwerionenforschung GmbH, 64291 Darmstadt, Germany

covered by a thin layer of organic solvent material. Other target fabrication methods include Pulsed Laser Deposition (PLD) [7], Polymer-Assisted Deposition (PAD) [8] and Drop-on-Demand inkjet printing (DoD) which was recently developed and characterized [9]. The Drop-on-Demand technique has some advantages when compared to the Molecular Plating technique in regard to the chemical purity and amount of the deposited material and is not limited to deposition on electrically conductive substrates. Several different targets and sources have recently been produced by this technique [10, 11]. Also with this technique, the final deposits are hygroscopic and may deteriorate at air.
To prevent such aging processes of freshly produced targets, they are usually converted into a long-term stable form. For this, the state-of-the-art relies on a well established on-line baking-in procedure with heavy-ion beams. During these irradiations, organic impurities are largely destroyed and the actinide species can be converted into the oxide [12]. To give just one recent example, we refer to [13], where ^{248}Cm targets were conditioned with a 5.6 MeV u^{-1} ^{48}Ca-beam on-line at the Separator for Heavy Ion reaction Products (SHIP). Alpha-spectra of the ^{248}Cm layer recorded before and after the baking-in procedure reveal a narrowing of the lines, indicating a loss of material in the layer while the activity stayed constant. It is already known that such transformations cannot be reproduced by heating up to 700 °C in an oxidizing or reducing gaseous atmosphere [14] and are not just caused by induced heat in the target layer during irradiation [15]. The field of the induced effects of such beams on target materials is well investigated by several groups. Some exemplary findings are phase transformations in cubic C-type lanthanide sesquioxides by electronic excitation [16] or beam induced electronic sputtering [17]. To date, though, it is still not well known, if similar effects of target conditioning can be achieved with ion or electron beams of substantially lower energies.

3.4 ODIn - a setup for Off-line Deposit Irradiation

As a new approach for investigations on the chemical and physical microprocesses during irradiations of target material with low-energy ion and electron beams, a new setup for Off-line Deposit Irradition (ODIn) was constructed at the Helmholtz Institute Mainz. This serves as a test bench and pilot facility for the development of a method to condition freshly produced actinide targets independently of on-line accelerator beam availability. ODIn provides electron beams up to 1.5 keV as well as ion beams of gaseous species up to 5 keV with currents of hundreds of µA. A general sketch is depicted in Fig. 3.1. The beam currents can be measured via a Faraday cup or by direct measurement of the current induced in the sample holder. Additionally, the irradiated samples as well as phosphor screens can be monitored by a camera through a viewport flange. A LabVIEW based remote control system was developed for the experiment and the beam profiles were measured with phosphor screens for several irradiation parameters. For commissioning, lead

samples were produced on gold plated Kapton foil by Molecular Plating and were irradiated with electron beams.

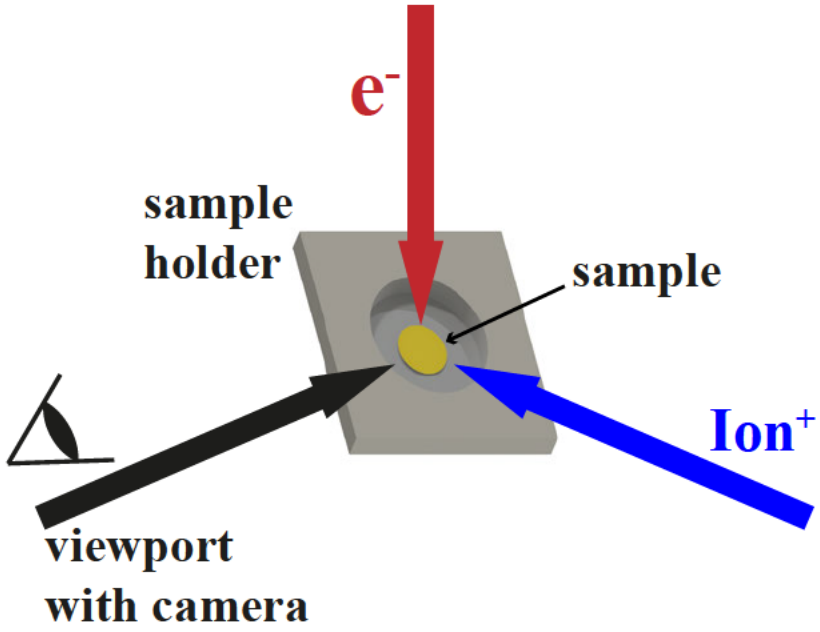

Figure 3.1: General sketch of the ODIn working principle.

3.4.1 Vacuum system and general setup

The technical drawing of the ODIn setup is given in Fig. 3.2. The setup comprises an electron gun (Kimball Physics, EFG-7 with EGPS-1017 power supply) and a sputter ion gun (tectra, IonEtch Sputter gun GenII) described in the following sections.

The irradiation chamber comprises both the electron gun and the ion gun as well as a viewport flange to monitor the sample, a cluster-flange with a Faraday cup (Kimball Physics Inc., FC-70, 0.063" aperture) mounted in the middle of a flange opposite to the ion gun and a turbo pump (Pfeiffer Vacuum, HiCube 300 H, 260 L min^{-1} for nitrogen, ultimate pressure at below 1×10^{-10} mbar). It takes one minute to reach a pressure of 1×10^{-5} mbar in the irradiation chamber after opening the gate valve to the airlock and 10 min more to reach a pressure below 1×10^{-6} mbar. This is ideal for the irradiation of many samples in one day without any heating of the vacuum parts and to keep a safe environment for the gun systems. Furthermore, the manually driven gate valve grants a slow release of the residual pressure of the airlock after it was pumped down to 1.5 mbar. An ultimate pressure of 2.5×10^{-8} mbar can be reached in the complete experiment if the gate valve is open. If the gate valve is closed, an ultimate pressure below 6×10^{-9} mbar can easily be reached without heating.

To allow sample changes without breaking vacuum in the irradiation chamber, a second chamber serving as an airlock is separated by a manually operated UHV

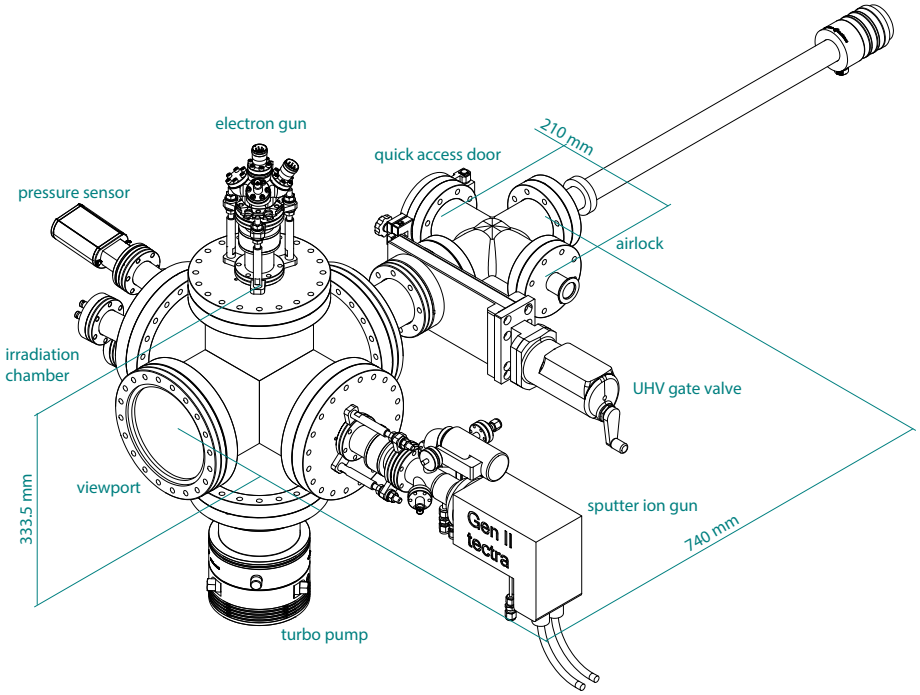

Figure 3.2: Technical drawing of the ODIn experiment.

gate valve. One small chamber (sample chamber) consists of a quick access door to enable easier sample changes and a rotary feedthrough to move the mounted sample or phosphor screen between both chambers and to arrange it towards a specific source by a turn of 90 °. The airlock can be evacuated by a membrane pump (Pfeiffer Vacuum, MVP 030-3 diaphragm pump, 30 L min^{-1}, ultimate pressure: below 2 mbar) in about 80 s to a pressure of 1.5 mbar and can be vented with nitrogen by a manual valve to avoid moisture from the air entering the airlock. The nitrogen gas is passed through a tube filled with dried $CaCl_2$ to remove residual moisture in the gas before entering ODIn.

3.4.2 Beam sources

The electron gun system (Kimball Physics, EFG-7 with EGPS-1017 power supply) is a commercially available, complete subsystem with included deflection electrodes. A simple scheme of the electron gun is given in Fig. 3.3 including all elements and their applied voltages. The beam energy, current and focus are adjustable over wide ranges. The gun system is able to produce electron beams within an energy range of 10 eV up to 1.5 keV at specified beam currents in the range of 1 nA up to 100 µA. At a working distance between 25 mm and 200 mm, spot diameters of 1 mm up to 100 mm can be achieved with Gaussian or uniform beam profile. In the used system a standard tantalum disc is used as a cathode and serves as the electron source. It is built inside a tubular structure with an aperture fixed to one end which is called Wehnelt or grid. By applying a negative voltage to this structure, the electric field

between the cathode and Wehnelt suppresses electron emission from the cathode perimeter, leaving only the center of the cathode to emit. By varying this voltage, a selection of either of the two previously mentioned beam profiles can be made. It can also be used to pulse the electron beam by adjusting a sufficiently high negative potential to cut off the beam. An aperture plate downstream of the Wehnelt acts as anode and is at ground potential. The potential difference between the cathode and anode determines the energy and trajectory of the electrons. The focusing lens is an Einzel lens with the first and third element at ground potential and the second element at negative focusing potential. At a given electron energy and working distance, the spot diameter is a function of focus voltage. The minimum spot diameter varies for different electron energies and is found by scanning the focus voltage as discussed in section 3.5.1. The last part of optics consists of two pairs of curved deflection plates for X- and Y-deflection, which allows scanning a specific area with a beam focused on the target and to correct the shape of the beam. To minimize the distortion of the beam, a small deflection can be applied, which results in a more circular spot shape. The gun system can be operated at pressures in the range of 1×10^{-11} mbar up to 1×10^{-5} mbar with manually driven source voltage and current or emission current control (ECC). With ECC the electron source is heated up slowly and the source voltage and current are continously adjusted to deliver a specific emission current. The beam current is in general about half of the emission current. The gun system is mounted on a port aligner for linear and angular adjustments at the irradiation chamber and the distance between the gun's aperture and the sample holder is about 80 mm.

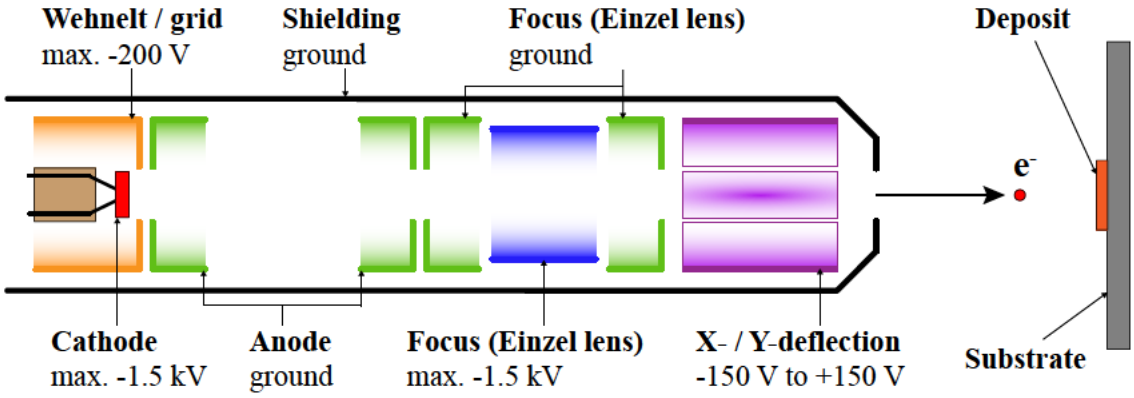

Figure 3.3: Scheme of the electron gun system including a simple illustration of all elements with their applied voltages.

The ion gun system (tectra, IonEtch Sputter gun GenII) is a commercially available filamentless ion source based on microwave plasma discharge. The principle of the source is coupling of microwave energy at 2.45 GHz into a coaxial waveguide and from there via evanescent wave coupling into a plasma chamber made of alumina. The intense oscillating electric fields produce a plasma discharge of the used gas.

Using microwaves to produce and sustain the plasma has some advantages, e.g., the ions can be extracted at very low energies down to 25 eV without the plasma collapsing and also the use of reactive gases such as oxygen and hydrogen is permitted, since there are no hot metal electrodes in the plasma. This allows the possibility to produce proton beams. The produced ions are extracted from the plasma using two single-hole extraction apertures and beam energies of up to 5 keV with a maximum beam current of 2 mA can be produced. The gun system is watercooled by an external chiller (Huber, HTS1, 650 W cooling capacity) and magnetron current, beam energy and extraction voltage can be controlled by its power supply. Furthermore, the magnetron current, beam current and voltages on the ion optics can be read out on the power supply. The investigated influence of the controllable parameters on the produced beam profiles and currents is discussed in section 3.5.2. Similar to the electron gun, also the ion gun is mounted on a port aligner at the irradiation chamber and the working distance is about 115 mm.

3.4.3 Sample introduction and monitoring

Either a target or a phosphor screen (e.g. GIDS, SCR-25-ITO-P43) is fixed between two titanium frames and can quickly be exchanged since it is just fixed with one screw in the sample holder. The maximum diameter of a target is restricted to 25 mm by the titanium frames. The holder itself is a single piece of titanium with an insertion slot for the titanium frames and is tilted at a 45 $^\circ$ angle towards both the gun systems and the viewport in the irradiation chamber. Thus, phosphor screens or targets can be monitored with a camera (Rauscher, Basler piA1000-60gc with camera lens MVL25M23 from Thorlabs) through the viewport in the irradiation chamber.

3.4.4 Control system

The power supplies of both gun systems as well as the camera system and the pressure readout can be controlled remotely. The user interface of the LabVIEW VI provided by Kimball Physics used for electron gun control is shown in Fig. 3.4. It provides control of all adjustable gun parameters (anode, grid and focus potentials, cathode voltage, deflection and scanning) and data logging. Additionally, the Emission Current Control (ECC) can be switched on, so the source voltage is adjusted automatically to deliver a steady emission current. The cathode temperature is also monitored in a third window, which is not shown in the figure.
The power supply of the sputter ion gun provides a D-Sub 9 pin connector for analog input remote control of the adjustable parameters of the ion gun. Three pins enable the remote control of a single gun parameter by applying a voltage of 5 V. Another three pins are used for metering by an applied voltage between 0 V and 10 V. One pin provides a voltage of 15 V with an internal resistance of 1.5 kΩ

and the residual pins are ground. For this connector, a remote control was developed using a commercially available microcontroller (Arduino Uno), threeMCP4725 digital-analog-converters (Adafruit, 12 bit, maximum 5 V output, controlled via I^2C) and three LM358 amplifier modules (LC Technology, working voltage 5 V to 12 V, 10 kΩ adjustable resistor for gain adjustment) for covering a metering region between 0 V to 10 V. The simplified circuit diagram is illustrated in Fig. 3.5. The remote control was also written in LabVIEW with a design matching that of the user interface shown in Fig. 3.4.
The readout of the dual gauge (Pfeiffer Vacuum, PT G28 290) is done in a separate LabVIEW VI. Both the pressure in front of the membrane pump as well as the pressure inside the irradiation chamber are monitored. The interlock for both gun systems is provided by the relay of the dual gauge and is not included in the LabVIEW remote control to avoid communication errors.
The camera is controlled by ethernet with a provided software from Basler. The camera can be operated in continous or single shot mode and its software provides several options for image enhancements. The pumps as well as the valves are all manually driven.

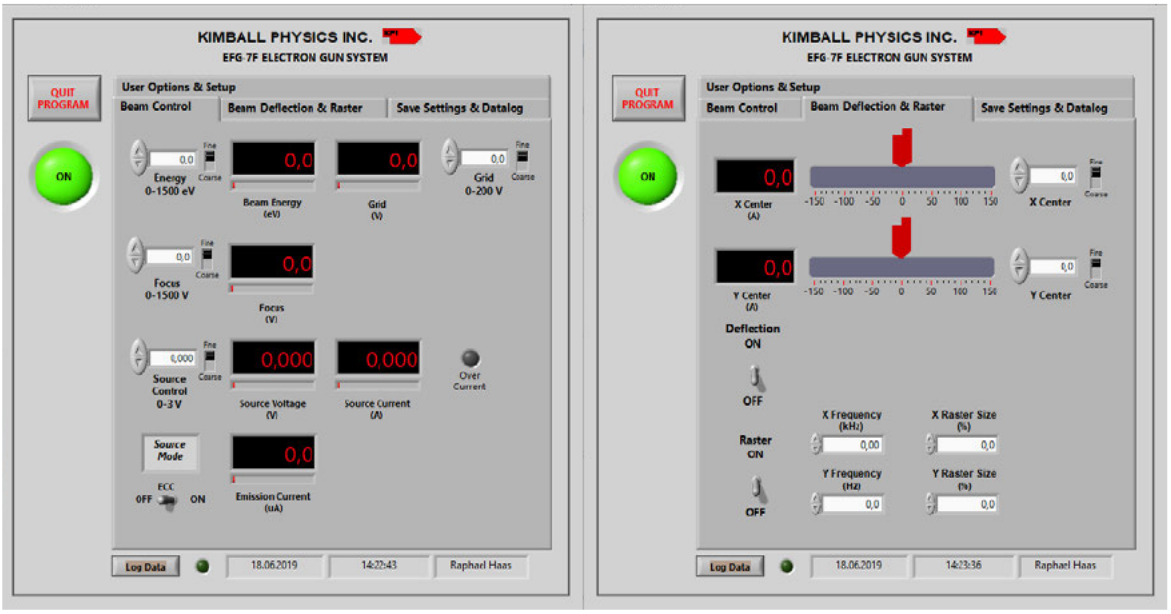

Figure 3.4: LabVIEW remote control user interface of the electron gun system delivered by Kimball Physics. (left) General beam control, setting and readout: Energy, grid, focus, source voltage and Emission Current Control (ECC) switch. (right) Deflection and area scan control.

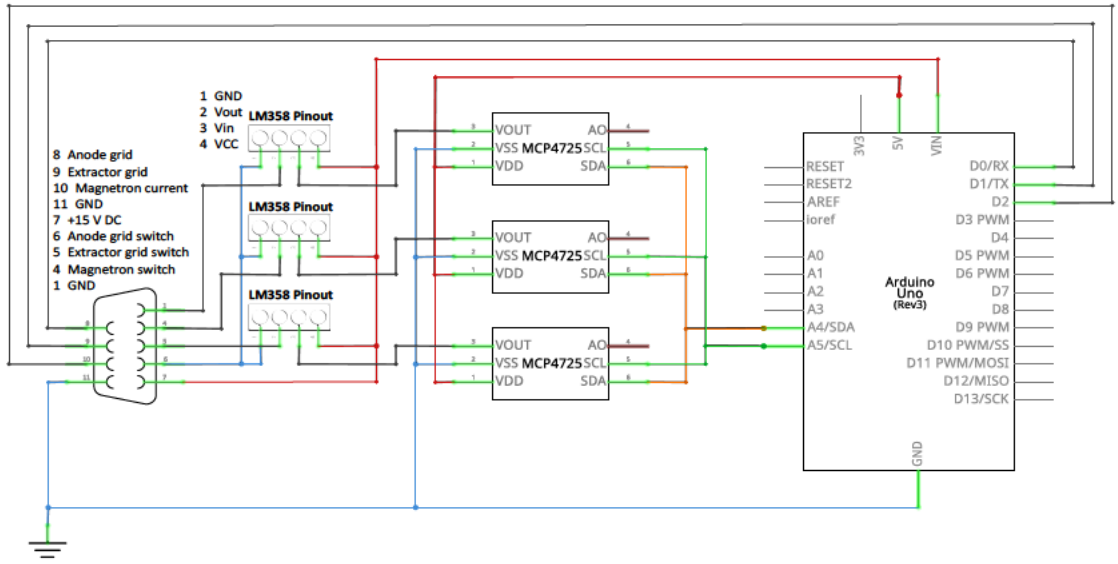

Figure 3.5: Simplified circuit diagram of the remote control for the ion gun power supply.

3.5 Characterization of the available beams

3.5.1 Electron beams

The beam profiles of the electron beam were investigated with a phosphor screen (GIDS, SCR-25-ITO-P43) monitored by a camera. The green channel of the taken pictures was used for the evaluation of the beam profiles with Gwyddion 2.5. A constant emission current of 10 µA was used for all beam tests. First, the beam spot diameter was investigated for different energies at 500 eV, 1000 eV and 1500 eV against different focus voltages with grid voltage fixed at 0 V. For instance, Fig. 3.7c) displays the beam spot shape observed on the phosphor screen at the energy 1500 eV. Due to the size of the phosphor screen, spot diameters above 25 mm are not measurable. The phosphor screen was fixed at the position of a target in the sample holder. The resulting spot diameters are illustrated in Fig. 3.6. The minimum spot diameter is reached for focus/energy = 0.66. It corresponds to the specification data sheet of the electron gun [18].

Then the influence of the grid voltage on the beam profile was investigated in different measurements for an energy of 1500 eV. At first, the grid voltage was varied between 10 V and 85 V and a focus voltage of 750 V. In a second measurement, the grid voltage was fixed at 83 V and the measurement of the spot diameter was repeated at focus voltages between 650 V and 990 V. The resulting beam profiles are illustrated in Fig. 3.7a) and Fig. 3.7b). Space charge effects are responsible for the donut-shaped profile. Depressions in central intensity are at

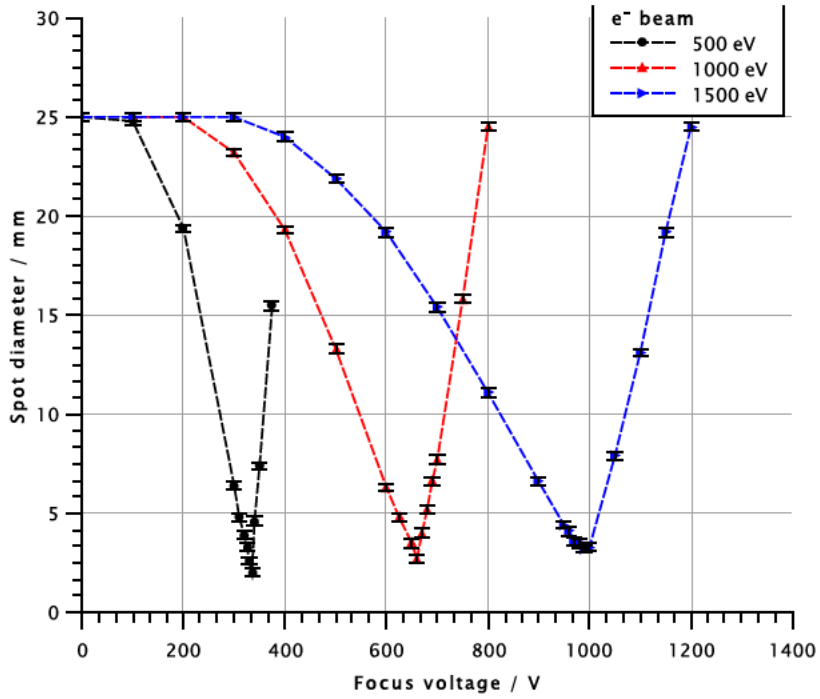

Figure 3.6: The effect of focus voltage on spot diameter at three different energies, showing minimum spots at focus/energy = 0.66.

least partially due to radiation damage at this position on the phosphor screen and are thus unrelated to the true beam profile.

During these measurements, the cathode temperature reaches a maximum of about 2000 K with the Grid voltage turned on and cools down after a warm up and with Grid voltage turned off to about 1700 K. An example graph of the evolution of the cathode temperature during operation of the electron gun is given in Fig. 3.8.

3.5.2 Ion beams

The ion gun was characterized in a comparable setup with the same camera system as in ODIn and the same dimensions of the vacuum chamber and working distance. The beam profiles were measured with a CsI phosphor screen (125 mm×95 mm×2 mm alumina plate coated with CsI) in a working distance of about 115 mm and the beam currents were measured with a Faraday cup (fabricated at GSI, 6 cm in diameter) on the opposite site of the ion gun in a working distance of about 317 mm.
In general, the beam current was measured against the variation of magnetron current, anode potential and extraction potential. At specific parameters, the phosphor screen was moved in front of the Faraday cup into the ion beam to measure the beam profile. Nitrogen gas was used to operate the ion gun. The gas flow was increased first for enough molecules to ignite the plasma and the chamber pressure was kept fixed at 3×10^{-4} mbar. The Faraday cup was polarized to suppress sec-

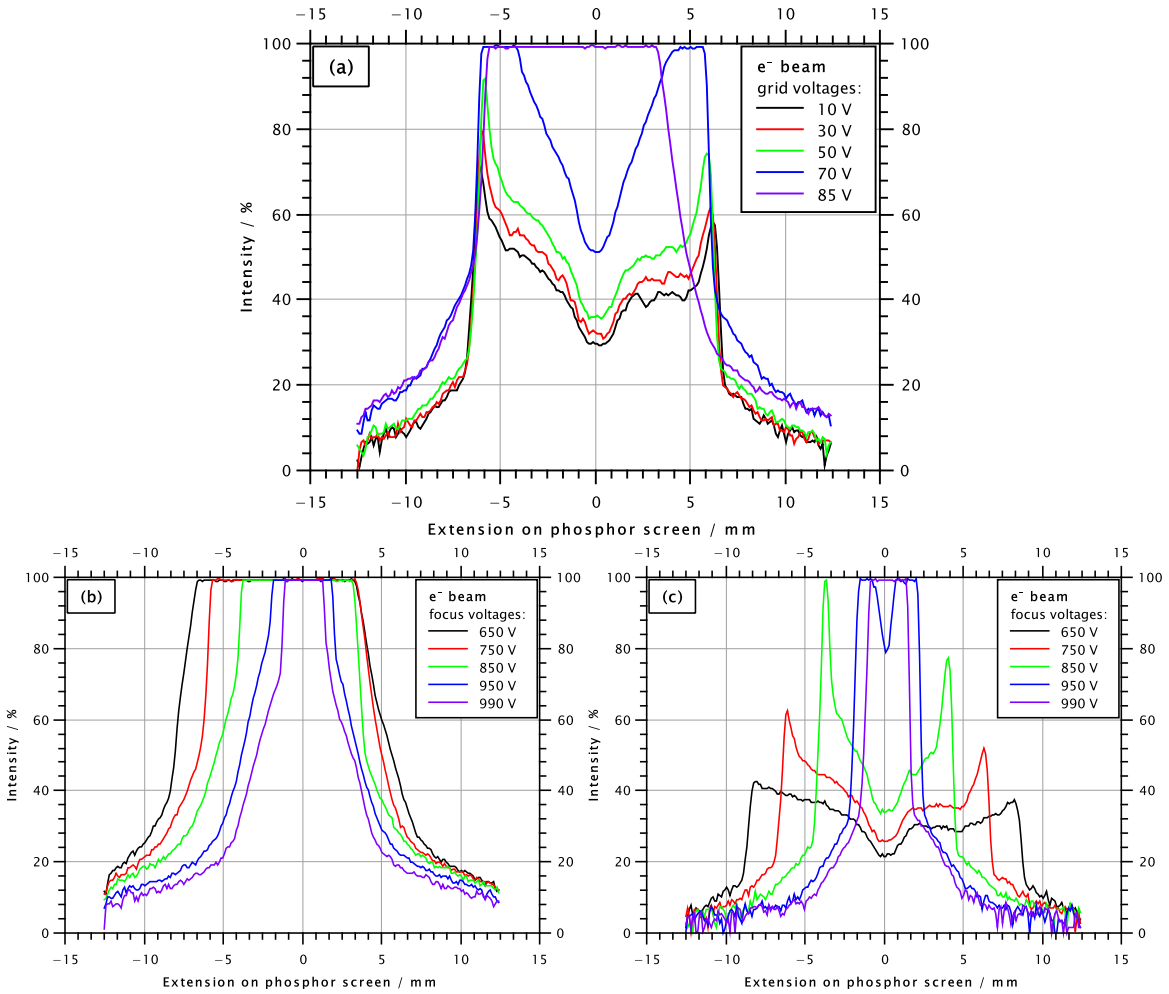

Figure 3.7: Beam profiles taken with different electron gun parameters at beam energy of 1500 eV: a) variation of grid voltage between 10 V and 85 V at focus voltage of 750 V, b) variation of focus voltage between 650 V and 990 V at grid voltage of 83 V and c) variation of focus voltage between 650 V and 990 V at grid voltage of 0 V.

ondary electrons. For the measurement of the beam current against the magnetron current, the anode potential was adjusted to 3.3 kV and the extraction voltage was adjusted to −0.9 kV. The current on the cup was limited to a maximum of 175 µA. A diagram of the measured current against the magnetron current is illustrated in Fig. 3.9a). Beam profiles were taken at magnetron currents of 6 mA, 12 mA and 20 mA as shown in Fig. 3.9b). The beam profiles were evaluated in the non-tilted axis after subtraction of the background fluorescence of the phosphor screen.

In another measurement the magnetron current was adjusted to 20 mA and extraction potential was kept at −0.9 kV. The anode potential was varied between 0.1 kV and 4 kV. The current on the cup was limited to a maximum of 163 µA. For a measurement of currents against even higher anode potentials, the extraction potential was increased to −1.1 kV and current on the cup was limited to a maximum

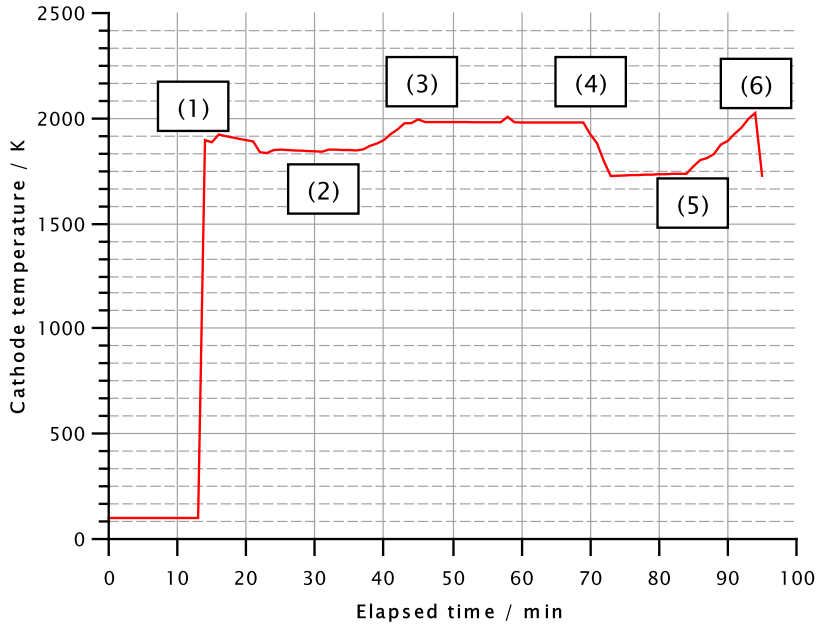

Figure 3.8: Cathode temperature of the electron gun during the measurements shown in Fig. 3.7. At (1), the source voltage is applied slowly to deliver an emission current of 10 µA. The cathode warms up and cathode temperature decreases a bit at (2). Then the grid voltage is slowly increased to 85 V at (3). At (4) grid voltage is turned off again and the cathode temperature decreases again from 2000 K to about 1700 K. At (5), grid voltage is increased to 83 V again and the cathode temperature rises to 2000 K. At (6), the source voltage is turned off.

of 109 µA. Then the anode potential was varied between 0.2 kV and 5 kV. Beam profiles were taken in the first measurement at 1.5 kV, 3 kV, 3.4 kV and 4 kV and in the second measurement at 1.4 kV, 2.6 kV, 3.6 kV, 4.5 kV and 5 kV. The diagram of the measured current against anode potential for different extraction potentials is given in Fig. 3.10a). The corresponding beam profiles are shown in Fig. 3.10b) for extraction potential of −0.9 kV and in Fig. 3.10c) for extraction potential of −1.1 kV.

In the last measurement the magnetron current was kept at 20 mA and the anode potential was adjusted to 3.7 kV. The extraction potential was varied between 0 kV and 2 kV. The current on the cup was limited to a maximum of 164 µA. Beam profiles were taken at extraction potentials of 0.3 kV, 0.8 kV, 1.1 kV and 1.9 kV. The diagram of the measured current against extraction potential is given in Fig. 3.11a). The corresponding beam profiles are shown in Fig. 3.11b).

3.5.3 Discussion on beam parameters

Electron beams

Electron beam spot diameters of 2 mm to 4 mm can be achieved with electrons in an energy range of 500 eV to 1500 eV. A small spot size is ideal to obtain a maximum

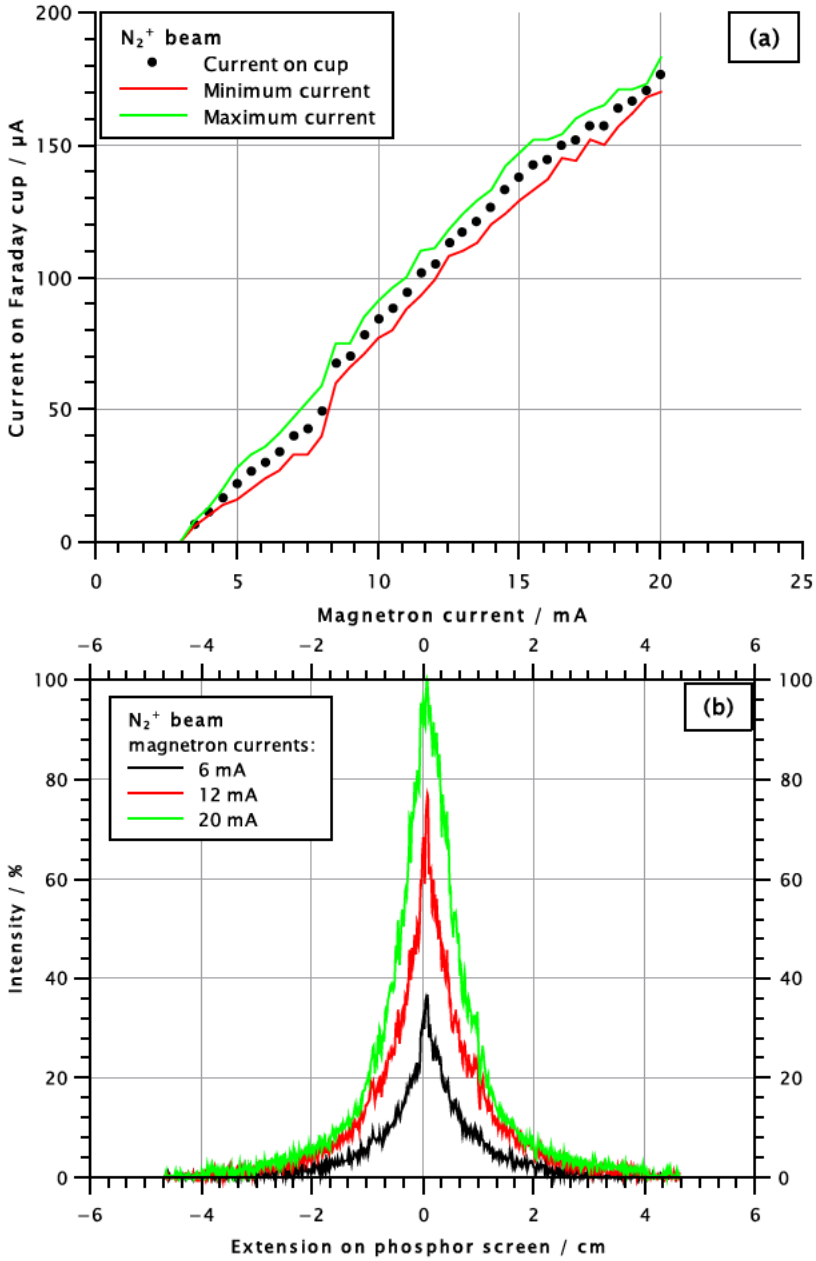

Figure 3.9: The measured current on Faraday cup against magnetron current of the ion gun with the anode potential at 3.3 kV and extraction voltage of −0.9 kV is shown in a). The red and green line represent the lowest and highest measured currents, respectively. The evaluated beam profiles are shown in b). They are presented as a function of the fluorescence intensity against the extension to the center of the screen. (For interpretation of the references to color in this figure legend, the reader is referred to the web version of this article.)

of deposited energy and flux per unit area and time. The scanning function of the electron gun allows irradiating areas that are larger than the spot diameter. The beam spot size and profile can be altered by varying the grid voltage (see Fig. 3.7b)

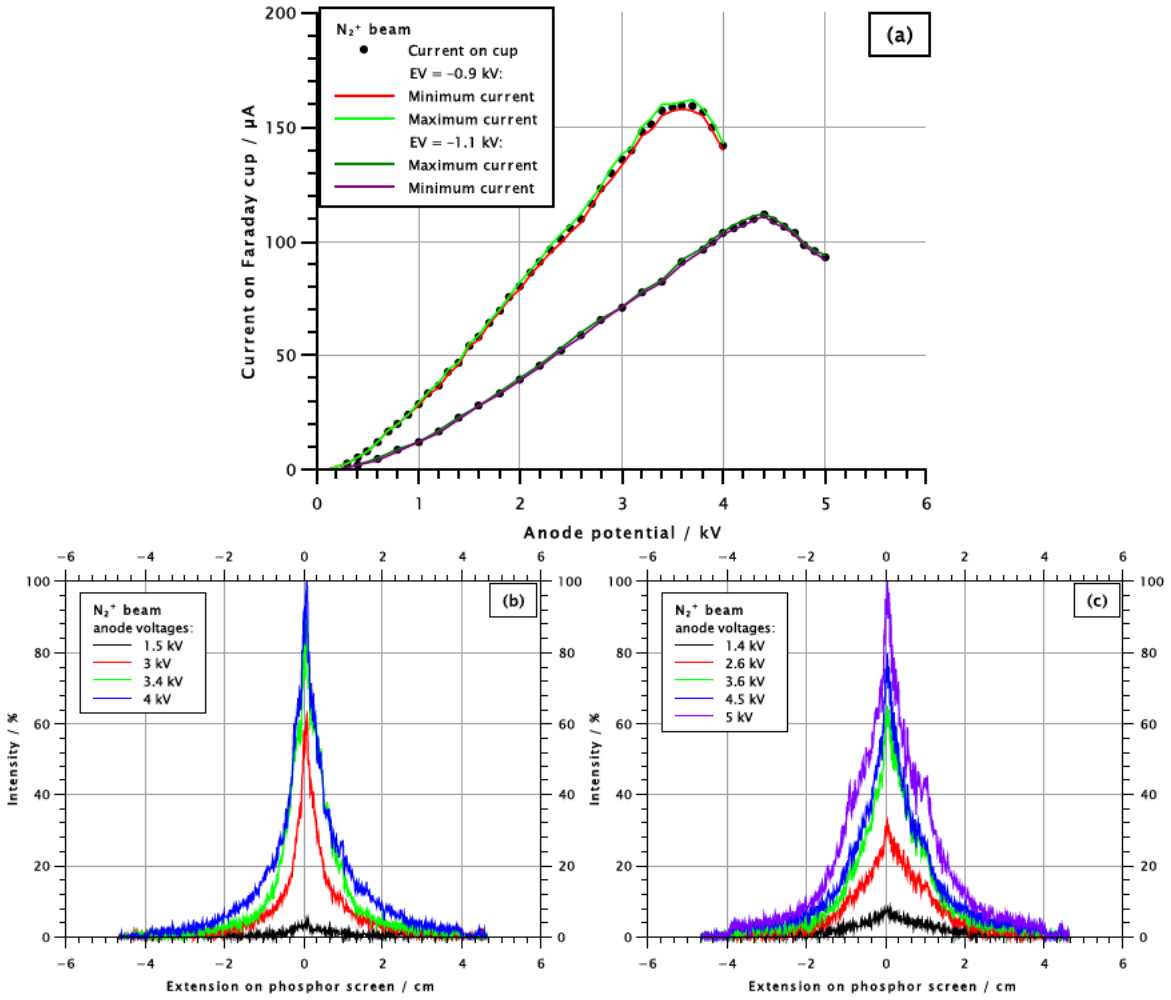

Figure 3.10: a) Measured current on Faraday cup against anode voltage of the ion gun is shown for a magnetron current of 20 mA and extraction voltages (EV) of −0.9 kV and −1.1 kV. The lines represent the lowest and highest measured currents, respectively. The evaluated beam profiles as a function of the fluorescence intensity against the extension to the center of the screen are shown for extraction voltages of −0.9 kV in b) and −1.1 kV in c).

and Fig. 3.7c)). In this way, the profile can be smoothed, and the influence of space charge effects can be reduced. For 1500 eV electrons, the ideal grid voltage was found to be 83 V. At voltages above 90 V, the beam is completely suppressed.

Ion beams

The effects of i) magnetron current, ii) anode potential, and iii) extraction potential on ion current and beam profile were studied for nitrogen ions. The beam current varies proportionally to the magnetron current (see Fig. 3.9a)). The beam current intensity depends on the anode and extraction potentials; the maximum current is obtained at 3.7 kV anode potential and 1 kV extraction potential. The corresponding

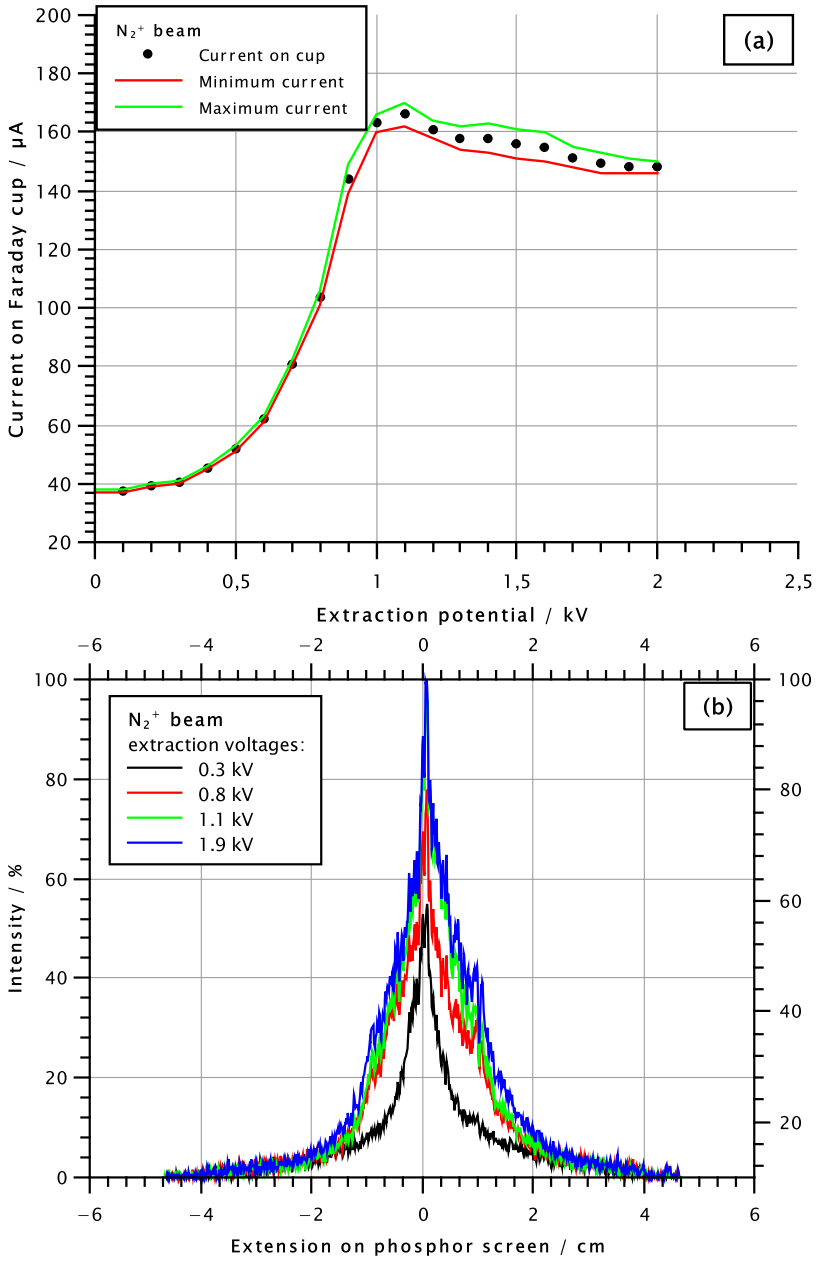

Figure 3.11: a) Measured current on Faraday cup against extraction voltage of the ion gun is shown for a magnetron current of 20 mA and anode potential of 3.7 kV. The lines represent the lowest and highest measured currents, respectively. The evaluated beam profiles as a function of the fluorescence intensity against the extension to the center of the screen are shown for an anode potential of 3.7 kV in b).

beam spot diameter is about 1 cm. In contrast to the electron beam, the ion beam cannot be scanned across the target area. Therefore, a variation of the beam spot size is the only option to change the irradiated area. To this end, the potential can be set to lower values than 3.7 kV and 1 kV, which will increase the beam spot size, at the expense of a reduced intensity.

3.6 First commission and irradiation of samples

3.6.1 Theoretical stopping powers and ranges of projectiles in matter

With the given electron and ion energies provided by the gun systems in ODIn, the different stopping powers and ranges in matter can be estimated. The software SRIM-2013 [19, 20] provides stopping powers and ranges for ions and target materials up to uranium. For stopping powers and ranges of electrons in matter, the National Institute of Standards and Technology (NIST) provides a database [21, 22] for many different pure element as well as common target materials like lead oxide or uranium oxide. Table 3.1 and table 3.2 give some total stopping powers and ranges of electron beams, light ion (hydrogen) and heavy ion (xenon) beams, which can be produced at ODIn, in exemplary target materials like amorphous carbon, metallic lead and uranium. The stopping powers and ranges in matter are given for the maximum beam energies which can be produced at ODIn.
The given values indicate that only deposits with a thickness lower than 100 µg cm^{-2} can be irradiated completely with the electron and ion beams provided by ODIn. With H^+ beams, the CSDA range is at its maximum with 260 µg cm^{-2} for metallic lead and at 220 µg cm^{-2} for metallic uranium. Therefore, H^+ beams seem to be most promising with respect to the ranges in matter. For ion beams of heavier gasous species, the stopping powers rise and the ion beams will probably induce more sputtering than transformations on the chemical species and will destroy the deposit. Sputtering could be used to remove organic impurities on the surface of the deposits.

Target material	Total stopping powers for different beams (MeV cm^2 g^{-1})		
	electron beam (1.5 keV)	H^+ beam (5 keV)	Xe^+ beam (5 keV)
Carbon (amorphous)	80.6	308.6	5773
Lead (metal)	15.6	35.26	978.1
Uranium (metal)	13.7	41.77	830.3

Table 3.1: Theoretical total stopping powers of different beams provided by the ODIn setup in three exemplary target materials. The values are given for the maximum beam energies which can be provided at ODIn. Data for electron and proton beams are taken from the NIST database [21, 22]. The data for Xe beams were calculated with SRIM-2013 [19, 20].

3.6.2 Irradiation tests of Pb samples

In a first irradiation test performed to commission the setup, molecular plated lead samples were irradiated with electron beams at 1500 eV and 100 µA emission

Target material	CSDA (continuous-slowing-down approximation) ranges in matter for different beams (mg cm^{-2})		
	electron beam (1.5 keV)	H^+ beam (5 keV)	Xe^+ beam (5 keV)
Carbon (amorphous)	<0.28	0.025	0.0016
Lead (metal)	<0.83	0.26	0.0041
Uranium (metal)	<0.89	0.22	0.0044

Table 3.2: Theoretical ranges in matter of different beams provided by the ODIn setup in three exemplary target materials. The values are given for the maximum beam energies which can be provided at ODIn. Data for the electron and proton beams are taken from the NIST database [21, 22]. The data for Xe beams were calculated with SRIM-2013 [19, 20].

current. This section is meant to give a short report of the first irradiation with ODIn. Further analytical investigations of the sample will be described elsewhere.

Reagents and materials

145.7 mg of lead nitrate (Sigma-Aldrich, 99.0 %) were dissolved in 10 mL of 0.1 M nitric acid, to give a concentration of 44 mmol L^{-1}. An aliquot of 20 µL was filled into the plating cell and was mixed with 1 mL of isopropanole and 9 mL of isobutanole. A round Kapton foil (Goodfellow, Polyimid - Film DuPont™ Kapton®, 25 µm thickness) with a diameter of 25 mm was cleaned with isopropanole, dried at air and then sputter coated with about 34 nm of gold on both sides. It was used as cathode. A palladium wire (Goodfellow, +99.99 %, 1 mm thickness) was used as anode.

Instrumentation and methods

Molecular Plating was performed in an upright cylindrical cell with 1.15 kV and 0.6 mA for 45 min. The contact area on the substrate (Kapton foil with gold coating) was 0.5 cm^2. After the plating process, the sample was dried at air in the fume hood for 24 h. Two identical samples were prepared by this method to have one sample for comparison after irradiation of the other one. In case of a 100 % yield in the molecular plating process, the deposit thickness is about 365 µg cm^{-2} which is about 59.4 µm.
The sample was carefully fixed on the sample holder in ODIn with conductive tape. It was irradiated with 1.5 keV electron beam and emission current of 100 µA with focus on the surface of the deposit. The focus voltage was at 990 V and grid voltage at 0 V. The spot diameter was about 3 mm. Due to a voltage on the deflection

electrodes during scanning and the angle of 45 ° on the sample surface, the beam spot shape was slighty deformed to a triangle. After a short moment, the surface turned dark at the spot where the focused beam impacted. The beam was then scanned slowly over the complete deposit surface until it turned completely dark by visual observation. The whole irradiation with an irradiance or flux density of about 2.1 W cm^{-2} took about an hour with an approximated deposited energy of 4.74×10^{16} MeV cm^{-2}. For electron gun power $\dot{Q}$ of 0.15 W, a thermal conductivity λ of the Kapton foil of 0.4 W m^{-1} K^{-1}, a beam spot radius r of 1.5 mm and the thickness of the Kapton foil d of 25 µm, the difference of temperature ΔT between the irradiated deposit and the sample holder can be calculated with Fourier's law

$$\dot{Q} = \lambda \cdot \pi \cdot r^2 \cdot \frac{\Delta T}{d} \tag{3.1}$$

and is about 1.3 K considering thermal conduction.

Results and Discussion

Both the non-irradiated and the irradiated sample were investigated with a light microscope (VHX-7000, Keyence). The surface of the irradiated deposit turned black during the irradiation with the 1.5 keV electron beam. The range of the electron beam into the deposit should be about 14 µm with respect to a stopping power of 17.43 MeV cm^2 g^{-1} (in lead oxide) [21]. Therefore, the beam was completely stopped in the deposit. The change in color indicates that a chemical or a crystal transformation occurred. The induced structural changes were investigated by confocal Raman spectroscopy (HR800 system, Horbia Jobin Yvon, λ_0 : 633 nm). The spectrometer was calibrated with a silicon sample. The microscopic pictures with three magnifications and the Raman spectra of both samples are shown in Fig. 3.12. The spectra indicate a chemical transformation from lead carbonate [23] to lead(II) oxide [24]. The observed changes in colour agree well with coulomb barrier irradiations of similar produced lead targets at UNILAC. A detailed follow-up spectroscopic investigation and comparison of lead targets irradiated off-line at ODIn and on-line at UNILAC is on its way. The investigation will show if it is possible to investigate the radiation-induced chemical reactions in target materials even without beam time at particle accelerators.

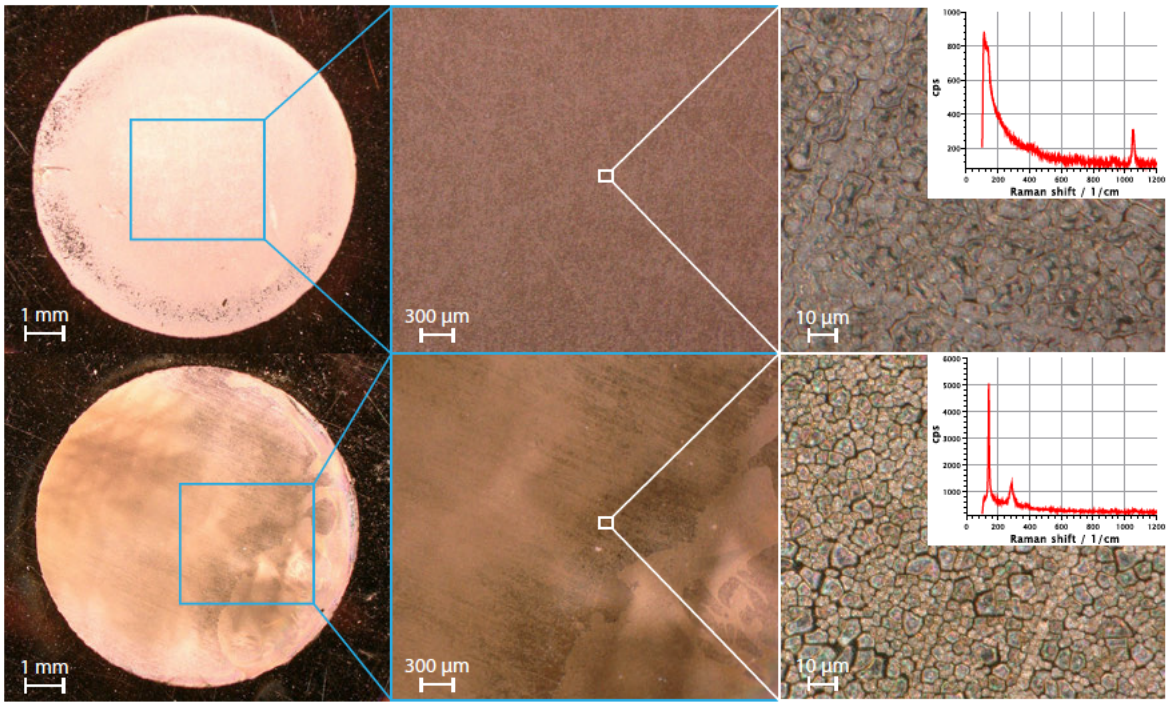

Figure 3.12: Optical microscope pictures of the non-irradiated lead sample (top) and of the electron-irradiated sample (bottom). The inset in the right-most pictures displays Raman spectra of the samples. These were recorded with a 633 nm excitation wavelength at 16 mW, using spectral autofocus. The change in the spectra indicates a chemical transformation of lead carbonate [23] to lead(II) oxide [24]. (For a colored high-resolution figure, the reader is referred to the web version of this article.)

3.7 Conclusion and Outlook

A new setup, named ODIn, was successfully constructed for the irradiation of samples with low energy electron and ion beams, characterized with regard to the electron gun and ion gun and tested for the first time with a molecular plated lead sample. The electron gun can generate up to 1.5 keV electron beams with up to 100 µA beam current. The spot diameters of the electron beam and beam profiles of the electron gun were investigated with a phosphor screen. Minimum spot diameters of 2 mm to 4 mm in diameter can be produced depending on the electron energy. The beam profile can be adjusted with the grid voltage from a nearly uniform to a Gaussian profile. Furthermore, the ion gun was characterized and the dependency of the beam current on different magnetron currents, anode voltages and extraction voltages was investigated. Also the beam profiles were investigated with a phosphor screen and they are more lorentzian shaped with a FWHM of about 2 mm to 3 mm. The complete setup can be controlled by remote with a delivered LabVIEW software for the electron gun and an Arduino-based remote control for the ion gun. The first irradiation of a lead sample with 1.5 keV electron beams showed

a visible changed on the deposit surface indicated by a change of color from orange to black. Raman analysis showed a chemical transformation of lead carbonate to lead(II) oxide. In future experiments, the irradiated samples of ODIn will be compared with samples irradiated with Coulomb-barrier heavy-ion beams at the UNILAC accelerator at GSI in Darmstadt and with samples irradiated with proton beams of tens of MeV energy at the IGISOL facility in Jyväskylä. Investigations of the chemical and crystal transformations on the surface of irradiated samples are currently ongoing, using analytical methods like Raman spectroscopy, scanning electron microscopy (SEM) as well as atomic force microscopy (AFM). These studies will help shedding light on the processes taking place in thin films irradiated with low energy particles. New insights into the chemical behavior of conventional target materials in the particle beam could be an important intermediate step in the development of new targets for the future generation of accelerators.

3.8 References

[1] W. Parker, R. Falk, Nuclear Instruments and Methods 16 (1962) 355–357.

[2] N. Trautmann, H. Folger, Nuclear Instruments and Methods in Physics Research Section A: Accelerators, Spectrometers, Detectors and Associated Equipment 282 (1989) 102–106.

[3] L. von der Wense, B. Seiferle, M. Laatiaoui, J. B. Neumayr, H.-J. Maier, H.-F. Wirth, C. Mokry, J. Runke, K. Eberhardt, Ch. E. Düllmann, N. G. Trautmann, P. G. Thirolf, Nature 533 (2016) 47–51.

[4] A. Vascon, S. Santi, A. Isse, T. Reich, J. Drebert, H. Christ, Ch. E. Düllmann, K. Eberhardt, Nuclear Instruments and Methods in Physics Research Section A: Accelerators, Spectrometers, Detectors and Associated Equipment 696 (2012) 180–191.

[5] A. Vascon, S. Santi, A. Isse, A. Kühnle, T. Reich, J. Drebert, K. Eberhardt, Ch. E. Düllmann, Nuclear Instruments and Methods in Physics Research Section A: Accelerators, Spectrometers, Detectors and Associated Equipment 714 (2013) 163–175.

[6] A. Vascon, N. Wiehl, T. Reich, J. Drebert, K. Eberhardt, Ch. E. Düllmann, Nuclear Instruments and Methods in Physics Research Section A: Accelerators, Spectrometers, Detectors and Associated Equipment 721 (2013) 35–44.

[7] A. Mitu, M. Dumitru, R. Suvăilă, A. Oprea, I. Gheorghe, P. Mereută, S. Brajnicov, I. Burducea, N. M. Florea, N. Mărginean, T. Glodariu, M. Dinescu, G. C. –. Danil, Vacuum 161 (2019) 162–167.

[8] M. A. Garcia, M. N. Ali, N. N. Chang, T. Parsons-Moss, P. D. Ashby, J. M. Gates, L. Stavsetra, K. E. Gregorich, H. Nitsche, Nuclear Instruments and Methods in Physics Research Section A: Accelerators, Spectrometers, Detectors and Associated Equipment 613 (2010) 396–400.

[9] R. Haas, S. Lohse, Ch. E. Düllmann, K. Eberhardt, C. Mokry, J. Runke, Nuclear Instruments and Methods in Physics Research Section A: Accelerators, Spectrometers, Detectors and Associated Equipment 874 (2017) 43–49.

[10] M. Weigand, T. Heftrich, Ch. E. Düllmann, K. Eberhardt, S. Fiebiger, J. Glorius, K. Göbel, R. Haas, C. Langer, S. Lohse, Physical Review C 97 (2018) 035803.

[11] K. Eberhardt, Ch. E. Düllmann, R. Haas, C. Mokry, J. Runke, P. Thörle-Pospiech, N. Trautmann, AIP Conference Proceedings 1962 (2018) 030009.

[12] P. R. Watson, W. Loveland, P. M. Zielinski, K. E. Gregorich, H. Nitsche, Nuclear Instruments and Methods in Physics Research Section B: Beam Interactions with Materials and Atoms 226 (2004) 543–548.

[13] S. Hofmann, S. Heinz, R. Mann, J. Maurer, J. Khuyagbaatar, D. Ackermann, S. Antalic, W. Barth, M. Block, H. Burkhard, The European Physical Journal A 48 (2012) 62.

[14] J. D. Burns, K. G. Myhre, N. J. Sims, D. W. Stracener, R. A. Boll, Nuclear Instruments and Methods in Physics Research Section A: Accelerators, Spectrometers, Detectors and Associated Equipment 830 (2016) 95–101.

[15] D. Mayorov, E. Tereshatov, T. Werke, M. Frey, C. Folden, Nuclear Instruments and Methods in Physics Research Section B: Beam Interactions with Materials and Atoms 407 (2017) 256–264.

[16] C. L. Tracy, M. Lang, F. Zhang, C. Trautmann, R. C. Ewing, Phys. Rev. B 92 (2015) 174101.

[17] L. Breuer, P. Ernst, M. Herder, F. Meinerzhagen, M. Bender, D. Severin, A. Wucher, Nuclear Instruments and Methods in Physics Research Section B: Beam Interactions with Materials and Atoms 435 (2018) 101–110.

[18] Kimball Physics Inc., EFG-7 / EGPS-1017 datasheet, https://www.kimballphysics.com/electron-gun-specs-efg-7-egps-1017, [Online; accessed 25-October-2019] (2016).

[19] J. F. Ziegler, M. Ziegler, J. Biersack, Nuclear Instruments and Methods in Physics Research Section B: Beam Interactions with Materials and Atoms 268 (2010) 1818–1823.

[20] James F. Ziegler, SRIM - The Stopping and Range of Ions in Matter, https://www.srim.org/, [Online; accessed 25-October-2019] (2013).

[21] M. J. Berger, J. S. Coursey, M. A. Zucker, J. Chang, Stopping-Power & Range Tables for Electrons, https://physics.nist.gov/PhysRefData/Star/Text/ESTAR.html, [Online; accessed 25-October-2019] (2017).

[22] M. J. Berger, J. S. Coursey, M. A. Zucker, J. Chang, Stopping-Power & Range Tables for Protons, https://physics.nist.gov/PhysRefData/Star/Text/PSTAR.html, [Online; accessed 25-October-2019] (2017).

[23] L. Burgio, R. J. H. Clark, Spectrochimica Acta Part A: Molecular and Biomolecular Spectroscopy 57 (2001) 1491–1521.

[24] L. Burgio, R. J. H. Clark, S. Firth, Analyst 126 (2001) 222–227.

Chapter 4

Publication III: Towards ^{233}U monolayer recoil ion sources

The following article was submitted as full article to *Radiochimica Acta* in 2020. The preprint is available on arXiv (arXiv:2004.02571). It deals with the production of very thin ^{233}U recoil ion sources by four different methods and their quantitative as well as qualitative characterization. Additionally, simulations were performed to investigate the influence of source characteristics on the resulting alpha spectra. The gained insights will be used for the production of recoil ion sources in the TACTICa experiment.

4.1 Own contributions

The theoretical calculations, SRIM and AASI simulations and the writing of the paper were performed self-directed. The mixed fit routine for a multiplett consisting of three peaks was developed and applied manually for all spectra. The production of the sources and their characterization was performed self-directed or by supervision.

Alpha spectrometric characterization of thin ^{233}U sources for $^{229(m)}Th$ production

R. Haas[1,2,3], M. Hufnagel[1], R. Abrosimov[1], Ch. E. Düllmann[1,2,3], D. Krupp[4], C. Mokry[1,2], D. Renisch[1,2], J. Runke[1,3], U. W. Scherer[4]

4.2 Abstract

Four different techniques were applied for the production of ^{233}U alpha recoil ion sources, providing ^{229}Th ions. They were compared with respect to a minimum energy spread of the ^{229}Th recoil ions, using the emitted alpha particles as an indicator. The techniques of Molecular Plating, Drop-on-Demand inkjet printing, chelation from dilute nitric acid solution on chemically functionalized silicon surfaces, and self-adsorption on passivated titanium surfaces were used. All fabricated sources were characterized by using alpha spectrometry, radiographic imaging, and scanning electron microscopy. A direct validation for the estimated recoil ion rate was obtained by collecting ^{228}Th recoil ions from ^{232}U recoil ion sources prepared by self-adsorption and Molecular Plating. The chelation and the self-adsorption based approaches appear most promising for the preparation of recoil ion sources delivering monochromatic recoil ions.

4.3 Introduction

Radioactive sources of alpha-decaying or spontaneously fissioning radionuclides are used in many experiments in nuclear chemistry and nuclear physics as a source for their daughter nuclei. In alpha-decaying recoil ion sources, the daughter nuclei are emitted from thin active layers owing to the short residual range of the daughters in matter. Such recoil ion sources were recently used in physics experiments, e.g., for investigations of the nuclear clock isomer ^{229m}Th [1–3] and for optimizations of the extraction of short-lived isotopes in buffer gas cells [4, 5]. The ^{233}U is used as example nuclide in the source fabrication, as it is of high current interest due to the production of ^{229m}Th and will be used as a recoil ion source in the experiment of the TACTICa[5] collaboration [6–8]. In the TACTICa experiment, the $^{229(m)}Th$ recoil ions will be decelerated by an electric field to less than 1 keV kinetic energy to allow their trapping in a linear Paul trap. In contrast to the approach employed,

[1]Department Chemie, Johannes Gutenberg-Universität Mainz, 55128 Mainz, Germany
[2]Helmholtz-Institut Mainz, 55128 Mainz, Germany
[3]GSI Helmholtzzentrum für Schwerionenforschung GmbH, 64291 Darmstadt, Germany
[4]Institut für Physikalische Chemie und Radiochemie, Hochschule Mannheim - University of Applied Sciences, 68163 Mannheim, Germany
[5]Trapping And Cooling of Thorium Ions with Calcium

e.g. in [1–3], where recoil ions were thermalized in buffer gas, stringent vacuum requirements and the desire to retain the initial charge state distribution [8] render purely electrostatic deceleration favorable for TACTICa. Ideal recoil ion sources for application in TACTICa consist of a monolayer of the mother nuclide ^{233}U to gain a high recoil efficiency with a minimal energy dispersion of the recoil ions. Due to the approximately fixed areal density of a monolayer, the activity of such an ion source is defined by the active area.
Different methods exist to fabricate targets or radioactive sources in many different geometries and thicknesses. A well established method is the Molecular Plating (MP) technique [9]. This method was well characterized and enhanced by Vascon et al. to fabricate smooth crack-free large-area thin films of alpha particle emitting ^{147}Sm [10]. These layers were investigated with X-ray photoelectron spectroscopy (XPS) and alpha spectrometry and showed that specific MP parameters, like the choice of plating solvent and the roughness of the substrate, lead to effects which influence the recoil efficiency and energy dispersion of the alpha-recoil ions. The thickness and morphology of the produced salt layer as well as cracked solvent fragments deposited on top of the radioactive source proved to influence the relative alpha detection efficiency by as much as 15 % [11]. Such alpha detection losses imply a critical influence on the recoil efficiency of the alpha daughter ions and their energy distribution. The MP technique needs further developments to fabricate more efficient recoil ion sources.
A novel fabrication technique is the Drop-on-Demand ink-jet printing method (DoD) [12], which is able to deposit dissolved material onto a variety of solid surfaces and is not restricted to electrically conducting substrates. It has a high printing accuracy as well as a reliable reproducibility of the deposited material [12]. This method has not yet been used to fabricate recoil ion sources consisting of a few atomic layers. Printing as well as solution parameters are well adjustable and, therefore, it should be possible to produce recoil ion sources suitable for application in, e.g. the TACTICa experiment.
In contrast to MP and DoD, where the material adheres mainly to the substrate by physisorption, there are two other possible ways to achieve effectively a monolayer of radionuclides, which is chemisorbed to the substrate. Krupp et al. developed a method to functionalize silicon surfaces of, e.g. passivated implanted planar silicon (PIPS) detectors for alpha spectrometry [13]. The silicon surfaces are functionalized with sulfonic acid groups, which chelate radionuclides from an acid solution. The chelation creates a chemisorption of the radionuclides, so that the surface can be rinsed afterwards with distilled water to remove non-bound radionuclides without loosing bound material. Theoretically, a saturated functionalized surface contains a single layer of radionuclides and seems promising for the production of ideal recoil ion sources.
Another way to produce chemisorbed monolayer films is to make use of the chemical equilibrium of radionuclides in solution on metal oxide surfaces, well

known as self-adsorption (SA) process. SA processes are well investigated for many radionuclides on a wide variety of metal oxides and soil material in the field of nuclear waste disposal [14–17]. Self-adsorption of thorium was used for the production of thin ^{229}Th films on CaF_2 surfaces [18] and is also promising for the production of ideal recoil ion sources for a high recoil efficiency with small kinetic energy dispersion of the emitted recoil ions.
In this article, the theoretical aspects of recoil ion sources concerning the stopping powers of alpha particles and recoil daughters in the source material as well as the achievable areal density of uranium depending on the fabrication method is discussed. Furthermore, Advanced Alpha spectrometric Simulations (AASI) [19–21] were performed for the investigation of the influence of different source parameters on the alpha spectra. The experimental and simulated spectra were parameterized using an adapted fit routine [22, 23] for a quantitative evaluation, allowing a comparison of recoil sources fabricated by different methods. At last, the recoil efficiencies were investigated of two sources produced by MP and SA by using the shorter-lived ^{232}U (half-life: 68.9 a).

4.4 Theoretical aspects

4.4.1 Stopping power in materials

The stopping powers of the alpha particles and the recoil daughter ions differ by about one order of magnitude. Furthermore, they depend on the chemical nature of the mother nuclide material. For the example nuclide ^{233}U (half-life: 1.59×10^5 a, E_α: 4824 keV (82.7 %), 4783 keV (14.9 %), 4729 keV (1.85 %)), the kinetic energy E_k of the ^{229}Th ions is about 84 keV while the alpha particle energy is about 4.8 MeV [derived from $E_k(^{229}\text{Th}) = Q_\alpha(^{233}\text{U}) - E_\alpha(^{233}\text{U})$, where Q_α is the Q-value of the alpha decay and E_α the kinetic energy of the alpha particle]. The stopping powers and ranges in different materials can easily be calculated with SRIM-2013 [24]. Due to the fact that the exact uranium compound is only known for DoD-produced sources, but not for the others, a number of different uranium compounds were used for the SRIM simulations. The stopping powers and ranges of both the ^{229}Th and the alpha particles in these compounds are given in Table 4.1 and Table 4.2. SRIM defines a monolayer of any material as 10^{15} atoms cm^{-2}. Therefore, the stopping powers describe the energetic loss per atomic layer. The data show how much more the ^{229}Th recoil ions are influenced by the mother nuclide material with ranges below 500 Å compared to the alpha particles with ranges above 10 µm in the same materials. Thus, alpha spectra of ^{233}U recoil ion sources cannot give detailed information on the kinetic energy distribution of the recoil ions. Even very thin sources with ten atomic layers of the mother nuclide material decelerate the emitted recoil ions by several keV. For a first semi-quantitative screening, a high-resolution alpha spectrum of an uranium recoil ion source allowing for a detailed evaluation

of the peak shape may give a hint about the thickness of the source, which can help determining the recoil efficiency and energy distribution of the thorium ions.

Table 4.1: Stopping powers and ranges of ^{229}Th recoil ions in different ^{233}U compounds. The initial kinetic energy of the recoil ions is set to 84 keV. The data were obtained with SRIM-2013 [24].

Compound	density / g cm^{-3} [25, 26]	Stopping Power of ^{229}Th / eV/(10^{15}atoms/cm^2)	Range / nm
$UO_2(OH)_2 \times H_2O$	5.0	348	28
UO_2CO_3	5.7	510	25
$UO_2(NO_3)_2$	2.8	457	45
UO_2	11.0	731	15
U_3O_8	8.4	664	19

Table 4.2: Stopping powers and ranges of alpha particles in different ^{233}U compounds. The maximum kinetic energy of the alpha particles is set to 4.824 MeV. The data were obtained with SRIM-2013 [24].

Compound	density / g cm^{-3} [25, 26]	Stopping Power of α-particle / eV/(10^{15}atoms/cm^2)	Range / µm
$UO_2(OH)_2 \times H_2O$	5.0	20.6	17.3
UO_2CO_3	5.7	29.5	15.6
$UO_2(NO_3)_2$	2.8	27.5	28.9
UO_2	11.0	43.1	10.7
U_3O_8	8.4	38.9	13.1

4.4.2 Theoretical areal density

As previously mentioned, a single layer of any material is defined in SRIM-2013 as 10^{15} atoms cm^{-2}, which is too crude for an approximation of all elements in one layer in order to be directly applicable in the present case. As an example, an areal density of about 2.23×10^{14} atoms cm^{-2} is calculated for a monolayer of uranium atoms in uranium dioxide. The areal uranium densities of this and other materials are given in Table 4.3. As the true chemical species and crystal structure is difficult to investigate for sources prepared by MP and DoD, a value of 10^{14} atoms cm^{-2} will be used for further discussions and for the calculation of the concentration of

solutions as used in the experimental section. The estimation of an areal uranium density gets more complicated for methods like chelation by sulfonic acid groups and SA, because there the areal uranium densities depend on the density and availability of binding partners on the surface of the substrate.

Table 4.3: Calculated areal uranium densities in various compounds. Basis of the calculations are crystal structure data from [25, 26].

Compound	areal uranium density / 10^{14} atoms cm^{-2}
$UO_2(OH)_2 \times H_2O$	1.41
UO_2CO_3	0.32
$UO_2(NO_3)_2$	0.51
UO_2	2.23
U_3O_8	0.93

For the chelation method, the areal density of sulfonic acid groups is important. An areal uranium density of about 4×10^{15} atoms cm^{-2} is achievable on PIPS detectors functionalized in that way [13]. For SA, the density of oxygen binding partners on the surface of the substrate influences the amount of adsorbed uranium atoms. Investigations in the field of nuclear waste disposal have shown the highest adsorption rate of uranium for titanium dioxide [17]. These investigations were always performed with titanium dioxide colloids, whereas source fabrication is performed on a titanium foil, which provides a lower density of oxygen binding partners than colloids do. To increase the source activity, the density of these binding partners can be increased, e.g., by passivation. There are several methods to achieve titanium passivation, e.g., by anodic oxidation or by heating [27]. Thermal treatment allows investigating the adsorption yield (and thus the achievable areal uranium density) by specifically producing one of two obtainable titanium dioxide modifications. This is carried out by the irreversible transformation of anatase→rutile at temperatures >600 °C at atmospheric pressure [27, 28]. The exact transformation temperature depends on impurities in the titanium. D. Velten et al. found transformations for amorphous→anatase and anatase→rutile in sol-gel powder samples after heat treatment [27]. Anatase, the modification found naturally on a passivation layer of titanium, is the most promising species for high adsorption yields. The areal oxygen density of both, anatase and rutile, was calculated for some ideal crystal faces to derive an average number. Calculations based on crystal structure data [26, 29, 30] are given in Table 4.4. The mean areal density of oxygen atoms on the surface of anatase and rutile is similar and is about 1.3×10^{15} atoms cm^{-2}. Due to the large ionic radius and coordination sphere of uranyl ions in carbonate solutions [14, 17], the uranyl ion will be coordinated to two oxygen atoms on the surface. This leads to an U:O ratio of 1:3 to 1:2, corresponding

to a maximum areal uranium density of 6.5×10^{14} atoms cm^{-2} with SA. The real areal density of adsorbed uranium is probably lower due to defects in the crystal surface. 10^{15} atoms cm^{-2} of ^{233}U have an activity of 138 Bq cm^{-2}, corresponding to an emission rate of ^{229}Th ions into a 2π solid angle of about 69 ions s^{-1} cm^{-2}.

Table 4.4: Calculated areal densities (ad) of oxygen available for self-adsorption on ideal crystal faces of anatase and rutile based on crystal structure data from [26, 29, 30]. The Miller indices of the individual crystal faces are given. The areal densities of oxygen are given for each crystal face and as average values for each modification.

	lengths / Å	crystal face	ad / 10^{15} atoms cm^{-2}	mean ad / 10^{15} atoms cm^{-2}
Anatase	a: 3.785	(001)	1.40	1.18
	c: 9.514	(100)	1.11	
		(101)	1.02	
Rutile	a: 4.594	(001)	1.51	1.36
	c: 2.962	(110)	0.98	
		(100)	1.60	

4.5 Peak fit model and AASIFIT

Alpha spectrometry is an important radioanalytical technique for the quantitative and qualitative investigation of alpha-emitting radionuclide samples in environmental and nuclear research [31]. High-resolution spectra of high-quality sources help characterizing samples with regard to alpha-decaying impurities, isotopic compositions and even qualitative characteristics like thickness and homogeneity of the sample [23]. Often, nearby peaks in alpha spectra overlap at least partially. For the deconvolution and interpretation of such spectra, several peak fit models were developed and improved in the last decades. One of the most successful models to represent a mono-energetic alpha peak consists of a Gaussian joined with an exponential distribution [22, 32]

$$f(u-\mu;\sigma,\tau) = \frac{A}{2\tau}\exp\left(\frac{u-\mu}{\tau}+\frac{\sigma^2}{2\tau^2}\right)\operatorname{erfc}\left[\frac{1}{\sqrt{2}}\left(\frac{u-\mu}{\sigma}+\frac{\sigma}{\tau}\right)\right] \tag{4.1}$$

where A is the peak area, u is the distance to the peak position μ, σ is the standard deviation of the Gaussian and τ is the tailing parameter. This model was improved by subtraction of the long tail distribution and a mix of two exponential functions with different lengths, $\tau_1 < \tau_2$, and a normalized weighting factor η [33]. In the present case of monolayer alpha recoil sources, the peaks are expected to be very narrow and the long tail distribution is expected to be non-existent, in

which case it can be neglected. Therefore, equation 4.1 was modified with the normalized weighting factor η and by a sum of three functions for the present nuclide of interest, ^{233}U, showing a multiplet of the three significant peaks

$$F(u) = \sum_{i=1}^{2} \sum_{j=1}^{3} \eta_i f_j (u - \mu_i; \sigma_i, \tau_i) \qquad (4.2)$$
$$1 = \eta_1 + \eta_2$$

with individual peak positions μ_1, μ_2 and μ_3 and two shared standard deviations of the Gaussian σ and tailing parameters τ, each pertaining to all three peaks. This mixed function contains eight free parameters

$$\begin{aligned} F(u) = {} & [\eta_1 f_1 (u - \mu_1; \sigma_1, \tau_1) + (1 - \eta_1) f_1 (u - \mu_1; \sigma_2, \tau_2)] \\ & + [\eta_1 f_2 (u - \mu_2; \sigma_1, \tau_1) + (1 - \eta_1) f_2 (u - \mu_2; \sigma_2, \tau_2)] \\ & + [\eta_1 f_3 (u - \mu_3; \sigma_1, \tau_1) + (1 - \eta_1) f_3 (u - \mu_3; \sigma_2, \tau_2)] \end{aligned} \qquad (4.3)$$

which was used for the determination of the individual, characteristic tailing parameters η_1 and τ_1 of spectra from ^{233}U sources produced by the four different methods. The ^{233}U spectra were fitted with QtiPlot [34]. An example of the applied fit function is given in Fig. 4.1.
Furthermore, for the investigation of effects of different source characteristics on the alpha spectrum, e.g., the thickness and RMS roughness, the simulation and fitting software AASIFIT was provided by STUK, Finland [19–21]. Numerous parameters of the detector setup, the source material and dimensions can be set in the software to give iterative Monte Carlo-simulated alpha spectra. Experimental data can be loaded into the software and can then be fitted on the basis of simulated spectra of specific isotopes [21]. Effects of source layer thickness, root mean square (RMS) roughness, homogeneity and source material on simulated alpha spectra will be discussed in Section 4.9.

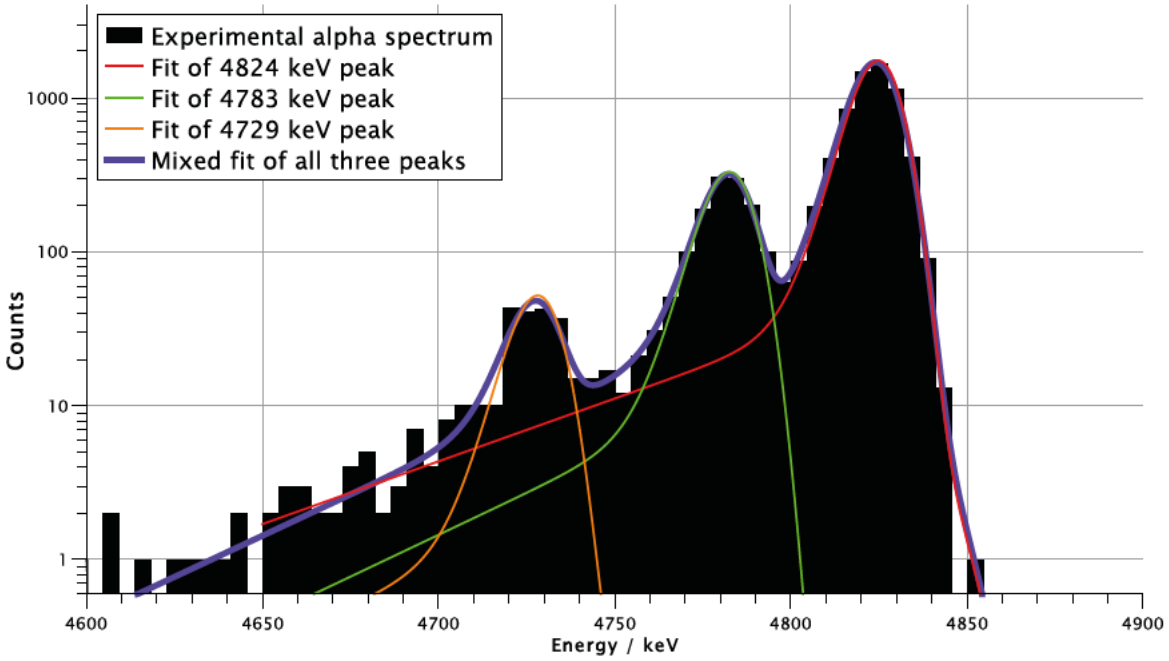

Figure 4.1: Exemplary QtiPlot fit of a 2k channel alpha spectrum of purified ^{233}U. A mixed fit including all three peaks of the multiplett (Eq. 4.3) as well as independent fits (Eq. 4.1) of the single peaks are shown.

4.6 Experimental

4.6.1 General instrumentation and methods

A light microscope (Bresser LCD Micro, 40x - 1600x magnification) was used for visual inspection of the sources. Scanning electron microscopy (SEM) was performed with a Philips XL 30 for the investigation of the topography of the sources in high resolution. Autoradiographic images (RI) weren taken with a Fujifilm FLA-7000 for information about the spacial distribution of radioactivity. Atomic force microscopy (AFM) was performed with a Semilab DS95 SPM System for the investigation of the topology (root mean square roughness) of the sources. For alpha spectrometry, different PIPS detectors and source-detector-distances were used for quantitative yield determination and for qualitative measurements. These are specified for each method in the following sections. A 16K channel analog-digital-converter (Canberra Nuclear Data ND581 ADC, used in 1K and 2K mode) with amplifier (Canberra 2015A AMP/TSCA) was used for data acquisition. A certified ^{241}Am source (Amersham Buchler, 290 Bq homogeneously distributed on an anodized aluminum disc with 16 mm in diameter and 150 µm thickness) was used for efficiency calibration of the used PIPS detectors.

4.6.2 Molecular Plating

Reagents and materials

A stock solution of column separated (in July 2017) ^{233}U as uranium nitrate in 0.1 mol L^{-1} HNO_3 (Merck, 65 %) with a concentration of 2.02 mg mL^{-1} was used for the preparation of all solutions. For MP, three solutions with concentrations of 38.9 µg mL^{-1}, 21.5 µg mL^{-1}, 5.25 µg mL^{-1} were prepared by dilution of aliquots from the stock solution in 0.1 mol L^{-1} HNO_3. Either N,N'-dimethylformamide (DMF) (Merck, 99.8 %) or a mixture of 10 % isopropanol (Merck, 99.8 %) and 90 % isobutanol (Merck, 99 %) was used as electrolyte in the plating cells. A palladium foil or a 1-mm thick palladium wire (>99.98 %) was used as anode. Silicon wafers (34 mm in diameter, 300 µm thickness) with a titanium coating (100 nm thickness) produced by magnetron sputtering as well as titanium foils (99.6 %, 25 mm in diameter, 25 µm thickness) were used as substrates. For cleaning of the titanium foils, distilled water, 6 mol L^{-1} HCl (Merck, 37 %), isopropanol and acetone (Merck, 99.5 %) were used.

Instrumentation and methods

For depositions on the titanium-coated silicon wafers, a horizontal cell design of A. Vascon et al. [10, 35] was used in combination with a HV power supply (Heinzinger LNC 3000-10 pos., 0 V to 3000 V, 0 mA to 10 mA). For depositions on the titanium foils, a vertical cell design [36] was used in combination with a different HV power supply (FUG MCP 350-1250, 0 V to 1250 V, 0 mA to 250 mA). Alpha spectra were recorded with a 2000 mm^2 PIPS detector (Canberra PD2000-40-300AM) in 5 mm distance for yield determination and a 25 mm^2 PIPS detector (Ortec ULTRA^{TM}, 11 keV FWHM intrinsic resolution) in 100 mm distance was used for recording high resolution spectra.

Source fabrication and characterization

The titanium foils were cleaned with 6 mol L^{-1} HCl, distilled water, isopropanol and acetone. The coated silicon wafers were cleaned with isopropanol to avoid damages to the titanium coating. An aliquot of 100 µL of the 5.25 µg mL^{-1} ^{233}U solution was mixed with 35 mL DMF using a vortex mixer for deposition on one silicon wafer. Another aliquot of 100 µL of the 34.4 µg mL^{-1} solution was mixed with 3.5 mL isopropanol and 31.5 mL isobutanol using a vortex mixer for deposition on another silicon wafer. For deposition on the titanium foils, aliquots of 20 µL of the 21.5 µg mL^{-1} solution were mixed with 1 mL isopropanol and 9 mL isobutanol. MP was performed at constant current of about 0.75 mA cm^{-2} for 1 h to 2 h. After deposition, the sources were carefully dried under an IR lamp in a fume hood. Alpha spectra for yield determination were taken with peak areas of at least 10^4 cts to reduce statistical counting errors below 1 %. Qualitative alpha spectra were taken

for several days to obtain adequate statistic. SEM pictures and RI were taken for visual inspection of the sources. Irradiation time for RI was about 2 h.

4.6.3 Drop-on-Demand inkjet printing

Reagents and materials

An aliquot of the stock solution was diluted to give three solutions with concentrations of 138 µg mL^{-1}, 74.2 µg mL^{-1} and 18.6 µg mL^{-1} of ^{233}U in 0.1 mol L^{-1} HNO_3 (Merck). Circular titanium foils (99.6 %, 34 mm in diameter, 25 µm thickness) were used as substrates. For cleaning of the titanium foils, distilled water, 6 mol L^{-1} HCl (Merck, 37 %), isopropanol, and acetone (Merck, 99.5 %) were used.

Instrumentation and methods

A DoD printer setup as described in [12] was used for printing. Tips with an inner diameter of 200 µm were used. Alpha spectra were recorded with a 2000 mm^2 PIPS detector (Canberra PD2000-40-300AM) in 5 mm distance for yield determination and a 25 mm^2 PIPS detector (Ortec ULTRA^{TM}, 11 keV FWHM intrinsic resolution) in 100 mm distance was used for recording high resolution spectra.

Source fabrication and characterization

Five sources were fabricated with a printing sequence containing 1413 drops within a circular area of 30 mm in diameter (see Fig. 4.2 (a)). For this, the 74.2 µg mL^{-1} solution and a drop volume of 5 nL at a stroke velocity of 100 µm ms^{-1} were used. Two additional sources were fabricated with a printing sequence containing 5637 drops within a circular area of 30 mm in diameter (see Fig. 4.2 (b)). Drop volume and stroke velocity were kept the same at 5 nL and 100 µm ms^{-1}, but the solutions with concentrations of 18.6 µg mL^{-1} and 138 µg mL^{-1} were used for these latter two sources. The sources were dried at air in the fume hood after fabrication. Alpha spectra, SEM pictures and RI were processed as described in section 4.6.2.

4.6.4 Chelation by sulfonic acid groups

Reagents and materials

An aliquot of the stock solution was diluted to give a solution with a concentration of 38.9 µg mL^{-1} of ^{233}U in 0.1 mol L^{-1} HNO_3 (Merck). Pieces of silicon wafers (300 µm thickness) in various forms with areas of about 6.4 mm^2 to 10 mm^2, functionalized with sulfonic acid groups according to [13], were used as substrates.

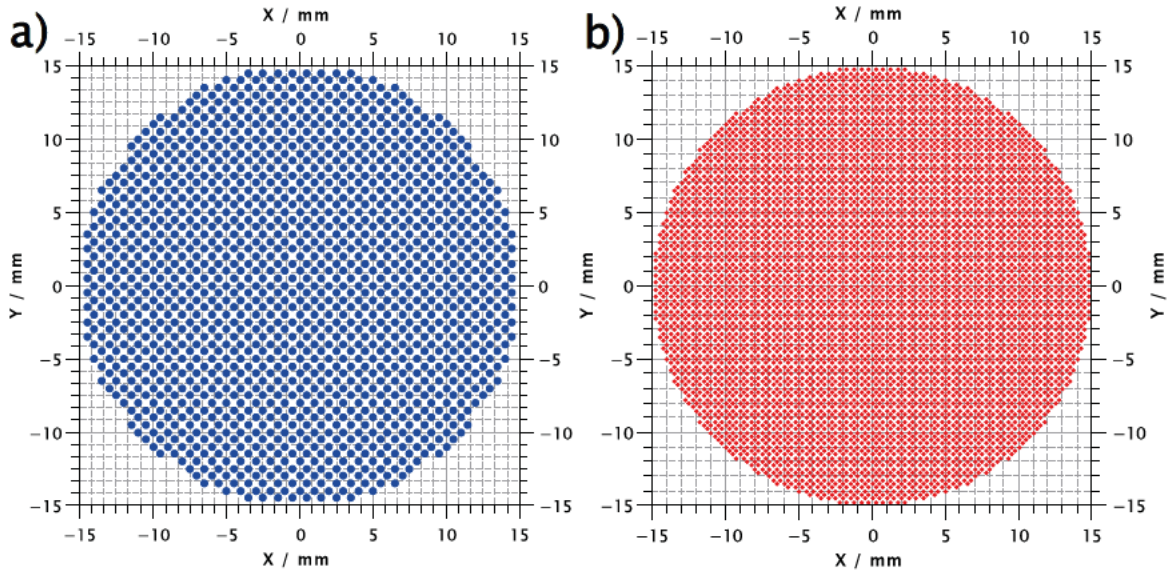

Figure 4.2: Printing sequences used for source fabrication. Panel a: Sequence containing 1413 coordinates. Panel b: Sequence containing 5637 coordinates. The distances between two coordinates are 0.7 mm (a) and 0.35 mm (b), respectively.

Instrumentation and methods

Alpha spectra were recorded with a 2000 mm^2 PIPS detector (Canberra PD2000-40-300AM) in 5 mm distance for yield determination and a 25 mm^2 PIPS detector (Ortec ULTRA^{TM}, 11 keV FWHM intrinsic resolution) in 100 mm distance was used for recording high resolution spectra.

Source fabrication and characterization

The functionalized wafers were placed in a crystallizing basin and covered with 10 mL of the ^{233}U solution. After 5 min, 15 min, 30 min, 60 min and 120 min the wafers were carefully removed from the solution, rinsed with distilled water and dried under an IR lamp. Alpha spectra, SEM pictures and RI were processed as described in section 4.6.2.

4.6.5 Self-adsorption

Reagents and materials

An aliquot of the stock solution was diluted with distilled water to give a concentration of 5.89 $\mu g\,mL^{-1}$ of ^{233}U. A titanium foil (99.6 %, 25 µm thickness) was used for preparation of the substrates. 0.1 $mol\,L^{-1}$ HNO_3 (Merck) was used for the adjustment of different pH values in the aqueous solutions. For cleaning of the titanium foils, distilled water, 6 $mol\,L^{-1}$ HCl (Merck, 37 %), isopropanol and acetone (Merck, 99.5 %) were used.

Instrumentation and methods

A muffle furnace (Nabertherm, LE 1/11/R7, max. 1100 °C) was used for thermal oxidation of the titanium foils at air. Alpha spectra were recorded with a 450 mm^2 PIPS detector (Ortec, CR-SNA-450-100) in 5 mm distance for yield determination and a 25 mm^2 PIPS detector (Ortec ULTRA^{TM}, CU-011-025-300, 11 keV FWHM intrinsic resolution) in 100 mm distance was used for recording high resolution spectra.

Source fabrication and characterization

In a first experimental series, solutions with different pH-values of 2 to 7 were generated as mixtures of 0.1 mol L^{-1} HNO_3 with distilled water. Pieces with dimensions of 10 mm x 10 mm were pretreated in the muffle furnace at 500 °C for one hour. The titanium pieces were put upright into small polyethylene flasks, containing a mixture consisting of 250 µL of the ^{233}U solution and 1 mL of the pH-adjusted solution, for one day. Afterwards, the titanium pieces were rinsed with distilled water and dried under an IR lamp in the fume hood. Yield determination was performed by alpha analysis of both sides of the titanium pieces as described in section 4.6.2.
In a second experimental series, Ti pieces with dimensions of 10 mm x 10 mm were thermally oxidized in the muffle furnace at different temperatures between 100 °C to 900 °C for one hour. The pieces were processed as described before in a solution with a pH value of 5. Yield determination was performed by alpha analysis of both sides of the titanium pieces as described in section 4.6.2. Three titanium foils, pretreated at temperatures of 20 °C, 450 °C, and 700 °C, were investigated by AFM. At last, two circular titanium foils with a diameter of 30 mm were processed at 450 °C and kept in ^{233}U solution at a pH value of 5. Another two titanium foils with the same dimensions were sand blasted in advance and processed exactly like the two other foils. Alpha spectra were recorded of one side of those foils. SEM pictures and RI were performed as described in section 4.6.2.

4.6.6 Investigation of the Th daughter recoil efficiency

Reagents and materials

A stock solution with 50 kBq of ^{232}U in 6.5 mL 0.1 mol L^{-1} HNO_3 (Merck) was evaporated under an IR lamp and dissolved again in 8 mol L^{-1} HCl (Merck). This process was repeated three times. A column (50 mm × 3 mm with Dowex AG 1x8 anion exchanger) was heated up to 55 °C and washed several times with 8 mol L^{-1} HCl. The ^{232}U solution was given onto the column and the daughter nuclides were eluted by 4 × 2 mL 8 mol L^{-1} HCl. The ^{232}U was stripped with 5 × 2 mL 0.5 mol L^{-1} HCl. The ^{232}U-containing eluate was evaporated to dryness again and the residue was dissolved in 1 mL HNO_3 solution at pH 5. Circular titanium foils

(Goodfellow, 99.6 %, 25 µm thickness, 25 mm in diameter) were used as substrates. For cleaning of the titanium foils, distilled water, 6 mol L^{-1} HCl (Merck, 37 %), isopropanol and acetone (Merck, 99.5 %) were used. A mixture of 10 % isopropanol (Merck, 99.8 %) and 90 % isobutanol (Merck, 99 %) was used as electrolyte for MP in the plating cells. A 1-mm thick palladium wire (>99.98 %) was used as anode for MP.

Instrumentation and methods

For depositions (SA and MP) on a limited area with 8 mm in diameter, a vertical cell design [36] was used. For MP, the cell was used in combination with a HV power supply (FUG MCP 350-1250, 0 V to 1250 V, 0 mA to 250 mA). Alpha spectra were recorded with a 450 mm^2 PIPS detector (Ortec CR-SNA-450-100) in 8 mm distance for yield determination and 450 mm^2 PIPS detectors (Canberra A450-18AM) in 50 mm distance inside an Alpha Analyst system (Canberra, Dual Alpha Spectrometer Upgrade Module 7200) were used for recording high resolution spectra with 4k channels.

Source fabrication and characterization

Self-adsorption

For the preparation of an SA source, a titanium foil was thermally oxidized in a muffle furnace for 1 h. Afterwards, it had a copper-colored surface. The oxidized titanium foil was fixed in the plating cell without a spacer disk. The ^{232}U solution was filled into the plating cell and Parafilm© was used to prevent evaporation. After 24 h, the solution was carefully removed with a pipette and the titanium foil was rinsed with distilled water and dried under an IR lamp.

Molecular Plating

For the preparation of the MP source, the residual solution was evaporated to dryness again and the residue was dissolved in 40 µL 0.1 mol L^{-1} HNO_3. The solution was mixed with 1 mL isopropanol and 9 mL isobutanol using a vortex mixer. A titanium foil was etched with 6 mol L^{-1} HCl and cleaned with distilled water, isopropanol and acetone. Both the titanium foil and the electrolyte solution were given into a plating cell and MP was performed at constant current of about 0.75 mA cm^{-2} for 2 h. After deposition, the source was carefully dried under an IR lamp in a fume hood. Alpha spectra for yield determination were taken of both sources with peak areas of at least 10^4 cts to reduce statistical counting errors below 1 %.

Recoil collection and investigation of the recoil efficiency

Both sources were kept in 5 mm distance to a titanium foil (25 mm in diameter) under vacuum at 8×10^{-3} mbar. Monte-Carlo simulations performed with AASI gave (30.9 ± 0.4) % of geometric efficiency for this setup. The collection times were 26 d for the SA source and 5.16 d for the MP source. After the collection, alpha spectra for yield determination were measured of both catcher foils with peak areas of at least 10^4 cts to reduce statistical counting errors below 1 %. Furthermore, qualitative alpha spectra were taken of both sources and the corresponding catcher foils.

4.7 Experimental results

4.7.1 Molecular Plating

The substrates, plating durations, deposit areas and quantitatively determined areal density of the MP sources are given in Table 4.5. The deposition area had a shiny surface. No material layer was observable with a light microscope. The qualitative alpha spectrum of source MP2 is shown in Fig. 4.3 together with a RI and a SEM picture. The three peaks of the ^{233}U multiplet are well resolved. The RI shows some inhomogeneities of the areal activity distribution. The surface of both, the coated wafer and the deposition area, look very smooth in the SEM picture except for some residues of the solvent.

Table 4.5: Parameters and yield of the MP-produced ^{233}U recoil ion sources. N,N'-Dimethylformamide (DMF) and mixtures of 90 % isopropanol and 10 % isobutanol were used as electrolytes. The areal density refers to ^{233}U atoms.

sample	conc. / $\mu g\,mL^{-1}$	sub-strate	electro-lyte	duration / h	area / cm^2	areal density / $10^{14}\,cm^{-2}$
MP1	5.25	wafer	DMF	1.0	7.1	0.69(1)
MP2	34.4	wafer	IP/IB	1.5	7.1	3.82(4)
MP3	21.5	Ti foil	IP/IB	1.0	0.5	2.48(3)
MP4	21.5	Ti foil	IP/IB	1.5	0.5	19.1(2)
MP5	21.5	Ti foil	IP/IB	2.0	0.5	19.8(2)

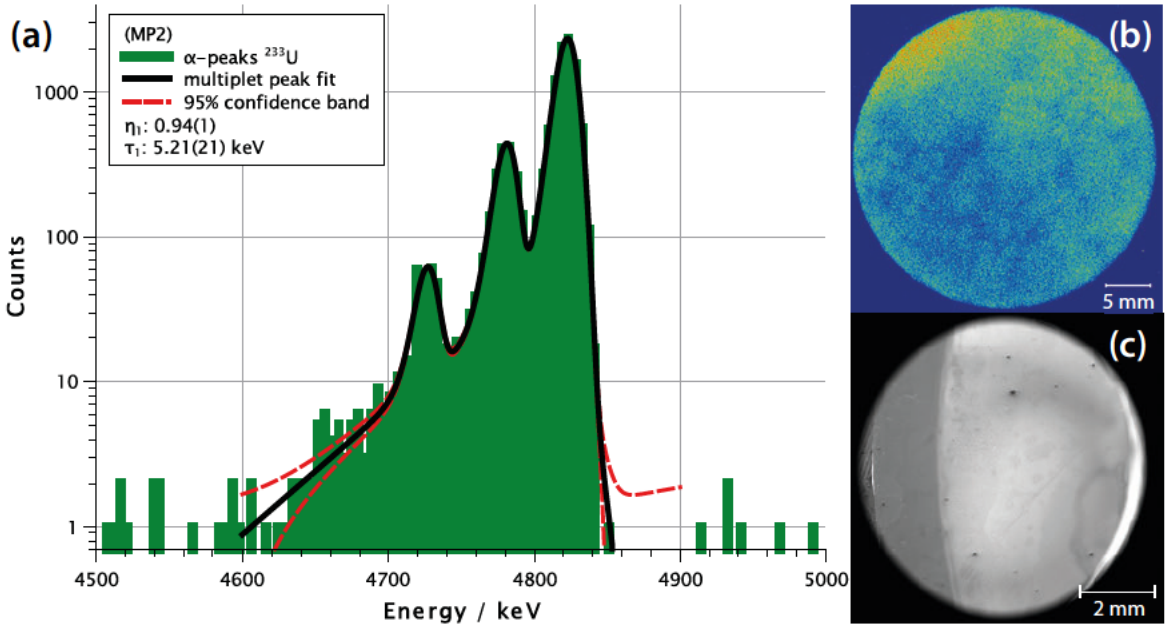

Figure 4.3: Qualitative alpha spectrum including a multiplet peak fit with confidence band (a), RI (b) and SEM picture (c) of a molecular plated ^{233}U recoil ion source (MP2). The source was fabricated on a titanium-coated silicon wafer from a mixture of 10 % isopropanol and 90 % isobutanol. Irradiation time for the RI was about 2 h.

4.7.2 Drop-on-Demand inkjet printing

The number of drops, drop volume, printed area and yield of the DoD sources are given in Table 4.6. The droplets dried within seconds during the printing process. No residues were observable with a light microscope. The qualitative alpha spectrum of the printed source DoD1 containing 1413 drops as well as its RI and SEM picture are given in Fig. 4.4. The three peaks are resolved. The RI shows a macroscopically homogeneous areal distribution of the activity. The size of the deposits varies within a range of about 200 µm due to surface effects of the titanium foil. The deposits of the single drops are faintly visible in the SEM picture thanks to a high height contrast by the rough surface of the titanium foil.

Table 4.6: Parameters for DoD printing and yield of the ^{233}U recoil ion sources. The areal density refers to the ^{233}U atoms on the area given in the table.

sample	conc. / $\mu g\,mL^{-1}$	drops	drop volume / nL	area / cm^2	areal density / $10^{14}\,cm^{-2}$
DoD1	74.2	1413	5.0	7.1	4.45(4)
DoD2	74.2	1413	5.0	7.1	4.60(5)
DoD3	74.2	1413	5.0	7.1	1.83(2)
DoD4	74.2	1413	5.0	7.1	1.81(2)
DoD5	74.2	1413	5.0	7.1	1.82(2)
DoD6	18.6	5637	5.0	7.1	1.23(1)
DoD7	138	5637	5.0	7.1	6.84(7)

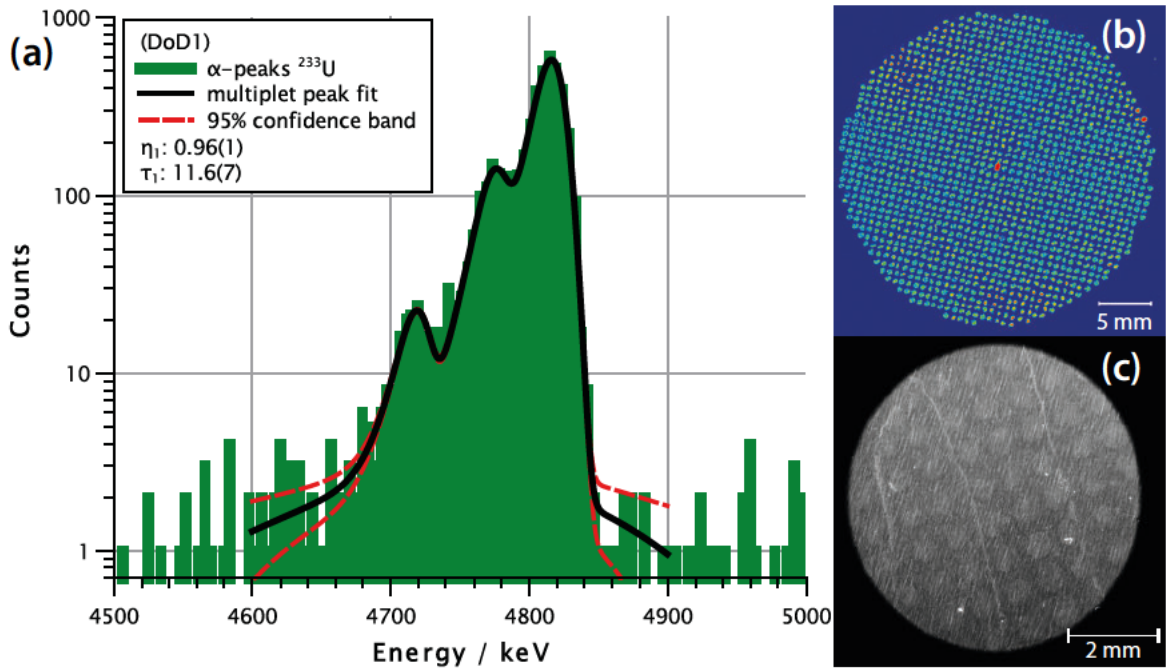

Figure 4.4: Qualitative alpha spectrum (a) of a DoD-printed ^{233}U recoil ion source (DoD1) on titanium foil as well as RI (b) and SEM picture (c). Irradiation time for the RI was about 2 h.

4.7.3 Chelation by sulfonic acid groups

The contact times, areas of the wafer pieces and areal densities of the chelated ^{233}U deduced from the quantitative alpha spectra are given in Table 4.7. No visible change occurred on the surface of the wafer pieces due to the fabrication process. The qualitative alpha spectrum of the source Ch6 including the multiplet peak fit is given in Fig. 4.5. Due to the very low areal density on the wafers, the count rate is very low. The three peaks are well-resolved and very narrow. The RI of the same

source in Fig. 4.5 shows a homogeneous, yet not very dense areal distribution of the activity.

Table 4.7: Parameters for chelation by sulfonic acid groups on silicon wafer pieces and areal densities. Contact time with the radioactive solution and areas of the silicon wafers are given. The areal density refers to ^{233}U atoms.

sample	contact time / min	area / cm^2	areal density / $10^{14}\,cm^{-2}$
Ch1	5	7.40	0.210(2)
Ch2	15	9.97	0.122(1)
Ch3	30	7.98	0.149(1)
Ch4	30	8.74	0.109(1)
Ch5	60	6.48	0.235(2)
Ch6	120	9.89	0.238(2)

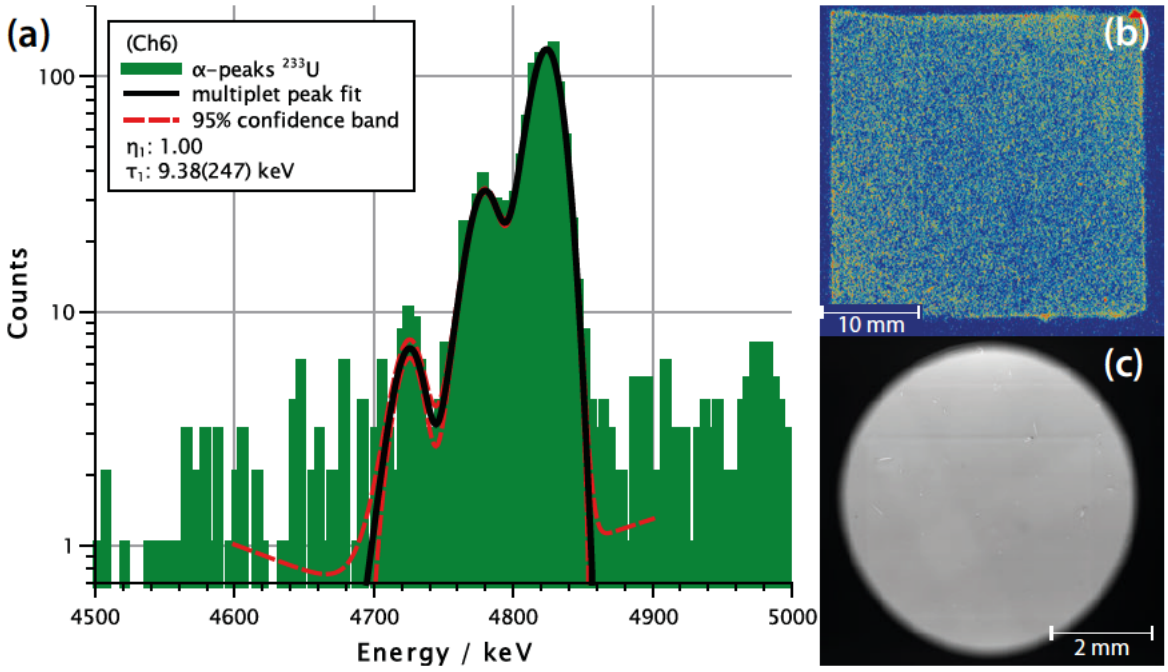

Figure 4.5: Qualitative alpha spectrum (a) of a ^{233}U recoil ion source (Ch6) fabricated by chelation on a functionalized silicon wafer piece as well as RI (b) and SEM picture (c). Irradiation time for the RI was about 1 h.

4.7.4 Self-adsorption

Fig. 4.6 shows the ^{233}U density of the SA sources as functions of the pH value of the solution (panel a) and the pretreatment temperature (panel b). The maximum yield was reached from a solution with a pH value of about 5, resulting in

about 40 ng cm^{-2} (10^{14} atoms cm^{-2}) on thermally oxidized titanium foils at 500 °C. This was increased to about 80 ng cm^{-2} (2×10^{14} atoms cm^{-2}) by changing the pretreatment temperature of the titanium foils to 450 °C. Sand-blasted titanium foils showed 270 ng cm^{-2} (7×10^{14} atoms cm^{-2}) of ^{233}U when prepared under the same conditions. To inspect a potentially big influence of different surface roughnesses, the corresponding values are listed in Table 4.8.

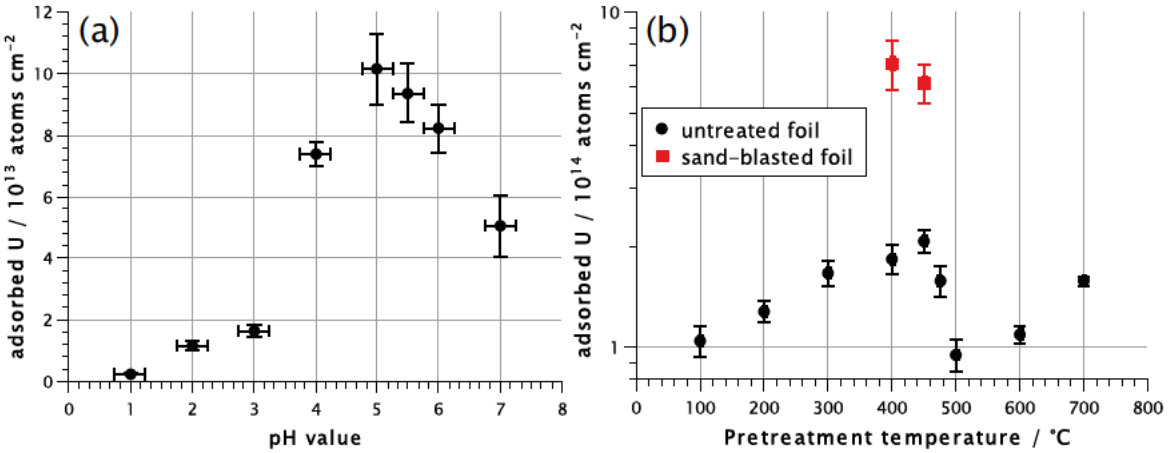

Figure 4.6: (a) Areal density of ^{233}U atoms on Ti foil thermally oxidized at 500 °C for 1 h as a function of pH value. (b) Areal density of ^{233}U atoms obtained at pH 5 on Ti foils as a function of the oxidation temperature applied before the adsorption exposure.

Table 4.8: Root mean square (RMS) roughness of titanium foils pretreated at different temperatures for 1 h. Atomic force microscopy was used for the investigation of the RMS roughness.

pretreatment temperature / °C	RMS roughness / nm
20	39(2)
450	24(10)
700	40(10)

The parameters for fabrication and yields of the SA sources are given in Table 4.9. No visible change occurred on the surface of the titanium foils after fabrication. The qualitative alpha spectrum of a source on a non-sand-blasted titanium foil (SA1) including the multiplet peak fit is given in Fig. 4.7 (a). The two peaks at lower energies are visible as shoulders of the peak at 4824 keV and are not well-resolved. The RI in Fig. 4.7 (b) shows a homogeneous areal distribution of activity. In the SEM picture in Fig. 4.7 (c), the height contrast of the titanium foil dominates, as this has a quite rough surface even without sand-blasting. No signal originating from the ^{233}U can be seen. The qualitative alpha spectrum of a source on a sand-blasted

titanium foil (SA3) as well as its RI and SEM pictures are given in Fig. 4.8. The left shoulder of the main alpha peak at 4824 keV is larger and the two peaks at lower energies can barely be identified. RI shows a quite homogeneous areal distribution of the activity but also shows artifacts due to the very rough surface structure of the foil, which is clearly visible in the SEM picture.

Table 4.9: Parameters for self-adsorption on preheated titanium foils and yields. The areal density refers to ^{233}U atoms.

sample	sand-blasted	pretreatment temperature / °C	area / cm^2	areal density / $10^{14}\,cm^{-2}$
SA1	no	450	7.07	2.33(2)
SA2	no	450	7.07	1.90(2)
SA3	yes	450	7.07	6.73(7)
SA4	yes	450	7.07	1.58(2)

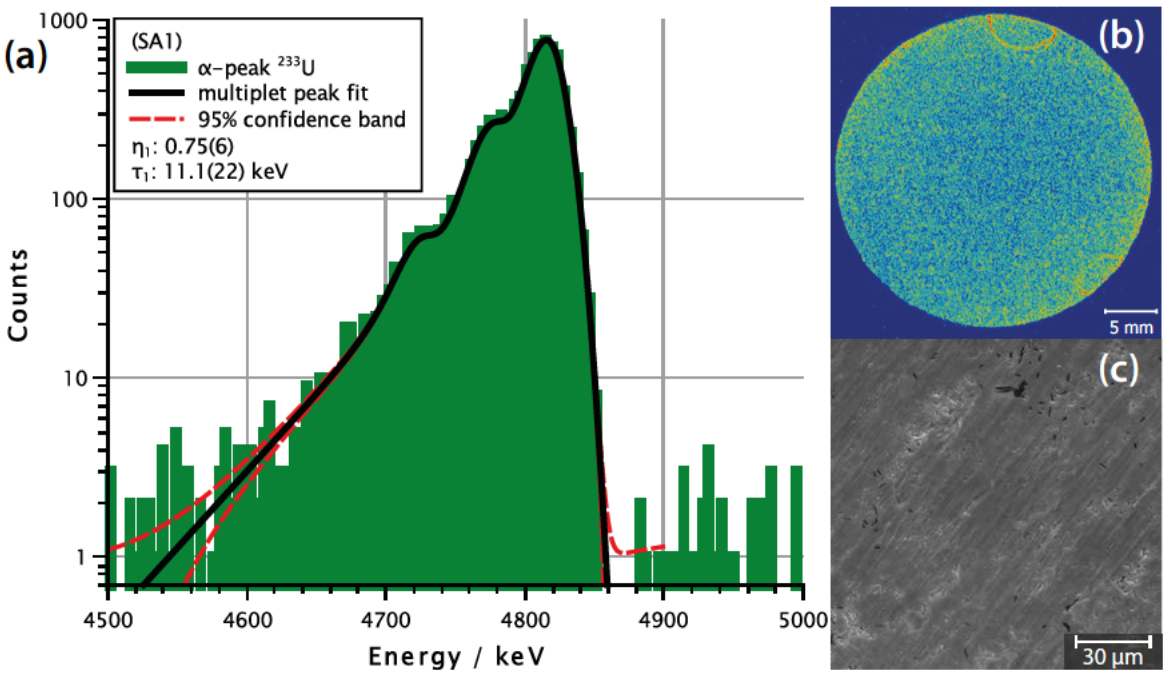

Figure 4.7: Qualitative alpha spectrum (a) as well as RI (b) and SEM picture (c) of a ^{233}U recoil ion source (SA1) fabricated by self-adsorption on a smooth titanium foil thermally oxidized at 450 °C for 1 h. Irradiation time for the RI was about 2 h.

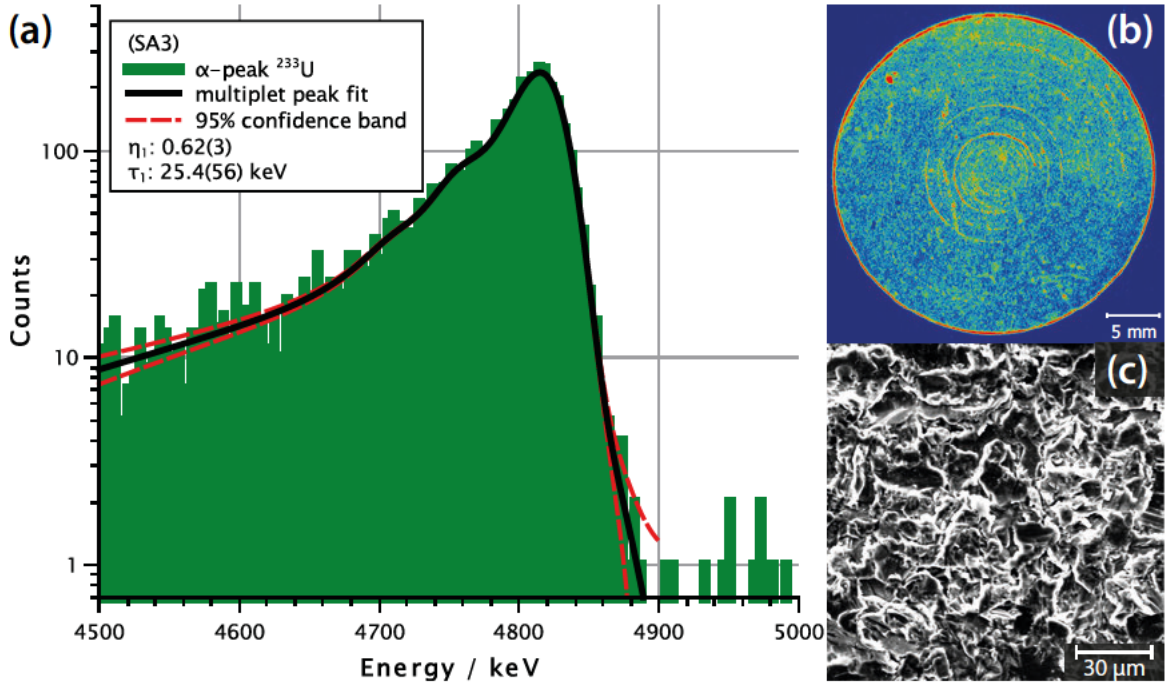

Figure 4.8: Qualitative alpha spectrum (a) as well as RI (b) and SEM picture (c) of a ^{233}U recoil ion source (SA3) fabricated by self-adsorption on a sand-blasted titanium foil thermally oxidized at 450 °C for 1 h. Irradiation time for the RI was about 2 h.

4.7.5 Comparison of fitting results of all four methods

A complete list including all results of the fit parameters is given in Table 4.11 in the appendix. The average values of the most significant parameters, η_1 and τ_1, are plotted against the average areal ^{233}U density for each fabrication method in Fig. 4.9. The fit parameter σ_1 is also significant for the qualitative evaluation, but is identical within error bars for all fabrication methods. Therefore, σ_1 is not included in the plots. The other parameters, σ_2 and τ_2, are less significant and have in general much higher values (see Table 4.11 in the appendix).

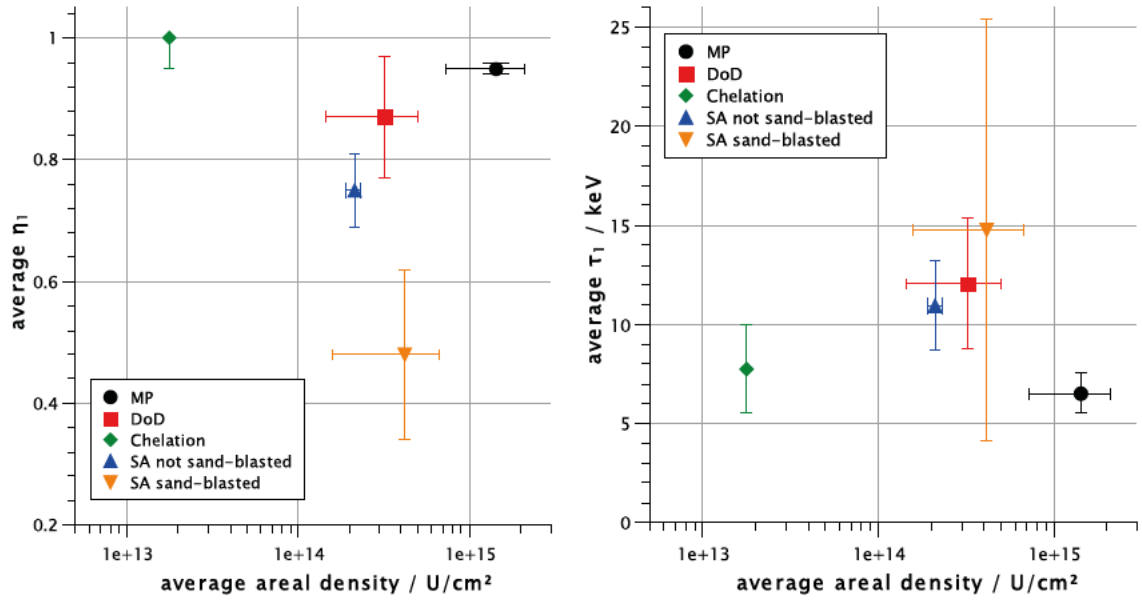

Figure 4.9: Plotted average fit parameters η_1 (left) and τ_1 (right) for each fabrication method against the average areal ^{233}U density of the sources.

4.7.6 Recoil efficiency of MP and SA prepared sources

The active areas of both fabricated sources were visible with the naked eye. The contact area of the SA source turned from copper-colored to violet and the deposition of the MP source had a bright yellow color. In contrast, no visible change occurred on the catcher foils. The geometric detection efficiency of the catcher foils was determined by Monte-Carlo simulations with AASI for the quantitative measurements. The determined ^{232}U source activities, the parameters and yields for the ^{228}Th recoil collection and the resulting recoil efficiencies are given in Table 4.10. The error of the recoil efficiency was calculated by a Gaussian error propagation, using the counting errors of the quantitative measurements as well as the errors of the geometric efficiencies for recoil collection and alpha detection. In Fig. 4.10, the qualitative spectra as well as the RI of the SA source and the corresponding catcher foil are depicted.

Table 4.10: ^{232}U activities of the SA and MP source and parameters and yields for the ^{228}Th recoil collection.

source	^{232}U activity / Bq	collection time / d	geometric efficiency (AASI) / %	collected ^{228}Th / Bq	recoil efficiency / %
SA	1300(9)	26.0	16.6(5)	10.7(1)	94.2(33)
MP	18800(60)	5.16	16.6(5)	3.13(2)	10.5(11)

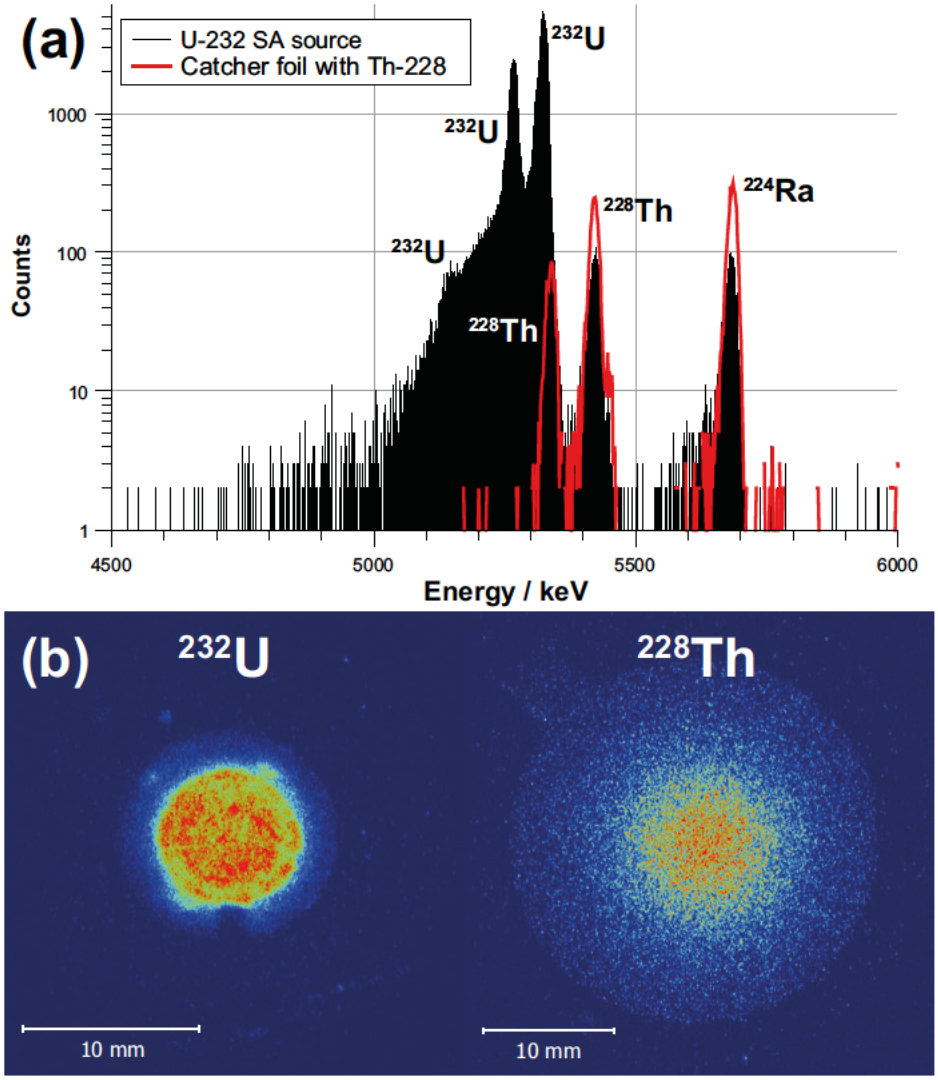

Figure 4.10: Qualitative alpha spectrum (a) and RI (b) of the ^{232}U SA source and the corresponding ^{228}Th recoil catcher foil. The spectra were measured for 1 h in case of the SA source and 5 h for the corresponding catcher foil, to obtain sufficient counts. The additional line at 5685 keV belongs to ^{224}Ra, the daughter nuclide of ^{228}Th. Irradiation time for the RI was about 15 min for the SA source and 2 h for the catcher foil.

4.8 Simulation results

As two fabrication methods (MP and DoD) cannot produce specifically monolayers, simulations are necessary to show the influence of several atomic layers on the alpha spectra of ^{233}U sources. The effects of different numbers of source layers (Fig. 4.11), different RMS roughnesses (Fig. 4.12) and different macroscopic layer shapes (Fig. 4.13) on simulated alpha spectra are shown. Convex and concave source shapes are described with a paraboloid of revolution, as described in [19]. The most important fit parameters, σ_1 and τ_1, are given in a legend for some simulated

spectra to show quantitatively the effect of different simulation parameters on the alpha spectrum. The residual fit parameters are given in Table 4.11. The influence of different chemical species (see Table 4.3) on simulated alpha spectra was also investigated, for sources having 10 atomic layers. The simulated spectra were identical and are therefore not plotted individually. The information on source material, backing and detector, which were used as parameters in AASI, is given in the caption of the figures. The varied parameters are given in the legends of the figures. A constant number of 10^6 simulated decays and a constant bin size of 5 keV was used for all simulations. The source-detector-distance was kept constant at 100 mm and the PIPS detector properties of the Ortec ULTRA™, as employed to obtain the qualitative spectra, were used to enable a direct comparison between experimental and simulated results. For a qualitative comparison of experimental spectra with these simulations, two exemplary alpha spectra of a molecular plated source (MP2) and a self-adsorbed source (SA1) were fitted with simulations in AASI. These are shown in Fig. 4.14.

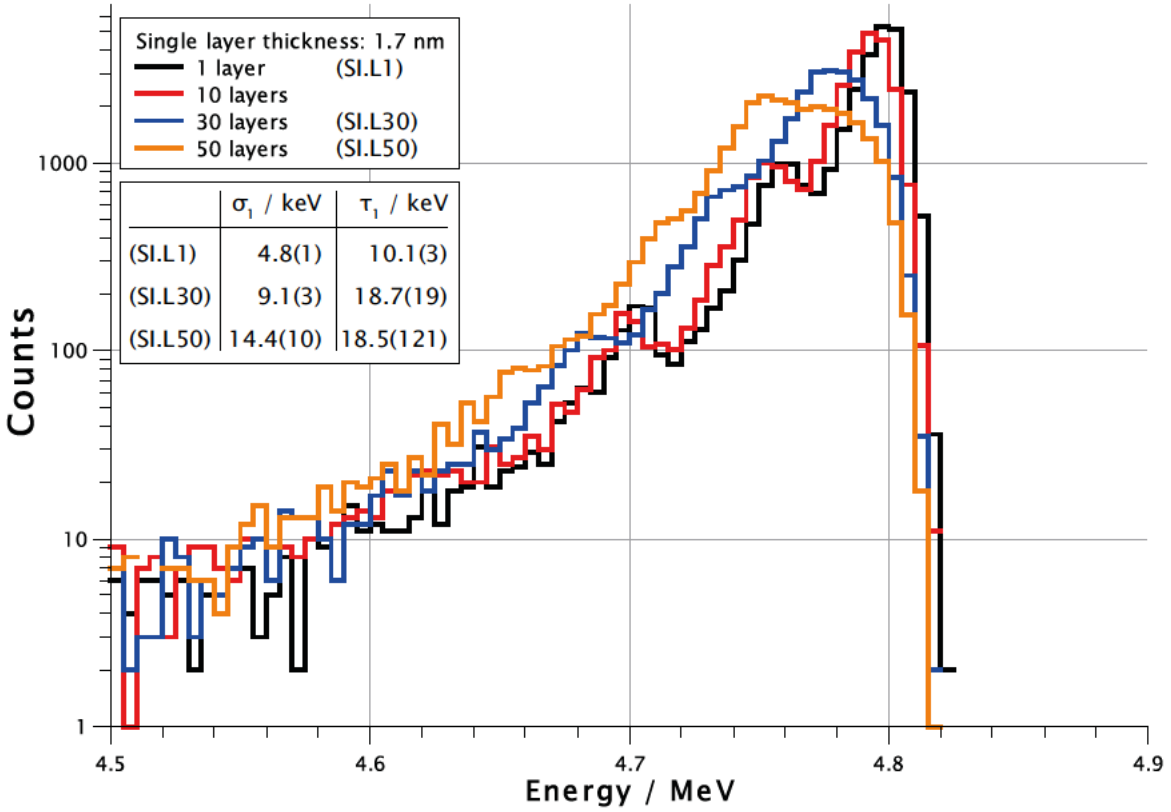

Figure 4.11: AASI simulations of ^{233}U sources with different numbers of atomic layers. The source material was set to $UO_2(OH)_2 \times H_2O$ with a diameter of 30 mm on a Ti backing with 25 µm thickness. The layer thickness was varied from 1.7 nm (representing a monolayer) up to 85 nm. The source-detector-distance was set to 100 mm and a number of 10^6 decays were simulated for each parameter variation.

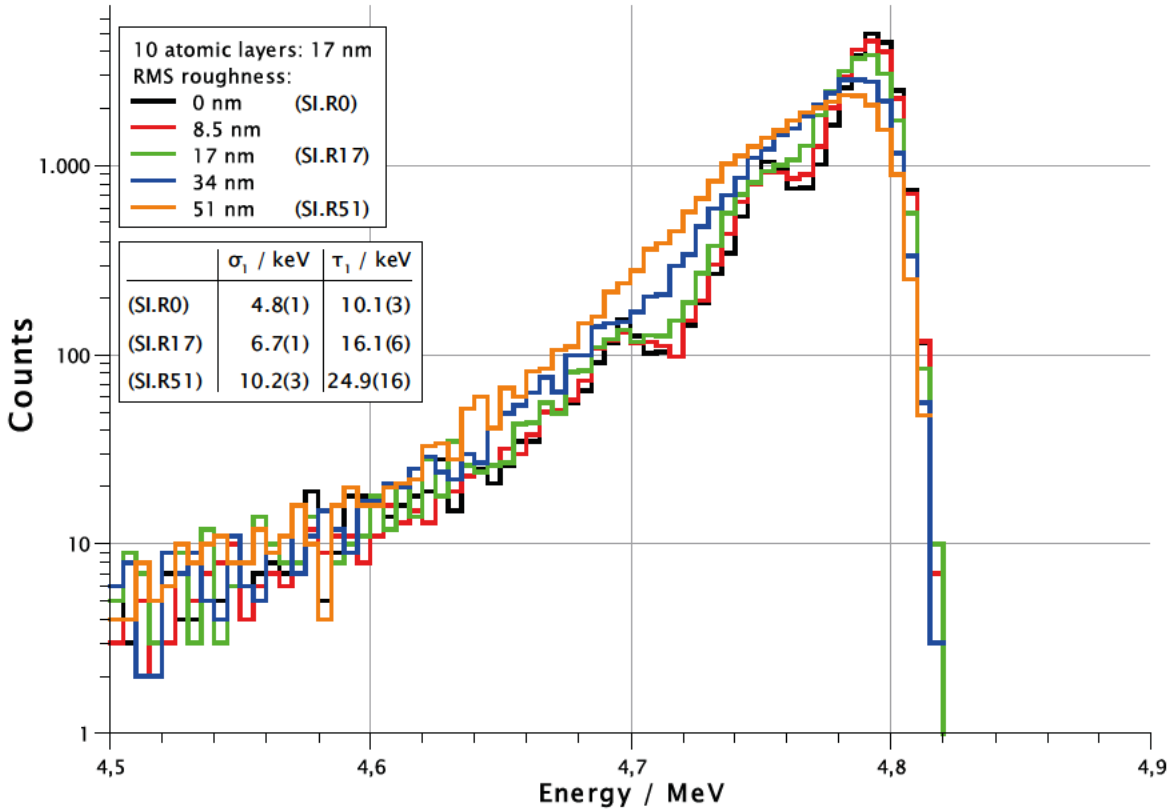

Figure 4.12: AASI simulations of ^{233}U sources with different root mean square roughnesses. The source material was set to $UO_2(OH)_2 \times H_2O$ with a diameter of 30 mm and a thickness of 17 nm (representing 10 atomic layers) on a Ti backing with 25 µm thickness. The source-detector-distance was set to 100 mm and a number of 10^6 decays were simulated for each parameter variation. The RMS roughness was varied in the range of 0 nm to 51 nm.

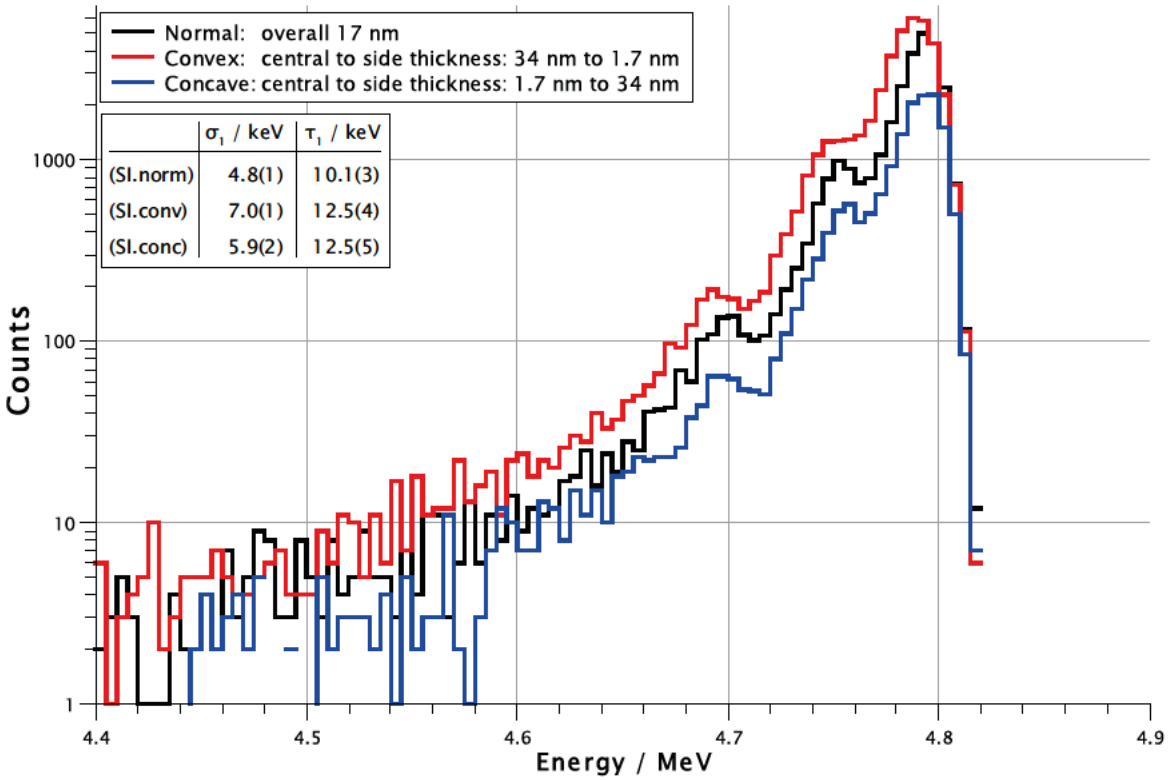

Figure 4.13: AASI simulations of ^{233}U sources with different layer shapes. Normal represents a cylindrical-shape, as the central thickness and the thickness at the side of the source layer are equal. Convex and concave source shapes are described with a paraboloid of revolution, as described in [19]. The source material was set to $UO_2(OH)_2 \times H_2O$ with a diameter of 30 mm and a thickness of 17 nm (representing 10 atomic layers) on a Ti backing with 25 µm thickness. The source-detector-distance was set to 100 mm and a number of 10^6 decays were simulated for each parameter variation.

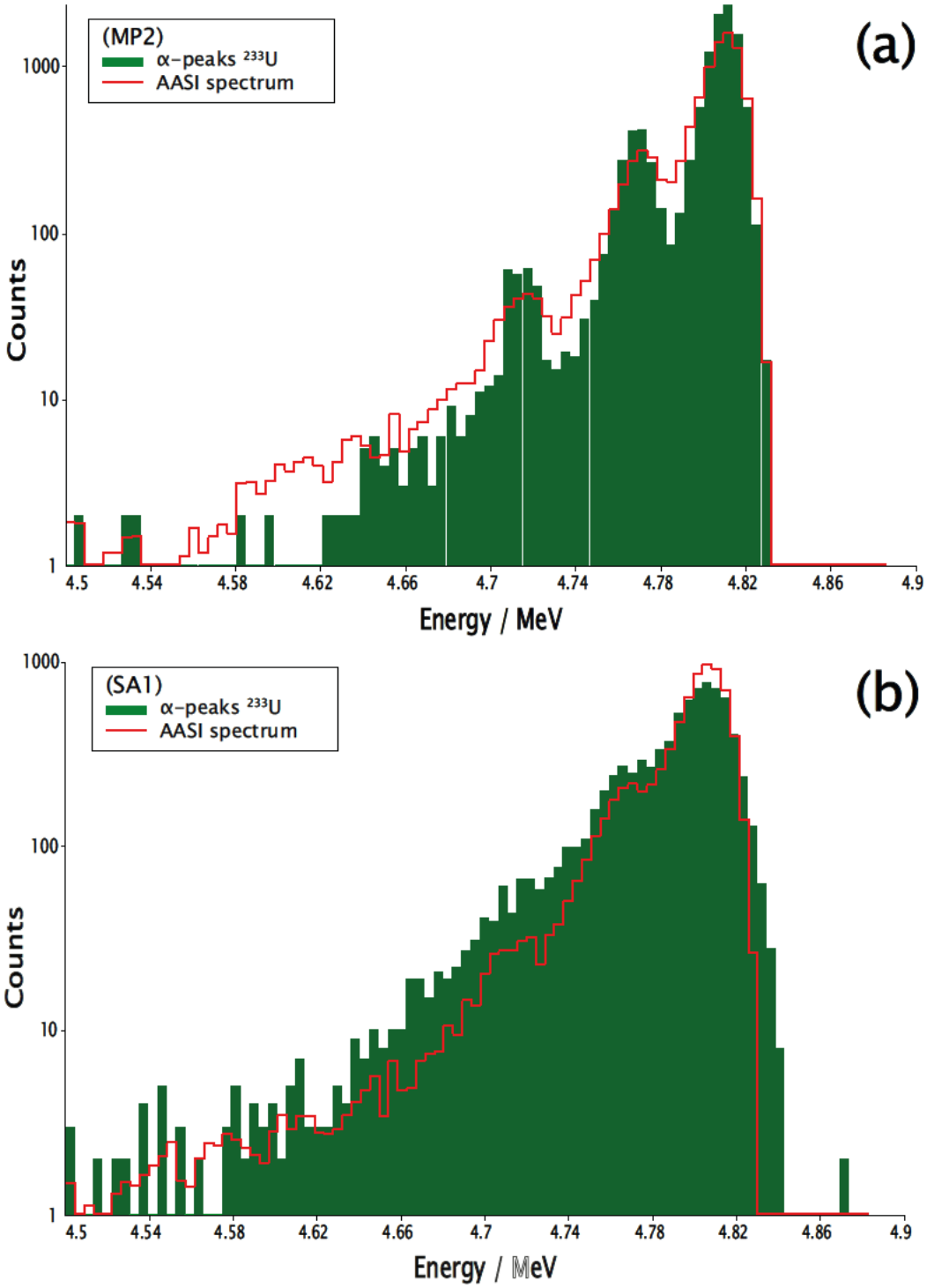

Figure 4.14: Qualitative comparison of experimental alpha spectra with AASI simulations. For the simulations, the source material was set to $UO_2(OH)_2 \times H_2O$ with a diameter of 30 mm and a thickness of 17 nm (representing 10 atomic layers) on a Ti backing with 25 µm thickness. The source-detector-distance was set to 100 mm and a number of 10^6 decays were simulated. In (a), for comparison with the molecular plated source (MP2), the RMS roughness was set to 0 nm, while for comparison with the self-adsorbed source (SA1) in (b) it was set to 34 nm.

4.9 Discussion

4.9.1 AASI simulations

The simulation results of Fig. 4.11 show that it is not simple to differentiate between a ^{233}U source containing a monolayer and one with 10 atomic layers based on the recorded alpha spectra. The difference can be seen by an energy shift of the peak maximum in the fit evaluation, because the error of the fitted peak position μ is about 0.5 keV. Both simulated spectra have the same shape, except for a slight shift of one bin (5 keV) to lower energies in case of the alpha source with 10 atomic layers. The systematic uncertainty of the alpha spectra collected with our used alpha-spectrometry setup is estimated to be about 10 keV; we are therefore not able to extract any information on the number of atomic layers from the peak positions in our experimental spectra. The Monte-Carlo simulations suggest this shift to occur predominantly because of alpha particles originating from inside the source material and less of these occurring from the top-most layers, as inferred from the fact that the number of decays did not increase proportionally to the number of atomic layers. At 20 to 30 atomic layers, the three single peaks are increasingly less well-resolved. At 50 atomic layers, only a single broad peak is visible. This indicates that with an increasing number of atomic layers in the source material, the alpha peak becomes broader, corresponding to an increase of σ_1 from (4.8 ± 0.1) keV to (14.4 ± 1.0) keV.
The simulation results depicted in Fig. 4.12 show a significant increase of the tailing with increasing RMS roughness. Also in this case it is not possible to differentiate between a source with a smooth surface and one with a RMS roughness of 8.5 nm with τ_1 at about 10 keV. The influence only becomes significant at higher RMS roughnesses. At 17 nm RMS roughness, the three single peaks start to merge due to a higher tailing τ_1 of about (16.1 ± 0.6) keV. At 51 nm RMS roughness, the three peaks are not distinguishable any more due to the very high tailing τ_1 of about (24.9 ± 1.6) keV. Additionally, the peak height starts to decrease but the peak area remains constant. The parameter σ_1 is linked to the increasing tailing, indicated by an increase from (4.8 ± 0.1) keV up to (10.2 ± 0.3) keV.
The simulation results of Fig. 4.13 pertain to the case of different shapes (convex/concave rotational paraboloid) of the source layer. The simulations show a minor, but clear difference of the alpha peak shape for the three cases. The fit parameters η_1, σ_1 and τ_1 are not significantly affected by the convex or concave layer shape. A slight broadening is indicated by an increase of σ_1 from (4.8 ± 0.1) keV to (7.0 ± 0.1) keV (convex) and (5.9 ± 0.2) keV (concave). Additionally, the tailing parameter τ_1 is increased in both cases from (10.1 ± 0.3) keV to about (12.5 ± 0.5) keV. More alpha particles reach the detector from a convex source while a concave source shows the opposite effect.

4.9.2 Molecular Plating

Thin ^{233}U sources with areal densities between 7×10^{13} atoms cm^{-2} to 2×10^{15} atoms cm^{-2} were produced by MP. The investigations by alpha spectrometry, RI and SEM showed no significant differences of the sources in this range of areal densities. The area in contact with the electrolyte was completely covered with active material, but differences in homogeneity occurred (see Fig. 4.3 (b)). These were not correlated with the concentration, substrate or electrolyte. The SEM picture shows a clearly visible contrast of the deposited material but a surface structure similar to the one of the pristine substrate. This is in agreement with measurements of A. Vascon et al. [10], who found the surfaces of thin sources on titanium-coated silicon wafers to be smoothest. The substrate roughness has a significant impact on the alpha spectra, as visible in Fig. 4.12 as an increase of the tailing τ_1 with increasing RMS roughness. Therefore, a smooth surface should be preferred for the source fabrication by MP. Furthermore, the alpha lines of the MP sources are well-resolved (see Fig. 4.3), with average σ_1 of (7.7 ± 1.6) keV. The average fit parameter η_1 is very close to 1 (0.95 ± 0.01) and the average tailing parameter τ_1 is (6.5 ± 1.0) keV, which is one of the lowest values when compared with those of the samples produced by the other fabrication methods (see Fig. 4.9). These results are in good agreement with AASI simulations of ^{233}U sources with less than 20 atomic layers (see Fig. 4.11). In summary, the MP sources show very good properties; with probably less than 20 atomic layers they should reach a recoil efficiency of ^{229}Th close to 100 %. Nevertheless, the investigation of the recoil efficiency from a ^{232}U source only showed an efficiency of (10.5 ± 1.1) %. This discrepancy to theoretical suggestions based on the ^{233}U experiments may have different reasons. First, the deposition of the ^{232}U was visible with the naked eye in contrast to all of the ^{233}U sources. Therefore, the deposited layer must be much thicker with lesser uranium atoms. This was checked by AASI simulations and comparison with a qualitative 4k alpha spectrum of the MP source. These AASI fits (with an areal uncertainty of 0.7 % and a χ^2 of 1.749) gave only a thickness of about 35 nm with a RMS roughness of about 90 nm and a density of 6.25 g cm^{-3} for the ^{232}U MP source. The unexpected high density can only be caused by metallic, inactive impurities, since the total amount of all determined ^{232}U and daughter atoms give a far lower weight (0.04 µg of a total simulated amount of 10.9 µg, including also lighter atoms like hydrogen and oxygen). These impurities might be palladium from the anode or other metals like iron, tin or zinc, which were not investigated beforehand. Another reason for the discrepancy could be sputter effects. The high activity of the MP source corresponds to a high recoil ion rate. High energetic recoil ions, e.g. ^{208}Pb from the alpha decay of the daughter nuclide ^{212}Po (E_{kin} =166.9 keV), may also ablate collected ^{228}Th from the catcher foil. This has to be investigated by further simulations before a final statement on the recoil efficiency of the MP sources can be made. The energy loss of the recoil ions is

difficult to estimate, since the exact chemical composition of the MP sources is not known and, e.g., organic impurities from the electrolyte, which do not substantially affect alpha particles, or impurities by daughter nuclides could have a significant impact on the recoil ion energy.

4.9.3 Drop-on-Demand inkjet printing

The DoD printed sources were very thin with areal densities in the range of 1–7×10^{14} atoms cm^{-2}. The deposits were not visually observable. SEM analysis was quite challenging, because the deposits were barely visible due to the height contrast of the titanium foils. The shape of the deposits on different regions of the titanium foils varied, probably due to differences in the surface properties. This also had an impact on the fit parameters η_1 and τ_1. Some spectra of sources with large deposits had smaller values of the fit parameters (see DoD1, DoD2, DoD4 and DoD6 in Table 4.11), whereas others with smaller deposits showed broader alpha peaks (see DoD3, DoD5 and DoD7 in Table 4.11). The broadening is probably an effect of the more convex lateral shape of the deposits, as indicated by AASI simulations (Fig. 4.13). In dependence on the surface properties (hydrophilic or hydrophobic) of the backing, the lateral cut of deposits of evaporated drops have a concave or convex shape [12]. The recoil efficiency for ^{229}Th might be close to 100 %, because the sources do not contain contamination of light elements in contrast to sources prepared by MP. Also the macroscopic areal distribution of the activity is homogeneous as shown in the RI in Fig. 4.4. The energy loss of the ^{229}Th recoil ions can be estimated more easily than for MP sources, because the chemical species, uranyl nitrate, is known. As the number of atomic layers is estimated to be below 20 from simulated spectra (Fig. 4.11) compared with the experimental alpha spectrum in Fig. 4.4, the maximum energy loss of the ^{229}Th recoil ions might be about (9 ± 2) keV based on the values of Table 4.1.

4.9.4 Chelation by sulfonic acid groups

The sources fabricated by chelation have the best quality by far as judged from the value of η_1 of about 1.0. The silicon surface provides a perfectly smooth surface for the sulfonic acid groups and therefore for the chelated ^{233}U. This can be seen both in the SEM picture and in the RI by a very homogeneous areal distribution of the activity (see Fig. 4.5). The RI and also the areal ^{233}U density indicate, though, that the densest occupation of the silicon surface by functional groups of about 10^{15} $-$OH $-$ groups cm^{-2} [37] has not yet been reached. The reason for the low areal density below 10^{15} atoms cm^{-2} could be due to two things. On one hand, preventing the formation of functional multilayers was problematic during the functionalization of the silicon surfaces. Therefore, conservative fabrication conditions were selected [37]. These may have led to fewer sites than needed to

reach the theoretically possible limit of 10^{15} atoms cm^{-2}. The optimal conditions for these silicon surfaces would have to be approached iteratively. On the other hand, the second step of the functionalization, the oxidation of the thiol groups to sulfonic acid groups, is also complex for extremely thin layers. The process is quite delicate, as a specific concentration of hydrogen peroxide is required to oxidize the thiols to sulfonic acid groups. If the concentration is too low or the contact time too short, the thiol groups on the surfaces will be only partially oxidized and there might be an intermediate stage containing disulfide bridges as a possible reaction product. If the hydrogen peroxide concentration is too high, the intermediate disulfide bridges are oxidized to sulfonic acid groups, but the functional layers are also destroyed. Still, the alpha spectra, as judged by the corresponding fit parameters, are the best when compared with those from sources fabricated by any other method. The fit routine had to be performed with a fixed $\eta_1 = 1$, because the multiplet peaks are too narrow and do not have a long tailing (parameterized by τ_2) at all. A problem with the alpha spectra was the very low statistics due to the low areal uranium content, which is reflected in the larger error bars of σ_1 and τ_1. The ^{233}U multiplet in the alpha spectra is even better resolved than suggested by the AASI simulation (see Fig. 4.11, black line). All this indicates that the sources fabricated by chelation might have an almost 100 % recoil efficiency of ^{229}Th recoil ions. We estimate the energy loss to just a few eV, due to breaking of chemical bonds.

4.9.5 Self-adsorption

The parameter studies for source fabrication by SA show optimal conditions at a pH value of 5 and on titanium foils thermally oxidized at 500 °C for 1 h. In this way, a maximum areal density of about 80 ng cm^{-2} (2×10^{14} atoms cm^{-2}) was reached. The findings of uranium adsorption on anatase fit well with results reported in [17]. The evolution of the adsorption rate as a function of treatment temperature of the titanium foils (Fig. 4.6) cannot be explained by an increase of the RMS roughness, as the AFM data in Table 4.8 show. Moreover, the evolution shows the adjustment of the titanium modification on the foil surface in the variation of the uranium adsorption. Two peaks of adsorbed uranium are visible and correspond to anatase (at 450 °C) and to rutile (at 700 °C). At room temperature up to 400 °C, amorphous titanium is present. Between 450 °C and 700 °C, a (semi-amorphous) mixture of both anatase and rutile is present. This fits well with x-ray diffraction measurements of sol-gel coated titanium films [27]. It was possible to increase the amount of adsorbed uranium from 80 ng cm^{-2} to 270 ng cm^{-2} on titanium foils that were sand-blasted and then pretreated at 450 °C. However, the roughness produced by sand-blasting was not well reproducible, as inferred from the large standard deviation of the amount of adsorbed uranium. The properties of sources prepared on untreated vs. sand-blasted Ti foils were very different. The areal distribution, shown on untreated foils in Fig. 4.7 (b), is very homogeneous. Only few artifacts

are visible, probably caused by the quite rough surface of the titanium foils (see SEM picture in Fig. 4.7 (c)), as it was also observed on the titanium foils of the DoD sources (see Fig. 4.4). The three single peaks of the ^{233}U multiplet are visible in the alpha spectra as shoulders of the next highest peak, due to the large average tailing τ_1 of (10.96 ± 2.26) keV, due to the rough surface of the titanium foil. The average τ_1 value is similar to that of the DoD sources, but τ_2 of (50.35 ± 5.39) keV has a higher weighting factor due to a lower value of η_1 of (0.75 ± 0.06) keV in the case of the untreated foils (see Fig. 4.9). The comparison with an AASI simulation in Fig. 4.14 (b) indicates that the reason for the differences in the peak shape is likely connected to the rough surface of the titanium foils. The RI and SEM pictures of the SA sources on sand-blasted foils show a much rougher surface and, therefore, more artifacts in the RI. Also the tailing in the alpha spectra is increased, leading to even lower values of η_1 of (0.48 ± 0.14) keV and higher values of τ_1 of (14.76 ± 10.68) keV. This supports the assumption that the tailing of the SA sources on untreated foils can be explained solely by the roughness of the foils. If the roughness of the substrates could be reduced, the SA sources would have the same quality as the sources fabricated by chelation with sulfonic acid groups concerning the recoil efficiency and the energy loss of ^{229}Th recoil ions. However, the SA method provides currently a higher areal density. The investigation of the recoil efficiency from a ^{232}U source produced on a limited area by SA gave an efficiency of (94.2 ± 3.3) %, which fits very well with the theoretical suggestions. The small discrepancy to an optimum value of 100 % might be caused by sputter effects due to high energetic recoil ions like ^{208}Pb coming from the source. The spectra depicted in Fig. 4.10 (a) support the theoretical suggestion that the layers produced by SA are single atomic layers, since no ^{232}U is visible in the spectrum of the catcher foil. In thicker deposits with several atomic layers, clusters of the source material are expected to be sputtered due to alpha decay collision cascades in deeper layers [38]. Furthermore, the areal distribution of ^{232}U in the RI is as homogeneous as the distribution of ^{233}U in the RI of Fig. 4.7 (b). Therefore, self-adsorption can also be carried out well on confined surfaces.

4.10 Conclusion

Four different fabrication methods were used to produce ^{233}U recoil ion sources delivering $^{229(m)}Th$ in a most narrow kinetic energy distribution. They were analyzed both quantitatively and qualitatively with respect to the resolution of the alpha spectra and the areal density of the ^{233}U layer. Simulations performed with AASI helped to understand the effects of different source characteristics like layer thickness, roughness, homogeneity and chemical species on the ^{233}U alpha spectrum. Both the information from the simulations and the experimental alpha spectra were used to make predictions on recoil efficiency and energy loss of ^{229}Th recoil ions. Additionally, experiments were performed with two ^{232}U sources produced by MP

and SA to investigate their ^{228}Th recoil efficiency. Sources produced by chelation with sulfonic acid groups are likely the best recoil ion sources with respect to energy sharpness of the ^{229}Th recoil ions. However, their areal density and hence the recoil ion rate is quite low. MP sources are very close in their quality to sources produced by chelation. However, they consist of several atomic layers and are therefore probably not ideal concerning the energy loss of recoil ions. This was proven with a ^{232}U source, for which a recoil efficiency of roughly 10 % was determined. Effects by metallic, inactive contaminants in the source material, which have caused a greater density in the deposit layer, have to be investigated by, e.g., neutron activation analysis in further experiments. They have to be removed before source production to achieve a higher recoil efficiency with MP sources. Also the methods of DoD and SA yielded promising sources. In contrast to MP and sources produced by chelation, they were fabricated on quite rough substrates. This induces a more pronounced tailing in the alpha spectra and decreases their quality. A method to control the shape of deposits produced by DoD is, e.g., to print on hydrophilic or even superhydrophilic surfaces. Such surfaces can be fabricated by anodic oxidation of titanium foils or by sol-gel coating of TiO_2 particles [27]. The deposits would then result in very broad and regular shapes and therefore the quality of DoD sources could probably be improved. The suggested method will also improve the quality of the SA sources. After the implementation of these improvements, the sources produced by chelation and by self-adsorption may well be the best recoil ion sources due to their guaranteed monolayer thicknesses. The investigation of a ^{232}U source produced by SA showed actually a ^{228}Th recoil efficiency close to 100 %, which fits perfectly to the proposed theoretical efficiency by alpha spectrometry analysis. MP and DoD would produce high qualitative recoil ion sources, but with a source thickness that can be less well controlled, and may, therefore, result in a larger energy spread and lower recoil efficiency of the ^{229}Th ions. All the presented data fit well to the experiments and theoretical suggestions of Pohjalainen et al. [39], where sources with much larger areal uranium densities of 74×10^{15} atoms cm^{-2} to 530×10^{15} atoms cm^{-2} were investigated and recoil efficiencies of about 16 % were measured. For the TACTICa experiment, the fabricated sources by SA appear well suited. The actual energy distribution of the ^{229}Th ions can be measured in the TACTICa ion source setup [8] to gain further insights into the characteristics of the produced sources.

4.11 References

[1] L. v. d. Wense, B. Seiferle, M. Laatiaoui, J. B. Neumayr, H.-J. Maier, H.-F. Wirth, C. Mokry, J. Runke, K. Eberhardt, Ch. E. Düllmann, N. G. Trautmann, P. G. Thirolf, Direct detection of the ^{229}Th nuclear clock transition, Nature 533 (2016) 47–51.

[2] J. Thielking, M. V. Okhapkin, P. Głowacki, D. M. Meier, L. v. d. Wense, B. Seiferle, Ch. E. Düllmann, P. G. Thirolf, E. Peik, Laser spectroscopic characterization of the nuclear-clock isomer ^{229m}Th, Nature 556 (2018) 321–325.

[3] B. Seiferle, L. v. d. Wense, P. V. Bilous, I. Amersdorffer, C. Lemell, F. Libisch, S. Stellmer, T. Schumm, Ch. E. Düllmann, A. Palffy, P. G. Thirolf, Energy of the ^{229}Th nuclear clock transition, Nature 573 (2019) 243–246.

[4] C. Droese, S. Eliseev, K. Blaum, M. Block, F. Herfurth, M. Laatiaoui, F. Lautenschläger, E. M. Ramirez, L. Schweikhard, V. Simon, P. Thirolf, The cryogenic gas stopping cell of SHIPTRAP, Nuclear Instruments and Methods in Physics Research Section B: Beam Interactions with Materials and Atoms 338 (2014) 126–138.

[5] S. Götz, S. Raeder, M. Block, Ch. E. Düllmann, M. Götz, E. Jäger, O. Kaleja, J. Krier, L. Lens, A. K. Mistry, C. Mokry, J. Runke, P. Thörle-Pospiech, A. Yakushev, Rapid extraction of short-lived isotopes from a buffer gas cell for use in gas-phase chemistry experiments. Part I: on-line studies with ^{219}Rn and ^{221}Fr, Nuclear Instruments and Methods in Physics Research Section A: Accelerators, Spectrometers, Detectors and Associated Equipment submitted (2020).

[6] K. Groot-Berning, F. Stopp, G. Jacob, D. Budker, R. Haas, D. Renisch, J. Runke, P. Thörle-Pospiech, Ch. E. Düllmann, F. Schmidt-Kaler, Trapping and sympathetic cooling of single thorium ions for spectroscopy, Phys. Rev. A 99 (023420) (2019).

[7] F. Stopp, K. Groot-Berning, G. Jacob, D. Budker, R. Haas, D. Renisch, J. Runke, P. Thörle-Pospiech, Ch. E. Düllmann, F. Schmidt-Kaler, Catching, trapping and in-situ-identification of thorium ions inside Coulomb crystals of $^{40}Ca^{+}$ ions, Hyperfine Interact. 240 (33) (2019).

[8] R. Haas, T. Kieck, D. Budker, Ch. E. Düllmann, K. Groot-Berning, W. Li, D. Renisch, F. Schmidt-Kaler, F. Stopp, A. Viatkina, Development of a recoil ion source providing slow Th ions including $^{229(m)}$Th in a broad charge state distribution, Hyperfine Interact. 241 (25) (2020).

[9] W. Parker, R. Falk, Molecular plating: A method for the electrolytic formation of thin inorganic films, Nucl. Instr. Methods 16 (1962) 355–357.

[10] A. Vascon, S. Santi, A. A. Isse, A. Kühnle, T. Reich, J. Drebert, K. Eberhardt, Ch. E. Düllmann, Smooth crack-free targets for nuclear applications produced by molecular plating, Nuclear Instruments and Methods in Physics Research Section A: Accelerators, Spectrometers, Detectors and Associated Equipment 714 (2013) 163–175.

[11] A. Vascon, N. Wiehl, T. Reich, J. Drebert, K. Eberhardt, Ch. E. Düllmann, The performance of thin layers produced by molecular plating as alpha-particle sources, Nuclear Instruments and Methods in Physics Research Section A: Accelerators, Spectrometers, Detectors and Associated Equipment 721 (2013) 35–44.

[12] R. Haas, S. Lohse, Ch. E. Düllmann, K. Eberhardt, C. Mokry, J. Runke, Development and characterization of a Drop-on-Demand inkjet printing system for nuclear target fabrication, Nuclear Instruments and Methods in Physics Research Section A: Accelerators, Spectrometers, Detectors and Associated Equipment 874 (2017) 43–49.

[13] D. Krupp, U. W. Scherer, Prototype development of ion exchanging alpha detectors, Nuclear Instruments and Methods in Physics Research Section A: Accelerators, Spectrometers, Detectors and Associated Equipment 897 (2018) 120–128.

[14] N. Jaffrezic-Renault, H. Poirier-Andrade, D. Trang, Models for the adsorption of uranium on titanium dioxide, Journal of Chromatography A 201 (1980) 187–192.

[15] M. Wazne, X. Meng, G. P. Korfiatis, C. Christodoulatos, Carbonate effects on hexavalent uranium removal from water by nanocrystalline titanium dioxide, Journal of Hazardous Materials 136 (2006) 47–52.

[16] K. Müller, H. Foerstendorf, T. Meusel, V. Brendler, G. Lefèvre, M. J. Comarmond, T. E. Payne, Sorption of U(VI) at the TiO_2–water interface: An in situ vibrational spectroscopic study, Geochimica et Cosmochimica Acta 76 (2012) 191–205.

[17] A. C. M. Lamb, F. Grieser, T. Healy, The adsorption of uranium (VI) onto colloidal TiO_2, SiO_2 and carbon black, Colloids and Surfaces A: Physicochemical and Engineering Aspects 499 (2016) 156–162.

[18] A. Yamaguchi, M. Kolbe, H. Kaser, T. Reichel, A. Gottwald, E. Peik, Experimental search for the low-energy nuclear transition in ^{229}Th with undulator radiation, New Journal of Physics 17 (2015) 053053.

[19] T. Siiskonen, R. Pöllänen, Advanced simulation code for alpha spectrometry, Nuclear Instruments and Methods in Physics Research Section A: Accelerators, Spectrometers, Detectors and Associated Equipment 550 (2005) 425–434.

[20] R. Pöllänen, T. Siiskonen, High-resolution alpha spectrometry under field conditions – fast identification of alpha particle emitting radionuclides from air samples, Journal of Environmental Radioactivity 87 (2006) 279–288.

[21] T. Siiskonen, R. Pöllänen, New Approach to Alpha Spectrum Analysis: Iterative Monte Carlo Simulations and Fitting, Prog. Nucl. Sci. Technol. 2 (2011) 437–441.

[22] G. Bortels, P. Collaers, Analytical function for fitting peaks in alpha-particle spectra from Si detectors, Appl. Radiat. Isot. 38 (1987) 831–837.

[23] S. Pommé, G. Sibbens, Alpha-particle Counting and Spectrometry in a Primary Standardisation Laboratory, Acta Chim. Slov. 55 (2008) 111–119.

[24] J. F. Ziegler, SRIM - The Stopping and Range of Ions in Matter, https://www.srim.org/, [Online; accessed 03-December-2019] (2013).

[25] I. Grenthe, J. Drożdżyński, T. Fujino, E. C. Buck, T. E. Albrecht-Schmitt, S. F. Wolf, Uranium, Springer Netherlands, Dordrecht, 2006, pp. 253–698.

[26] D. Lide, CRC Handbook of Chemistry and Physics, 84th Edition, CRC Handbook of Chemistry and Physics, Taylor & Francis, 2003.

[27] D. Velten, V. Biehl, F. Aubertin, B. Valeske, W. Possart, J. Breme, Preparation of TiO_2 layers on cp-Ti and Ti_6Al_4V by thermal and anodic oxidation and by sol-gel coating techniques and their characterization, Journal of Biomedical Materials Research 59 (2001) 18–28.

[28] N. Xiliang, Z. Shuping, M. Gloria, K. Sohlberg, Doping of TiO_2 Polymorphs for Altered Optical and Photocatalytic Properties, International Journal of Photoenergy 2009 (2009) 1–22.

[29] K. Persson, Materials Data on TiO2 (SG:141) by Materials Project, https://materialsproject.org/docs/calculations (2014).

[30] K. Persson, Materials Data on TiO2 (SG:12) by Materials Project, https://materialsproject.org/docs/calculations (2014).

[31] S. K. Aggarwal, Alpha-particle spectrometry for the determination of alpha emitting isotopes in nuclear, environmental and biological samples: past, present and future, Anal. Methods 8 (2016) 5353–5371.

[32] A. L'Hoir, Study of the asymmetrical response of silicon surface barrier detectors to MeV light ions. Application to the precise analysis of light ions energy spectra I. Helium ions, Nuclear Instruments and Methods in Physics Research 223 (1984) 336–345.

[33] T. Babeliowsky, G. Bortels, ALFA: A program for accurate analysis of complex alpha-particle spectra on a PC, Applied Radiation and Isotopes 44 (1993) 1349–1358.

[34] I. Vasilef, QtiPlot - Data Analysis and Scientific Visualisation (2013).

[35] A. Vascon, S. Santi, A. A. Isse, T. Reich, J. Drebert, H. Christ, Ch. E. Düllmann, K. Eberhardt, Elucidation of constant current density molecular plating, Nuclear Instruments and Methods in Physics Research Section A: Accelerators, Spectrometers, Detectors and Associated Equipment 696 (2012) 180–191.

[36] N. Trautmann, H. Folger, Preparation of actinide targets by electrodeposition, Nuclear Instruments and Methods in Physics Research Section A: Accelerators, Spectrometers, Detectors and Associated Equipment 282 (1989) 102–106.

[37] D. K. Aswal, S. Lenfant, D. Guerin, J. V. Yakhmi, D. Vuillaume, Self assembled monolayers on silicon for molecular electronics, Analytica Chimica Acta 568 (2006) 84–108.

[38] K. A. Nekrasov, D. D. Seitov, A. A. Pomosova, A. Y. Kupryazhkin, S. K. Gupta, A. B. Usseinov, Sputtering of material from the surface of PuO_2 crystals by collision cascades impact. A molecular dynamics study, Nuclear Instruments and Methods in Physics Research Section B: Beam Interactions with Materials and Atoms 475 (2020) 39–43.

[39] I. Pohjalainen, I. D. Moore, T. Sajavaara, Characterization of ^{233}U alpha recoil sources for $^{229(m)}$Th beam production, Nuclear Instruments and Methods in Physics Research Section B: Beam Interactions with Materials and Atoms 463 (2020) 441–448.

4.12 Appendix

Table 4.11: Fit parameters of the qualitative alpha spectra of all fabricated sources, sorted by the fabrication method, and of some simulated spectra. Constants are marked with a $*$ inside the error brackets because their error could not be determined. When η_1 was set to 1.0, the peak had no significant tailing and therefore had to be fitted only with τ_1 and σ_1. As the second term of the fit function is multiplied with η_2=0, σ_2 and τ_2 can be neglected. "DoF" is short for "degrees of freedom".

Experimental spectra								
sample	channels	η_1	σ_1 / keV	σ_2 / keV	τ_1 / keV	τ_2 / keV	χ^2/DoF	R^2
MP1	2048	1.00(*)	7.51(137)	–	15.4(51)	–	1.55	0.7131
MP2	2048	0.94(1)	5.28(9)	12.5(21)	5.21(21)	49.7(50)	0.74	0.9965
MP3	2048	1.00(*)	10.6(21)	–	2.4(107)	–	1.41	0.8370
MP4	2048	0.96(1)	9.63(31)	104(52)	6.32(91)	54.4(235)	0.75	0.9884
MP5	2048	0.96(1)	8.13(22)	84(32)	8.04(56)	65.1(173)	0.68	0.9915
DoD1	2048	0.96(1)	7.13(23)	93.2(590)	11.6(7)	95.4(381)	0.72	0.9897
DoD2	1024	0.95(1)	6.57(19)	30.0(*)	9.94(45)	125(14)	6E-6	0.9911
DoD3	1024	0.72(6)	5.92(38)	12.3(15)	15.8(16)	63.0(57)	4E-6	0.9881
DoD4	2048	0.93(2)	9.27(55)	93.2(*)	8.29(152)	72.3(438)	1.09	0.9660
DoD5	2048	0.93(2)	6.31(48)	93.2(*)	19.9(19)	80.3(475)	0.996	0.9662
DoD6	1024	0.96(1)	7.04(24)	75.0(*)	7.98(52)	259(84)	3E-6	0.9872
DoD7	2048	0.67(7)	8.34(40)	14.2(12)	11.0(20)	52.9(52)	0.97	0.9903
Ch1	2048	1.00(*)	8.55(83)	–	7.95(206)	–	3.58	0.8840
Ch2	1024	1.00(*)	10.9(14)	–	5.12(334)	–	2.72	0.7269
Ch3	1024	1.00(*)	8.73(140)	–	9.32(344)	–	3E-6	0.8499
Ch4	1024	1.00(*)	10.1(22)	–	3.75(682)	–	6E-6	0.7034
Ch5	1024	1.00(*)	6.86(106)	–	11.1(22)	–	5E-6	0.8578
Ch6	2048	1.00(*)	9.24(96)	–	9.38(247)	–	1.70	0.8974
SA1	2048	0.75(6)	10.8(4)	5.00(258)	11.1(22)	50.7(56)	0.92	0.9912
SA2	2048	0.75(6)	9.79(48)	16.8(17)	10.8(24)	50.0(52)	1.38	0.9886
SA3	2048	0.62(3)	12.6(10)	30.1(43)	25.4(56)	215(57)	0.90	0.9800
SA4	2048	0.33(9)	8.17(601)	8.92(569)	4.08(300)	75.7(45)	3.80	0.9798

continued on next page

continued from previous page

Simulated spectra								
sample	channels	η_1	σ_1 / keV	σ_2 / keV	τ_1 / keV	τ_2 / keV	χ^2/DoF	R^2
L1	2048	0.91(1)	4.8(1)	6.6(21)	10.1(3)	65.7(44)	1.18	0.9973
L30	2048	0.96(3)	9.1(3)	11.0(*)	18.7(19)	116(74)	6.93	0.9846
L50	2048	0.94(*)	14.4(10)	17.5(*)	18.5(121)	96.5(491)	33.2	0.9297
R0	2048	0.91(1)	4.8(1)	6.6(21)	10.1(3)	65.7(44)	1.18	0.9973
R17	2048	0.94(*)	6.7(1)	6.8(*)	16.1(6)	95.0(67)	2.05	0.9954
R51	2048	0.95(2)	10.2(3)	13.5(*)	24.9(16)	124(62)	4.47	0.9896
norm	2048	0.91(1)	4.8(1)	6.6(21)	10.1(3)	65.7(44)	1.18	0.9973
conv	2048	0.93(*)	7.0(1)	7.0(*)	12.5(4)	86.5(43)	1.98	0.9970
conc	2048	0.91(*)	5.9(2)	5.9(*)	12.5(5)	67.6(38)	1.65	0.9933

Chapter 5

Publication IV: Recoil ion source development for TACTICa

The following article is a conference proceeding of PLATAN 2019, 1st International Conference, Merger of the Poznan Meeting on Lasers and Trapping Devices in Atomic Nuclei Research and the International Conference on Laser Probing, Mainz, Germany 19-24 May 2019. It was published in *Hyperfine Interactions*, Springer, volume 241, article 25 in 2020. It deals with the conceptional problem of a recoil ion source providing decelerated recoil ions in their initial charge state distribution. Furthermore, the technical design of the recoil ion source as well as ion flight simulations for this design are presented.

5.1 Own contributions

Mayor contributions were delivered for the conceptualization and design of the experiment. The development of the required monolayer sources was performed and contributions were delivered for successful ion flight simulations. The poster for the PLATAN 2019 conference as well as the corresponding conference proceeding were prepared self-directed.

Development of a recoil ion source providing slow Th ions including $^{229(m)}$Th in a broad charge state distribution

R. Haas[1,2,3,4], T. Kieck[1,2], D. Budker[2,4,5,6], Ch. E. Düllmann[1,2,3,4], K. Groot-Berning[6], W. Li[2,4], D. Renisch[1,2], F. Schmidt-Kaler[2,6], F. Stopp[6], A. Viatkina[2,6]

5.2 Abstract

Ions of the isomer ^{229m}Th are a topic of high interest for the construction of a "nuclear clock" and in the field of fundamental physics for testing symmetries of nature. They can be efficiently captured in Paul traps which are ideal for performing high precision quantum logic spectroscopy. Trapping and identification of long-lived $^{232}Th^{+}$ ions from a laser ablation source was already demonstrated by the TACTICa collaboration on Trapping And Cooling of Thorium Ions with Calcium. The ^{229m}Th is most easily accessible as α-decay daughter of the decay of ^{233}U. We report on the development of a source for slow Th ions, including ^{229m}Th for the TACTICa experiment. The ^{229m}Th source is currently under construction and comprises a ^{233}U monolayer, from which ^{229m}Th ions recoil. These are decelerated in an electric field. Conservation of the full initial charge state distribution of the ^{229m}Th recoil ions is one of the unique features of this source. We present ion-flight simulations for our adopted layout and give a final source design. This source will provide Th ions in their original charge state at energies suitable for capture in a linear Paul trap for spectroscopy investigations.

5.3 Introduction

The ^{229m}Th became a nuclide of high interest in the field of quantum physics in recent years because of its low-energy isomeric nuclear state [1]. This is considered a promising candidate for the development of a nuclear clock [2] and is an interesting nuclide in the search for physics beyond the standard model [3]. Basic features of the ^{229m}Th were experimentally studied in recent years [4–7]. Its low excitation energy [7] in principle allows direct optical excitation with existing laser technology, but the excitation energy is presently not known with sufficient accuracy. Recently, the isomeric state of ^{229}Th was successfully populated in the β^{-}-decay of the artificial nuclide ^{229}Ac [8] and via synchrotron X-ray pumping to the second excited state at 29.19 keV [9]. At the moment, the simplest experimental access to ^{229m}Th is via

[1]Department Chemie, Johannes Gutenberg-Universität Mainz, 55128 Mainz, Germany
[2]Helmholtz-Institut Mainz, 55128 Mainz, Germany
[3]GSI Helmholtzzentrum für Schwerionenforschung GmbH, 64291 Darmstadt, Germany
[4]PRISMA Cluster of Excellence, Johannes Gutenberg-Universität Mainz, 55128 Mainz, Germany
[5]Department of Physics, University of California, Berkeley, CA 94720-7300, USA
[6]QUANTUM, Institut für Physik, Johannes Gutenberg-Universität Mainz, 55128 Mainz, Germany

α-decay of its mother nuclide ^{233}U, which proceeds through the isomeric state in 2 % of all decays [6, 10]. The aim of the collaboration TACTICa[1] is to capture ^{229m}Th and further Th isotopes inside a $^{40}Ca^{+}$ Coulomb ion crystal by sympathetic laser cooling in a Paul trap for precision spectroscopy experiments. This has successfully been demonstrated with $^{232}Th^{+}$ ions from a laser ablation source [11, 12]. There, the $^{232}Th^{+}$ ions became a high mass defect inside the $^{40}Ca^{+}$ Coulomb crystals [12]. The used segmented Paul trap is capable of capturing singly-charged ions with kinetic energies of up to 1 keV. It operates at a maximum background pressure of 1×10^{-10} mbar. Owing to these specifications, the loading of ^{229}Th recoil ions from the decay of ^{233}U with a kinetic energy of E_k = 84 keV [derived from $E_k(^{229}\text{Th}) = Q_\alpha(^{233}\text{U}) - E_\alpha(^{233}\text{U})$, where Q_α is the Q-value of the α-decay and E_α the kinetic energy of the α-particle] becomes challenging. Additionally, the ions emerge from the sample in a rather wide charge-state distribution. This was studied in ^{222}Ra from ^{226}Th [13] and is isotope-specific, as it depends on the nuclear structure and transitions of the individual nuclei. Whereas in [4–7], $^{229}Th^{3+}$ has been successfully extracted as low-energy ion beam from a buffer-gas-stopping-cell based setup, this approach cannot be used for deceleration in our setup due to the gas load, which is incompatible with the pressure requirements in the TACTICa Paul trap. Additionally, this technique leads to a loss of the higher charge states, which are of interest for spectroscopic investigations of the isomeric state. There are good reasons to perform atomic spectroscopy of highly charged ions of Th. To start with, little experimental information is available about the energy levels of Th for ionization stages higher that 2+ [14], even though recent calculation were carried out for Th^{4+} [15]. Apart from serving as a test of atomic theory, spectroscopy in highly charged states of Th may enable studies directly relevant to the isomeric nuclear excitation via processes such as the so-called "electron bridge" (see, e. g., [16], which describes this process in 3+ ions). Therefore, a novel ion source has been developed, which will provide low-energy $^{229m}Th^{n+}$ ions produced as recoil daughter products in the α-decay of ^{233}U. The concept of the source is based on electrostatic deceleration of ions from the ^{233}U recoil ion source. It will consist of a monolayer sample of ^{233}U to provide a monochromatic $^{229m}Th^{n+}$ beam. The source will be set to a high negative potential to decelerate the recoil ions emitted from the source surface when running up against ground potential, at which the vacuum chamber is kept. The absence of gas encounters provides the opportunity to study ^{229m}Th in various charge states like in the case of ^{222}Ra from ^{226}Th-decay [13]. In addition to the recoil ion source, a laser-ablation ion source [11] will also be installed to provide ions of Th isotopes that are available as macroscopic samples. The combination of the ablation and recoil ion sources offers the possibility to study a variety of Th isotopes (see Fig. 5.1) in several charge states. The ions will be captured by a Paul trap, sympathetically cooled using a crystal of laser-cooled Ca^{+}

[1] TACTICa (Trapping And Cooling of Thorium Ions with Calcium)

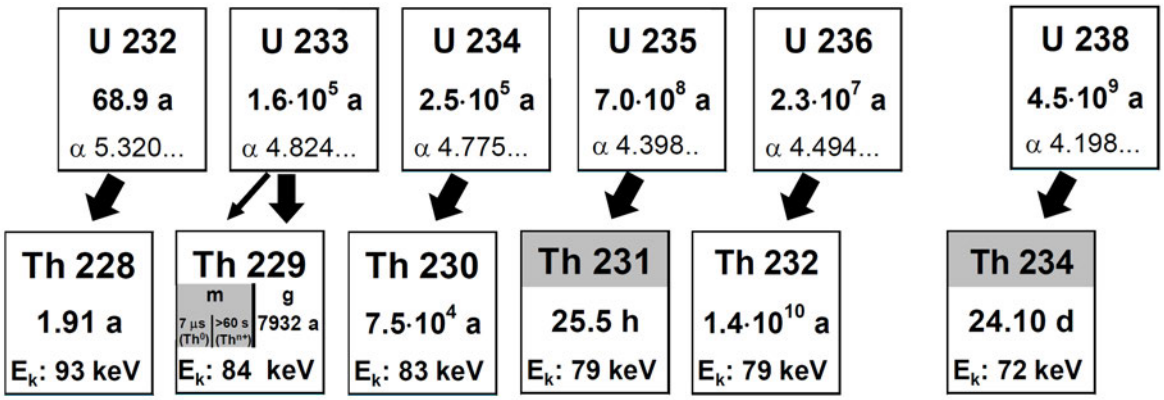

Figure 5.1: Excerpt of the nuclear chart showing thorium isotopes of interest for TACTICa. Long-lived uranium α-decay precursor isotopes are also shown. The half-lives of all isotopes are indicated. For the uranium isotopes, the α-particle energies are given in MeV. For the thorium isotopes, the kinetic energies, E_k, of the recoil ions populated in the α-decay are given. Many of the thorium isotopes are available in macroscopic quantity, suitable for ablation source production. Those indicated in gray are only available as α-decay products from the recoil ion source.

ions and be available for precision spectroscopy. This is of interest, e.g., for the verification of hypothetical extensions of the theoretical description of the isotope shift using the nonlinearity of the King plot and thus for the search for new particles [17].

5.4 Electrostatic deceleration

In the following, we use ^{229m}Th as the example nuclide. The kinetic energy of the ^{229m}Th recoil ions of about 84 keV has to be reduced before the ions enter the Paul trap to allow their capture. As mentioned in section 5.3, the maximum acceptable kinetic energy of singly-charged ^{229m}Th ions is around 1 keV. A recoil ion source provides ^{229m}Th recoil ions in a 2π angular distribution. Ion cooling provides both the reduction of the transverse component of the ions' velocity and longitudinal deceleration of the recoil ions. This would be the ideal solution for a 2π source to produce an ion beam. The most efficient cooling method is buffer gas cooling as used in other ^{229m}Th experiments [4–7]. Owing to charge exchange collisions in a buffer gas cell, the charge state distribution collapses to low charge states. In [4–7], predominantly 2+ and 3+ ions were extracted. To retain higher charge states, which are expected to be populated in the α-decay of ^{233}U, gas-free cooling methods are required.

We decided to use electrostatic deceleration of the recoil ions by a negative potential on the source. For this approach, a source with a high recoil efficiency as well as a sharp recoil energy spectrum without any loss of the high charge

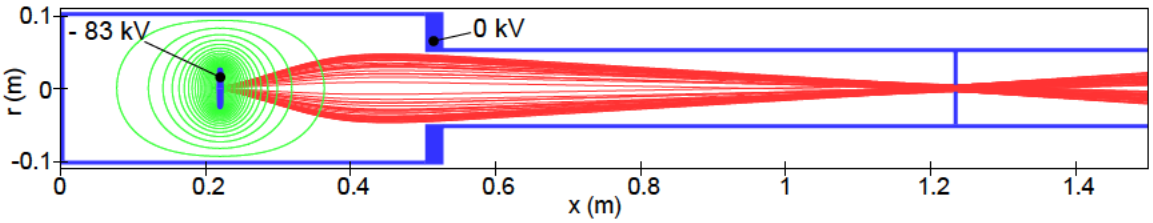

Figure 5.2: Flight trajectories of the singly-charged recoil ions that clear the aperture and equipotential lines. The ion energy is about 1000 eV after exiting the electrostatic deceleration chamber.

states is needed. This is typically given by an ideal recoil ion source consisting of a single atomic layer of ^{233}U. Such sources can be efficiently produced by several methods, e.g., in the Nuclear Chemistry section of the Department of Chemistry in Mainz. A comparison of the different source fabrication methods will be published separately [18]. The basic idea of the electrostatic deceleration of recoil ions in the TACTICa source is to use the potential difference between the source (kept at negative voltage) and the trap entrance (at ground potential). Because of the kinetic energy of the recoil ions of about 84 keV, a high negative potential between 83 keV to 84 keV is needed to decelerate singly-charged ^{229}Th^{+} ions to an energy below 1 keV. For higher charge states, correspondingly lower voltages are sufficient. At a specific voltage, the source will deliver the chosen charge state with proper energy as well as lower charge states with higher energy due to lower deceleration. Higher charge states will always be suppressed.

The advantage of this source type concerning charge-state conservation comes with the disadvantage of low efficiency, because of low angular acceptance caused by emittance conservation (Liouville's theorem). 50 % of all ions are emitted into the substrate and therefore lost. The emittance of the residual ions is preserved regardless of ion optics and could only be reduced by cooling mechanisms. Many of these (e.g., buffer gas [4], stochastic [19], electron [20], laser [21]) are not applicable here. In our design, the source is kept at high voltage matching the charge state and only the vacuum chamber at ground potential acts as an ion-optical element. In our simulation model used for the optimizations of the source, the ions are emitted from a round surface with a diameter of 30 mm in 2π angular distribution with an energy of 84 keV randomized in position and angle with the Mersenne Twister 19937 algorithm [22]. Several ion-flight simulations were performed with the open-source software IBSimu [23] to evaluate the transmission efficiency of the recoil ions through the first aperture with a diameter of 100 mm. The simulation setup including solid ion-optics, equipotential lines and flight pathways of the aperture-transmitting ions is given in Fig. 5.2.

5.5 Final design

The final design of the TACTICa source is kept simple and is shown schematically in Fig. 5.3. As mentioned in section 5.4, the electrostatic deceleration of the recoil ions can be achieved with a high negative potential on the source and the vacuum chamber at ground potential. The ^{233}U source is fixed in the center of a tubular chamber of a 500 mm length and an inner diameter of 200 mm. After deceleration at the end of the tubular chamber, the ions enter a section with a microchannel plate detector (MCP) for beam-analysis. The source chamber as well as the beam analysis chamber can be separated from the main chamber containing the trap with a gate valve (GV1) for maintenance and source exchange. A 90 ° electrostatic quadrupole bender is the connection point of both the recoil ion source and the laser ablation ion source with the trap. It is used to switch between the ion beams of both sources. In the ablation ion source, singly-charged ions are produced by means of a pulsed laser. The laser pulses serve as time-stamps, leading to precisely known ion arrival times at the Paul trap, which can therefore be closed at times synchronized with incoming ions, thus ensuring the ions' capture [11]. To prevent ions other than Th from entering the trap, a Wien filter is used, which selects the right mass-to-charge ratio. In case of the recoil ion source, ion production by α-decay of the mother nuclide occurs at a random time, and no timing information is available in this case. Therefore, a small chamber housing a tagging section to obtain timing information of passing recoil ions is placed in front of the Paul trap. This will provide the signal necessary to know when exactly the trap needs to be closed. The tagging methods under investigations are by image charge detection [25], by fluorescence detection [24] and by energy loss in the ion crystal [26] followed by doppler-recooling measurement [27, 28]. The section with the ablation ion source, the quadrupole bender and the tagging station can also be separated for maintenance from the Paul trap with a gate valve (GV2), to keep the trap under ultra-high vacuum conditions also when the vacuum has to be broken outside of the trap.

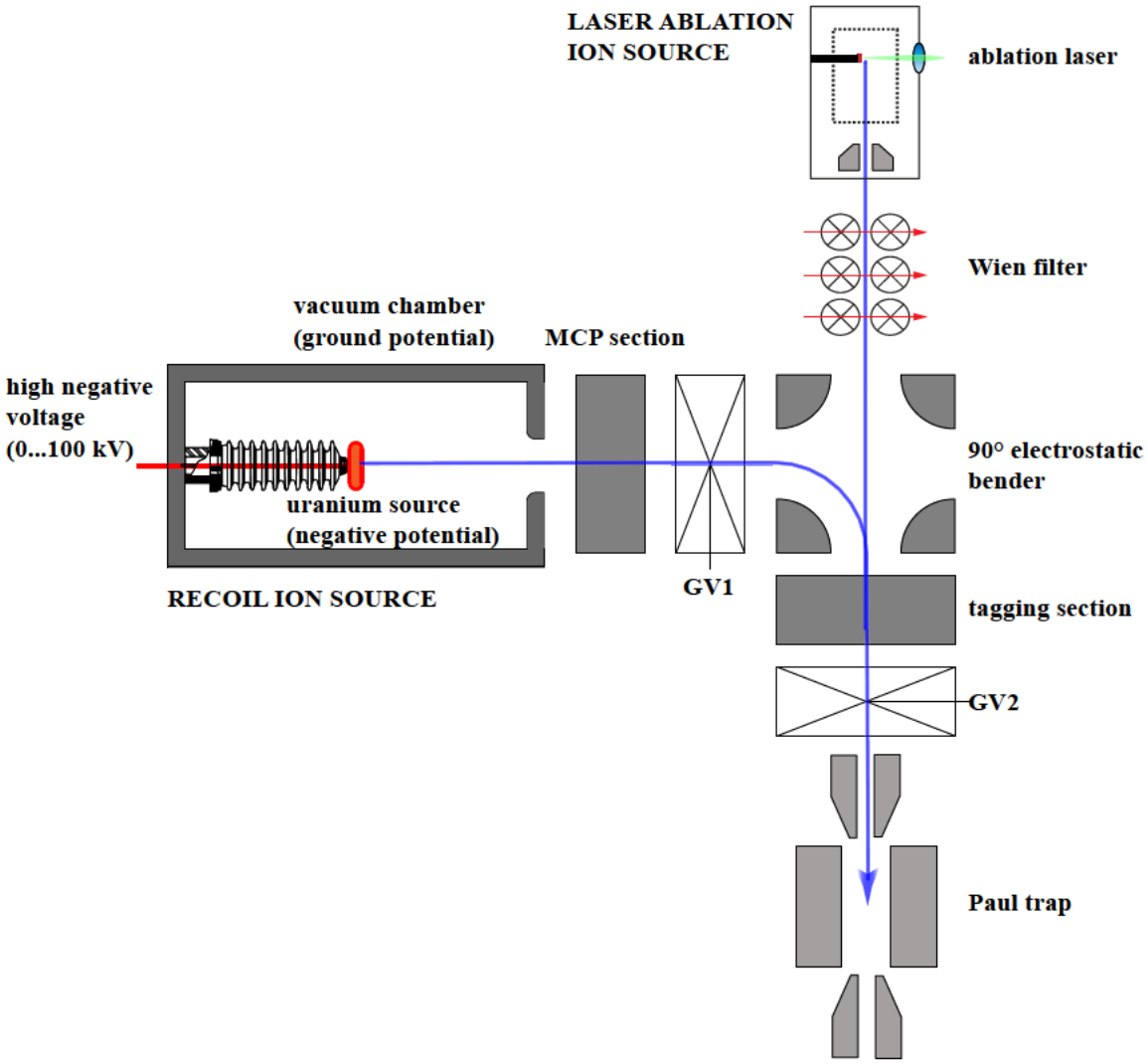

Figure 5.3: Schematic illustration of the TACTICa experimental setup including both the recoil ion source and the laser ablation ion source (not to scale). See text for details.

5.6 Conclusion

We present the design of a recoil ion source setup using electrostatic deceleration for the TACTICa experiment. This source will deliver Th^{n+} recoil ions of a variety of Th isotopes (including ^{229m}Th) from a uranium monolayer source. The kinetic energy for trapping of the ions has to be below 1 keV. The most promising way to decelerate the ions and to retain them in their original charge states is via electrostatic deceleration. It allows to select a single charge state of the full initial charge state distribution [13]. Furthermore, electrostatic bending removes expected contamination of ^{228}Th ions due to their higher kinetic energy of 93 keV. Detailed simulations with IBSimu [23] are ongoing to optimize the setup with respect to the transmission rate. The rate of the most interesting ion ^{229m}Th will nevertheless be low, as it is restricted by both the activity of approximately 13 Bq cm^{-2} determined by the source size and half-life of ^{233}U and a population rate of 2 % into the isomeric state. Thus tagging of the ions in flight is essential to obtain a timing signal determining the optimum time for closing the Paul trap with an ion inside. Finally, a design for the setup of the TACTICa source is given which includes the possibility to load both recoil ions or ions from a laser ablation ion source into the Paul trap. The construction of the setup is ongoing.

5.7 References

[1] M. S. Safronova et al., Search for new physics with atoms and molecules, Rev. Mod. Phys., 90, 025008 (2018)

[2] E. Peik et al., Nuclear laser spectroscopy of the 3.5 eV transition in Th-229, Europhys. Lett., 61, 181 (2003)

[3] V. V. Flambaum, Enhanced Effect of Temporal Variation of the Fine Structure Constant and the Strong Interaction in ^{229}Th, Phys. Rev. Lett. 97, 092502 (2006)

[4] L. von der Wense et al., Direct detection of the ^{229}Th nuclear clock transition, Nature, 533, 47 (2016)

[5] B. Seiferle et al., Lifetime Measurement of the ^{229}Th Nuclear Isomer, Phys. Rev. Lett., 118, 042501 (2017)

[6] J. Thielking et al., Laser spectroscopic characterization of the nuclear-clock isomer ^{229m}Th, Nature, 556, 321 (2018)

[7] B. Seiferle et al., Energy of the ^{229}Th nuclear clock transition, Nature, 573, 243 (2019)

[8] Y. Shigekawa et al., Observation of internal-conversion electrons emitted from ^{299m}Th produced by β decay of ^{229}Ac, Phys. Rev. C, 100, 044304 (2019)

[9] T. Masuda et al., X-ray pumping of the ^{229}Th nuclear clock isomer, Nature, 573, 238 (2019)

[10] V. Barci et al., Nuclear structure of ^{229}Th from γ-ray spectroscopy study of ^{233}U α-particle decay, Phys. Rev. C, 68, 034329 (2003)

[11] K. Groot-Berning et al., Trapping and sympathetic cooling of single thorium ions for spectroscopy, Phys. Rev. A, 99, 023420 (2019)

[12] F. Stopp et al., Catching, trapping and in-situ-identification of thorium ions inside Coulomb crystals of $^{40}Ca^{+}$ ions, Hyperfine Interact., 240, 33 (2019)

[13] K. Gunter et al., Charge and energy distributions of recoils from ^{226}Th alpha decay, Phys. Rev. Lett., 16, 9 (1966)

[14] A. Kramida et al., NIST Atomic Spectra Database (ver. 5.7.1), [Online]. Available: https://physics.nist.gov/asd (2019, November 14th)

[15] M. S. Safronova et al., Atomic properties of actinide ions with particle-hole configurations, Phys. Rev. A, 97, 012511 (2018)

[16] R. A. Müller et al., Theoretical analysis of the electron bridge process in $^{229}Th^{3+}$, Nucl. Instrum. Meth. Phys. Res. B, 408, 84 (2017)

[17] V. V. Flambaum et al., Isotope shift, nonlinearity of King plots, and the search for new particles, Phys. Rev. A, 97, 032510 (2018)

[18] R. Haas et al., to be submitted to Radiochim. Acta.

[19] D. Moehl et al., Physics and technique of stochastic cooling, Physics Reports 58, 73 (1980)

[20] G. I. Budker et al., Experimental studies of electron cooling, Particle Accelerators 7, 197 (1976)

[21] S. Schroeder et al., First laser cooling of relativistic ions in a storage ring, Phys. Rev. Lett. 64, 2901 (1990)

[22] M. Matsumoto et al., Mersenne Twister: A 623-Dimensionally Equidistributed Uniform Pseudo-Random Number Generator, ACM TOMACS 8, 3 (1998)

[23] T. Kalvas et al., IBSIMU: A three-dimensional simulation software for charged particle optics, Rev. Sci. Instrum. 81, 02B703 (2010)

[24] R. F. Garcia Ruiz et al., Development of a sensitive setup for laser spectroscopy studies of very exotic calcium isotopes, J. Phys. G: Nucl. Part. Phys., 44, 044003 (2017)

[25] P. Räcke et al., Detection of small bunches of ions using image charges, Nature Scientific Reports, 8, 9781 (2018)

[26] L. Schmöger et al., Deceleration, precooling, and multi-pass stopping of highly charged ions in Be^+ Coulomb crystals, AIP Rev. Sci. Instrum., 86, 103111 (2015)

[27] J. H. Wesenberg et al., Fluorescence during Doppler cooling of a single trapped atom, Phys. Rev. A, 76, 053416 (2007)

[28] G. Huber et al., Transport of ions in a segmented linear Paul trap in printed-circuit-board technology, New J. Phys., 10, 013004 (2008)

Chapter 6

Conclusion and Outlook

This work has involved both technical developments and experiments that have not only used new methods for the radiochemical fabrication of both targets as well as recoil ion sources, but have also helped to gain new insights into existing and novel methods, individually and in comparison, to produce better radiochemical sources in the future. Furthermore, an experimental setup was developed and constructed in collaboration with physicists, where novel recoil ion sources consisting of a monolayer of active material are used in a high electrostatic field to deliver low-energetic recoil ions in their full initial charge state distribution for high-precision quantum logic spectroscopy in a Paul trap.

The Drop-on-Demand inkjet printing method, which was developed and characterized before this work, was previously only used for the production of deposit patterns, which resulted from the evaporation of single droplets. In this work, the DoD method was used for the first time for the fabrication of a target with a closed layer consisting of isotopically enriched ^{170}Er. The homogeneous layer was achieved by stepwise drying under IR light and adding further material by printing onto the dried deposits. The thereby fabricated target was successfully used for the validation of the 66.7 keV γ-line intensity of ^{171}Tm by neutron activation analysis and laid the foundation for further measurements of the neutron capture cross section of ^{171}Tm, which is of great importance as a branch point in the astrophysical s-process. This technical achievement placed the DoD method on an equal level of importance in target production with molecular plating.

Nevertheless, the problem of how targets produced by DoD perform in particle beams, e.g. during conditioning for accelerator experiments, and which chemical microprocesses are involved in the irradiation of targets with low-energetic electron and ion beams remained open. Based on earlier findings, many of the freshly produced targets from MP and, as it should turn out, also DoD are not stable under normal laboratory conditions and deteriorate by humidity and oxygen over long storage periods. The base-of-the-art was therefore to condition the targets

in parasitic ion beams with reduced energies and intensities at accelerators to convert unstable hygroscopic chemical compounds on the targets into more stable compounds. Due to the cost- and time-intensive nature of such conditioning with accelerator beams and the difficult availability of beam time due to modifications to the particle accelerator at GSI, a method was developed providing particle beams for the conditioning of targets independent of accelerator beam times. A pilot experimental setup for "Off-line Deposit Irradiation" (ODIn) was constructed and characterized, to investigate the induced effects of low-energetic electron and ion beams (<5 keV) on target layers produced by MP and DoD. The first insights were that lead targets produced by MP were successfully converted from the lead carbonate into lead(II) oxide by irradiation with 1.5 keV electron beams. Furthermore, the pilot setup is the foundation for the development of a method to regularly condition targets for accelerator experiments in the future.

In addition to target production, the fabrication of recoil ion sources consisting of alpha-decaying nuclides is also of great importance for many nuclear physics applications. One of such applications is the investigation of the isomer of ^{229}Th with its very low excitation energy below 10 eV. The easiest way to obtain this state is by internal conversion processes in the alpha decay from the mother nuclide ^{233}U. Therefore the MP and DoD methods, which were already well established in target fabrication, were used for the fabrication of very thin layered ^{233}U sources. Ideally, single layers of ^{233}U should be fabricated in order to achieve the highest possible recoil efficiency with the lowest possible scattering of the emitted ^{229}Th recoil ions. In order to better investigate the sources produced by MP and DoD with respect to their layer thickness, they were compared with sources produced by two new methods that should theoretically produce pure monolayers. These are based on chelation by functional groups and self-adsorption processes of actinides on metal oxides. The sources produced by all four methods were characterized quantitatively and qualitatively by several methods including alpha spectrometry, scanning electron microscopy and radiographic imaging. A fit routine was developed and used on qualitative alpha spectra in order to gain comparable parameter like the tailing and FWHM of the ^{233}U alpha peak. Additionally, these experimental spectra were compared with advanced alpha spectrometric simulations, where the influence of several source parameters including number of atomic layers, surface roughness and layer shape on the alpha peak were investigated. The sources produced by SA and MP were additionally investigated in their recoil efficiency by the collection of ^{228}Th recoil ions from ^{232}U, resulting in nearly 100 % recoil efficiency for SA sources. Therefore, sources produced by SA are the best recoil ion sources with respect to the recoil efficiency, but the actual energy distribution of the recoil ions has to be investigated in further experiments.

At last, a design was proposed and ion flight simulations were performed for a recoil source setup using the previously described monolayer sources and electrostatic deceleration to deliver low-energetic $^{229(m)}$Th ions in high charge states >3+

for high-precision quantum logic spectroscopy in the TACTICa experiment. The application of electrostatic deceleration was discussed with ion flight simulations giving pathways of ions in the proposed setup as well as extraction efficiencies. The latter is comparable low as the geometric efficiency. Thus, effective methods for ion detection in flight were discussed since the low extraction efficiency has to be balanced with a high capture efficiency in the Paul trap. The proposed experimental setup will consist of the recoil ion source section, a laser ablation ion source to provide ions from bulk material, a tagging section for detection of ions in flight and a section for ion beam analysis. The construction of the setup is still ongoing.

Future experiments with targets produced by DoD will show how they perform in accelerator beams. Additionally, further experiments with the ODIn pilot setup will shed light on the chemical microprocesses involved during the irradiation of targets with ion beams and how to develop a method for regular conditioning of targets. The proposed improvements on actual fabrication methods for recoil ion sources will provide a great variety of high-qualitative sources, which can be applied for different experiments. Still, the method based on self-adsorption has to be studied further with other actinides and on other substrates and the real energy distribution of the ^{229}Th ions from different recoil ion sources has to be investigated in the TACTICa experiment.

With this thesis, the fabrication of targets and recoil ion sources has been improved significantly to deliver tailor-made targets and sources suitable for the needs of future applications in nuclear physics.

List of Figures

List of Tables

Acknowledgements

An dieser Stelle möchte ich gerne all jenen danken, die mich im Laufe meines Studiums und meiner Promotion begleitet und unterstützt haben:

Allen voran möchte ich ganz besonders meinem Doktorvater [redacted] danken, der mich schon im Studium während meiner Bachelor- und Masterarbeit betreut hat und mir die Möglichkeit gab, die Promotion in seiner Arbeitsgruppe abzulegen. Ich danke ihm auch dafür, dass er mir in der gesamten Zeit alle Freiheiten gelassen hat, meine Fähigkeiten und Interessen in der Wissenschaft nicht bloß einzusetzen, sondern mich auch darin unterstützt und ermutigt hat, mich weiterzubilden und dadurch meine Fähigkeiten noch weiter auszubauen. Ich bin für die Wertschätzung, Unterstützung, aber auch die Anstöße zur Perfektion sehr dankbar.

Außerdem danke ich auch [redacted] und [redacted] für die gute Betreuung und für viele gute Ratschläge während meiner Promotion. Im Einzelnen danke ich [redacted] für die Ermöglichung eines Forschungspraktikums bei SHIPTRAP an der GSI während meines Masterstudiums, was mir sehr interessante Einblicke in große experimentelle Aufbauten und wertvolle Erfahrungen für meine eigene Arbeit ermöglicht hat. Meinem Mentor [redacted] danke ich für den öfteren interessanten und hilfreichen Ideenaustausch und viele fesselnde Gespräche.

Ein ganz besonderer Dank gilt auch [redacted], [redacted] und [redacted] für die Betreuung während meiner Bachelor- und Masterarbeit, für ihre Zusammenarbeit mit mir und dafür, dass sie mir alle wichtigen Techniken im Bereich der Targetherstellung und Probencharakterisierung beigebracht haben.

Ich danke allen Mitarbeitern und Kollegen aus der Kernchemie, aus dem Helmholtz-Institut und der GSI für die tolle Zusammenarbeit und viele schöne Momente bei Institutsfeiern, Ausflügen und anderen Veranstaltungen.

Ich danke auch sehr meiner Arbeitsgruppe, den “Superheavies”, für die familiäre Atmosphäre, das gute Arbeitsklima und die schöne Zusammenarbeit bei vielen Projekten. [redacted], [redacted], [redacted] und [redacted] möchte ich dabei ganz besonders danken für die enge Zusammenarbeit, viele hilfreiche Ratschläge, tatkräftige Unterstützung und den guten Ideenaustausch. Den beiden Letzteren danke ich auch für die schöne Büroatmosphäre.

[redacted] und [redacted] danke ich für die Erlaubnis zur Verwendung der Veröffentlichung zu den ^{170}Er-Arbeiten in meiner Dissertation und die gute Zusammenarbeit bei dem Projekt.

[redacted] und [redacted] danke ich ebenfalls für die gute Zusammenarbeit und den Ideenaustausch bei den Arbeiten zu den Rückstoßionenquellen.

[redacted], [redacted], [redacted] und [redacted] möchte ich für die Hilfe bei den Bestrahlungen von Bleitargets an TASCA danken. Den Targetmachern an der GSI, insbesondere [redacted], möchte ich danken für die Herstellung vieler Substrate, die essentiell waren für die Herstellung vieler

Targets und anderer Proben.

Ich möchte auch [redacted] und der Larissa-Gruppe danken für die Unterstützung, Beratung und gute Zusammenarbeit in vielen Projekten. Außerdem danke ich ihnen für den herzlichen Umgang und ebenfalls viele schöne Momente.

Ein herzlicher Dank geht auch an alle meine Freunde, sowohl vergangene als auch neue, für die Unterstützung und Begleitung, besonders in schwierigen Zeiten.

Meiner Familie danke ich besonders für die moralische und finanzielle Unterstützung während meines Studiums und meiner Promotion. Vorallem danke ich dabei meiner Mutter [redacted] und meinem Bruder [redacted], die immer für mich da waren. Zuletzt danke ich auch meinem verstorbenen Großvater [redacted], der mir die Faszination für die Natur nahe gebracht, meine handwerklichen Fähigkeiten gefördert und sowohl meine Neugier als auch meinen Forschergeist geprägt hat wie kein anderer.

Vielen herzlichen Dank!

Curriculum Vitae

Raphael Haas

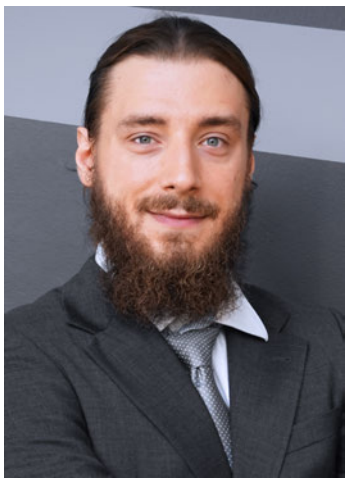

[redacted]

Persönliche Daten

Geburtstag/-ort	[redacted]
Staatsangehörigkeit	deutsch

Bildungsweg

05/2017 - 09/2020	Promotion, Fachrichtung Chemie Johannes Gutenberg-Universität Mainz Titel der Dissertation: Tailor-made thin radionuclide layers for targets and recoil ion sources in nuclear applications 1. Gutachter: [redacted] 2. Gutachter: [redacted]
10/2014 - 01/2017	Master-Studium Chemie Johannes Gutenberg-Universität Mainz Titel der Masterarbeit: Herstellung von Dünnschichten aus Lanthan auf Graphenoberflächen mittels elektrochemischer Abscheidung und mittels der Drop-on-Demand-Drucktechnologie 1. Gutachter: [redacted] 2. Gutachter: [redacted]

10/2011 - 09/2014	Bachelor-Studium Chemie Johannes Gutenberg-Universität Mainz Titel der Bachelorarbeit: Radiochemische Holmium-Probenpräparation für den RISIKO Massenseparator für das ECHo-Projekt 1. Gutachter: [redacted] 2. Gutachter: [redacted]
08/2002 - 06/2011	Abitur Gymnasium Taunusstein

Publikationen

[1] R. Haas, M. Hufnagel, R. Abrosimov, Ch. E. Düllmann, D. Krupp, C. Mokry, D. Renisch, J. Runke, U. W. Scherer, Alpha spectrometric characterization of thin ^{233}U sources for $^{229(m)}$Th production, Radiochimica Acta (2020) [accepted].

[2] S. Rau, F. Heiße, F. Köhler-Langes, S. Sasidharan, R. Haas, D. Renisch, Ch. E. Düllmann, W. Quint, S. Sturm, K. Blaum, Penning trap mass measurements of the deuteron and the HD^+ molecular ion, Nature 585 (2020) 43–47.

[3] R. Haas, T. Kieck, D. Budker, Ch. E. Düllmann, K. Groot-Berning, W. Li, D. Renisch, F. Schmidt-Kaler, F. Stopp, A. Viatkina, Development of a recoil ion source providing slow Th ions including $^{229(m)}$Th in a broad charge state distribution, Hyperfine Interactions 241 (2020) 25.

[4] R. Haas, C. C. Meyer, S. Böhland, Ch. E. Düllmann, J. Mäder, K. Tinschert, ODIn — A setup for Off-line Deposit Irradiations of thin layers for nuclear physics applications, Nuclear Instruments and Methods in Physics Research Section A: Accelerators, Spectrometers, Detectors and Associated Equipment 957 (2020) 163366.

[5] F. Stopp, K. Groot-Berning, G. Jacob, D. Budker, R. Haas, D. Renisch, J. Runke, P. Thörle-Pospiech, Ch. E. Düllmann, F. Schmidt-Kaler, Catching, trapping and in-situ-identification of thorium ions inside Coulomb crystals of $^{40}Ca^+$ ions, Hyperfine Interactions 240 (2019) 33.

[6] K. Groot-Berning, F. Stopp, G. Jacob, D. Budker, R. Haas, D. Renisch, J. Runke, P. Thörle-Pospiech, Ch. E. Düllmann, F. Schmidt-Kaler, Trapping and sympathetic cooling of single thorium ions for spectroscopy, Physical Review A 99 (2019) 023420.

[7] T. Heftrich, M. Weigand, C. E. Düllmann, K. Eberhardt, S. Fiebiger, J. Glorius, K. Göbel, C. Guerrero, R. Haas, S. Heinitz, J. Lerendegui-Marco, F. Käppeler, J. D. Kaiser, U. Köster, C. Langer, S. Lohse, F. Ludwig, R. Reifarth, D. Renisch, K. Scheutwinkel, D. Schumann, N. Wiehl, C. Wolf, Thermal (n, γ) cross section and resonance integral of ^{171}Tm, Physical Review C 99 (2019) 065810.

[8] L. C. von der Wense, B. Seiferle, C. Schneider, J. Jeet, I. Amersdorffer, N. Arlt, F. Zacherl, R. Haas, D. Renisch, P. Mosel, P. Mosel, M. Kovacev, U. Morgner, Ch. E. Düllmann, E. R. Hudson, P. G. Thirolf, The concept of laser-based conversion electron Mössbauer spectroscopy for a precise energy determination of ^{229m}Th, Hyperfine Interactions 240 (2019) 23.

[9] K. Eberhardt, C. E. Düllmann, R. Haas, C. Mokry, J. Runke, P. Thörle-Pospiech, N. Trautmann, Actinide targets for fundamental research in nuclear physics, AIP Conference Proceedings 1962 (2018) 030009.

[10] M. Weigand, T. Heftrich, Ch. E. Düllmann, K. Eberhardt, S. Fiebiger, J. Glorius, K. Göbel, R. Haas, C. Langer, S. Lohse, 66.7-keV γ-line intensity of ^{171}Tm determined via neutron activation, Physical Review C 97 (2018) 035803.

[11] H. Dorrer, K. Chrysalidis, T. D. Goodacre, C. E. Düllmann, K. Eberhardt, C. Enss, L. Gastaldo, R. Haas, J. Harding, C. Hassel, K. Johnston, T. Kieck, U. Köster, B. Marsh, C. Mokry, S. Rothe, J. Runke, F. Schneider, T. Stora, A. Türler, K. Wendt, Production, isolation and characterization of radiochemically pure ^{163}Ho samples for the ECHo-project, Radiochimica Acta 106 (2018) 535–547.

[12] R. Haas, S. Lohse, Ch. E. Düllmann, K. Eberhardt, C. Mokry, J. Runke, Development and characterization of a Drop-on-Demand inkjet printing system for nuclear target fabrication, Nuclear Instruments and Methods in Physics Research Section A: Accelerators, Spectrometers, Detectors and Associated Equipment 874 (2017) 43–49.

[13] L. Gastaldo, K. Blaum, K. Chrysalidis, T. Day Goodacre, A. Domula, M. Door, H. Dorrer, C. E. Düllmann, K. Eberhardt, S. Eliseev, C. Enss, A. Faessler, P. Filianin, A. Fleischmann, D. Fonnesu, L. Gamer, R. Haas, C. Hassel, D. Hengstler, J. Jochum, K. Johnston, U. Kebschull, S. Kempf, T. Kieck, U. Köster, S. Lahiri, M. Maiti, F. Mantegazzini, B. Marsh, P. Neroutsos, Y. N. Novikov, P. C. O. Ranitzsch, S. Rothe, A. Rischka, A. Saenz, O. Sander, F. Schneider, S. Scholl,

R. X. Schüssler, C. Schweiger, F. Simkovic, T. Stora, Z. Szücs, A. Türler, M. Veinhard, M. Weber, M. Wegner, K. Wendt, K. Zuber, The electron capture in ^{163}Ho experiment – ECHo, The European Physical Journal Special Topics 226 (2017) 1623–1694.

[14] F. Schneider, K. Chrysalidis, H. Dorrer, C. E. Düllmann, K. Eberhardt, R. Haas, T. Kieck, C. Mokry, P. Naubereit, S. Schmidt, K. Wendt, Resonance ionization of holmium for ion implantation in microcalorimeters, Nuclear Instruments and Methods in Physics Research Section B: Beam Interactions with Materials and Atoms 376 (2016) 388–392.

Forschungsaufenthalte

11/2018	Einwöchige Strahlzeit an IGISOL University of Jyväskylä, Finnland

Konferenzbeiträge

09/2019	Jahrestagung der Fachgruppe Nuklearchemie 2019, Dresden, Germany Oral presentation: ”Vergleich verschiedener Herstellungsverfahren zur Erzeugung von Monolagen alpha-zerfallender Actinidenisotope als ideale Rückstoßquellen ihrer Tochterkerne”
08/2019	6th International Conference on the Chemistry and Physics of the Transactinide Elements, Wilhelmshaven, Germany Poster presentation: ”ODIn – Off-line Deposit Irradiation as a baking-in procedure for heavy-element targets”
05/2019	International Conference Merger of the Poznan Meeting on Lasers and Trapping Devices in Atomic Nuclei Research and the International Conference on Laser Probing, Helmholtz Institute Mainz, Germany Poster presentation: ”Source Development and Simulations of Ion Optics for an Ion Source providing slow highly charged ^{229m}Th ions”

02/2019	NUSPRASEN Workshop 2019, GSI, Darmstadt, Germany Oral presentation: ”Target performance under beam influence: Comparison of different production methods and different incident projectiles”
09/2017	GDCh Wissenschaftsforum 2017 - Jahrestagung der Fachgruppe Nuklearchemie, Berlin, Germany Oral presentation: ”Development, characterization and first applications of a Drop-on-Demand inkjet printing system for nuclear target fabrication”
09/2017	16th Workshop on Recoil Separator for Superheavy Element Chemistry, GSI, Darmstadt, Germany Oral presentation: ”Development, characterization and first applications of a Drop-on-Demand inkjet printing system for nuclear target fabrication”

Auszeichnungen

10/2019	Giersch Excellence Award for outstanding scientific work during the PhD
08/2019	IUPAC Poster Prize, 6th International Conference on the Chemistry and Physics of the Transactinide Elements, Wilhelmshaven, Germany

Sonstige Tätigkeiten

02/2018 - 03/2020	Koordinator und leitender Assistent des kernchemischen Grundpraktikums im ehemaligen Institut für Kernchemie, Johannes Gutenberg-Universität Mainz
05/2017 - 02/2018	Vorlesungsassistent in der Grundvorlesung “Chemie für Physiker und Geowissenschaftler”, Johannes Gutenberg-Universität Mainz

01/2017 - 04/2017	Wissenschaftliche Hilfskraft in der Arbeitsgruppe Düllmann bei der Charakterisierung und Anwendung des DoD-Druckers im Bereich radiochemischer Probenherstellung
04/2013 - 10/2016	Aktives Mitglied des Fachschaftsrates im Fachbereich Chemie, Pharmazie und Geowissenschaften an der Johannes Gutenberg-Universität Mainz, Aufgabenbereiche: Veranstaltungsplanung, Erstsemesterbetreuung, Sharepointverwaltung, Vertretung studentischer Interessen in der Lehre